## REVIEW

Check for updates

# Porphyrin-containing materials for photodegradation of organic pollutants in wastewaters: a review

Sara R. D. Gamelas, [iD][a] João P. C. Tomé, [iD] *[b]
Augusto C. Tomé [iD] *[a] and Leandro M. O. Lourenço [iD] *[a]

Industrialization and town urbanization have led to an exponential need for clean water and new wastewater treatment strategies. Currently, photocatalysis is the most appealing method to destroy organic pollutants in water, and the use of sunlight, with the assistance of a solid photocatalyst, is considered one of the most sustainable approaches. The use of heterogeneous photocatalysts has unique advantages, namely their recovery and reuse for several cycles without loss of activity. Due to their remarkable optical and photophysical properties, porphyrin (Por) dyes can be used in homogenous and heterogeneous photocatalysis. Different supports can be used to immobilize Pors, allowing the final material to extend its absorption into the white light region since most of the supports only absorb UV light. This review focuses on the photocatalytic performance of non-immobilized and immobilized porphyrins in the photodegradation of organic pollutants for wastewater treatment application.

## 1. Introduction

Water is the most important natural resource on earth and must be preserved. However, it has been contaminated because of anthropogenic activities. Industrialization and town urbanization have led to enormous problems regarding effluent gathering and treatment. In many countries, most industries discard their wastewater directly into aquatic environments without previous suitable treatment. In India, for instance, most of the industrial effluents are coloured due to the untreated wastewaters from the painting and textile industries. This leads to loss of water quality, which can be hazardous to aquatic life and human health. Because most synthetic dyes are slowly degraded in the environment, it is necessary to remove or degrade those contaminants as much as possible before the effluents are discharged into the rivers to solve or mitigate this problem.[1–4]

Researchers have developed sustainable wastewater treatment strategies in the past few decades.[5–10] When developing a new approach for water treatment, its safety and sustainability must be considered. In this context, photocatalysis arises as a green alternative to currently used methods (rapid sand filtration, upflow roughing filters, and slow sand filtration, among others) that show several disadvantages such as high maintenance and expensive costs.[11]

In the case of photocatalysis, it only requires a photocatalyst and light to produce reactive oxygen species (ROS) that will degrade the pollutant. The use of sunlight, with the assistance of a solid photocatalyst (which may be recycled and reused),[12,13] is a valuable and green approach to destroy organic contaminants. During the photocatalytic process with semiconductors, the adsorption process plays an important role since it is necessary for the dye first to be adsorbed into the photocatalyst's surface. This process is based on a surface phenomenon using a solution which has an adsorbable solute (like dyes) that comes in contact with the adsorbent with a highly porous surface.[14] Adsorption was already used as an effective separation technique due to its high efficiency in removing dyes. In fact, activated carbon was already used to remove phenols, pesticides, and dyes.[15]

The efficiency of a photocatalytic process depends on the nature of the photocatalyst as well as the source of light. When irradiated, the catalyst is photo-activated by photons with the same or higher energy than its band gap energy. Typically, higher irradiation intensity leads to higher photocatalytic efficiency.[16] Knowing that sunlight is a safe and renewable energy, its use in photodegradation studies offers many advantages, such as cleanness and abundance. However, it requires the development of catalysts that can be activated by sunlight.[17]

Titanium dioxide has become the most widely used photocatalyst in the past few years due to its high stability,

[a] LAQV–REQUIMTE, Department of Chemistry, University of Aveiro, 3810-193 Aveiro, Portugal. E-mail: actome@ua.pt, leandrolourenco@ua.pt
[b] Centro de Química Estrutural, Institute of Molecular Sciences & Departamento de Engenharia Química, Instituto Superior Técnico, Universidade de Lisboa, 1049-001 Lisboa, Portugal. E-mail: jtome@tecnico.ulisboa.pt

**2352** | *Catal. Sci. Technol.*, 2024, **14**, 2352–2389

This journal is © The Royal Society of Chemistry 2024

cheapness, non-toxicity, and high efficiency. Furthermore, $TiO_2$ can absorb near-UV light (315–400 nm) and form electron ($e^-$)–hole ($h^+$) pairs which can directly oxidize or reduce substrates. Nonetheless, there are several drawbacks in using bare $TiO_2$ in photocatalysis which include a relatively large band-gap and its wavelength light absorption being restricted to UV light.[18,19] Therefore, to improve the use of sunlight, it is necessary to modify $TiO_2$ to extend its wavelength absorption to white light. This modification includes non-/transition-metal ion doping[20–22] and dye sensitization.[23] Besides $TiO_2$, it is also common to find zinc oxide,[24] silicon dioxide,[23] polymers[25] and g-$C_3N_4$ (ref. 26) that can also be modified to increase their absorption spectra to white light.[27,28] Among many dye sensitizers, porphyrins (Pors)[29,30] have received particular attention due to their valuable features in water treatment. In fact, due to their strong absorption in the visible region and photoelectrical properties, Pors have been extensively used as catalysts for the photooxidation of organic pollutants.[23]

Pors are aromatic tetrapyrrolic macrocycles with interesting absorption spectra,[31] typically displaying a strong absorption band around 400 nm (the Soret band) and other bands with lower intensity in the 500–650 nm region (the Q bands).[32,33] Por derivatives can undergo several reaction types, including inner core complexation with metal ions such as Zn(II), Cu(II), Co(II), Sn(III), and Fe(II), among others.[34–36] The presence or absence of a metal ion in the macrocycle core can significantly modify its reactivity and photocatalytic performance.[37,38] Due to their biological, photophysical, and photochemical properties, tetrapyrrolic macrocycles have also been applied in areas such as sensors,[39–41] artificial oxygen transporters,[42] biomimetic models,[43] semiconductors[44] and medicine.[45–48] However, considering the water pollution problems, (photo)catalysis is one of the most relevant areas where these dyes can be used.[49,50] Moreover, Pors combined with (or supported on) inorganic materials, such as $TiO_2$, ZnO, $SiO_2$, mixtures of two inorganic supports (e.g., $TiO_2$–$SiO_2$, etc.) or nanoparticles, among others, act as photocatalytic materials for wastewater treatment that give rise to higher degradation rates, allow their facile recovery and their reusability without significant loss of activity.[51]

This review presents several successful examples regarding the photocatalytic degradation of water pollutants using non-immobilized and immobilized porphyrins.

## 2. Mechanism of the photocatalytic degradation of organic pollutants

The degradation of pollutants may occur by indirect photolysis in the presence of immobilized or non-immobilized porphyrins that can absorb irradiation and subsequently generate ROS such as singlet oxygen ($^1O_2$), hydroxyl (HO·), peroxyl (ROO·), and superoxide anion ($O_2^{·-}$) radicals.[23,52] This methodology requires light, a photosensitizer (PS), and molecular oxygen ($^3O_2$). As depicted in Fig. 1, a PS is excited from the ground state ($S_0$) to
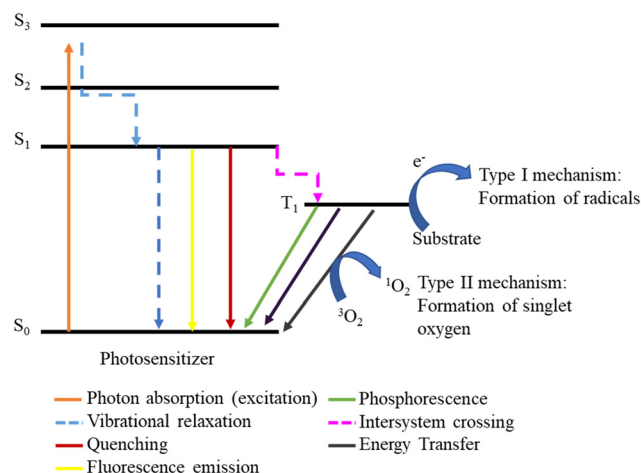


**Fig. 1** Modified Jablonski's diagram to elucidate the formation of ROS.

an excited singlet state ($S_1$ or $S_3$) after irradiation. From this point, the excited molecule can return to the ground state by different processes, including emission (fluorescence) and vibration (heat) or by reacting with substrates. However, an excited triplet state ($T_1$) with a much longer lifetime can be formed if the decay can go through an intersystem crossing. From this point, the PS can perform photoreactions by two competitive mechanisms: type I mechanism, an electron transfer from the PS to the substrate occurs, leading to the formation of reactive radicals, while in the type II mechanism there is an energy transfer from the PS's triplet state to molecular oxygen, generating $^1O_2$.[53]

Some Pors have high quantum yields for triplet state formation, determining their increased ability to generate ROS.[54] This quantum yield can be increased by the insertion of some metal ions in their inner core.[55]

## 3. Photocatalytic degradation of organic pollutants in water with non-immobilized porphyrins

Non-immobilized porphyrins are frequently evaluated as photocatalysts, namely in preliminary assays aiming to study the adequate experimental conditions for the photodegradation of pollutants before their immobilization in organic or inorganic matrixes. In cases where the applied porphyrins are water-insoluble, their recovery and reuse do not necessarily require immobilization in any support. A brief discussion concerning the photodegradation of common organic water pollutants (e.g., dyes, nitroaromatics, phenols, medicines) by non-immobilized porphyrins is presented in this section.

Natural nitroaromatic compounds are rare, but they are frequently used as dyes, pesticides, or explosives, for instance. Their use has become so intensive that it led to the contamination of soil and groundwater.[56] To find efficient ways to degrade 2,4,6-trinitrotoluene (2,4,6-TNT), Hikal and Harmon[57] developed a crystalline structure (Fig. 2) by self-

This journal is © The Royal Society of Chemistry 2024

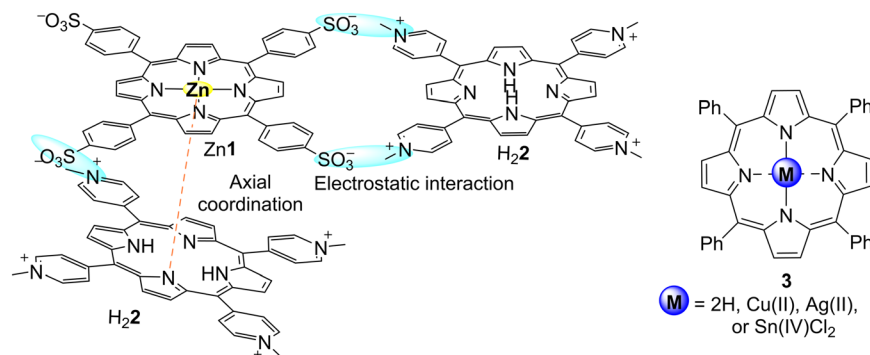*Catal. Sci. Technol.*, 2024, **14**, 2352–2389 | **2353**

**Fig. 2** Representation of the interactions between Zn1 and H$_2$2 in the solid-state; and structures free-base and metal M3.

assembly of porphyrins Zn1 and H$_2$2, which bear sulfonato and pyridinium groups, respectively. Crystals of Zn1–H$_2$2 were characterized by optical microscopy to determine that, depending on the molar ratio of the porphyrins in the starting solution, they may reach a length between 30–55 μm and width of 2–50 μm. Moreover, it was observed that the UV–vis spectrum of the crystalline structure and the spectra of the two monomers are quite different (broadened and blue and/or red-shifted Soret and Q bands). It is essential to highlight that the formation of the crystals led to a dramatic reduction of the intensity of the emission bands accompanied by a red-shift and split of the bands. These materials were able to reduce 80% of 2,4,6-TNT under a tungsten lamp for 3 h, with the photocatalyst being highly photostable under the experimental conditions (Table 1). The authors studied the degradation products and identified trinitrobenzene.

Methyl orange (MO) is a water-soluble dye used as a pH indicator in textiles, foodstuffs, farming chemical products, paper, leather industries, *etc.* However, its release into the environment, even in low quantities, causes serious pollution problems. In this sense, Salker and co-worker[58] used *meso*-tetraphenylporphyrin (H$_2$3) and the corresponding metalloporphyrins M3 (M = Cu(ɪɪ), Ag(ɪɪ), or Sn(ɪv)Cl$_2$, Fig. 2 and Table 1) for the photocatalytic degradation of MO. The fluorescent H$_2$3 and Sn3Cl$_2$ were revealed to be more efficient for MO photodegradation than the non-fluorescent Cu3 and

Ag3.[58] Although only small amounts of porphyrin are needed for these photocatalytic studies, the porphyrins used in this work could be recovered, which is a very relevant point for this type of application.

# 4. Wastewater treatment using polymeric porphyrins or porphyrins immobilized on polymers

In the past few years, due to their low-cost and facile synthesis along with appropriate mechanical properties and excellent electrical and electrochemical activities, organic polymers have attracted increased attention as materials for solar cells, fuel cells, catalysts, adsorption, light emitting diodes, separation processes, magnetism, and rechargeable lithium batteries.[25]

Both polymeric porphyrins and porphyrins immobilized on polymers have been used as photocatalysts to degrade organic pollutants in water. A few examples are discussed in the following sections.

### 4.1. Polymeric porphyrins

Rahman and co-workers[59] described that Congo red (CR), a stable water-soluble anionic azo dye with a benzidine core (a cancer-causing substance), is hard to degrade. This dye is dangerous for human health and has a high ecotoxicity in the

**Table 1** Non-immobilized porphyrins used to degrade TNT and MO pollutants

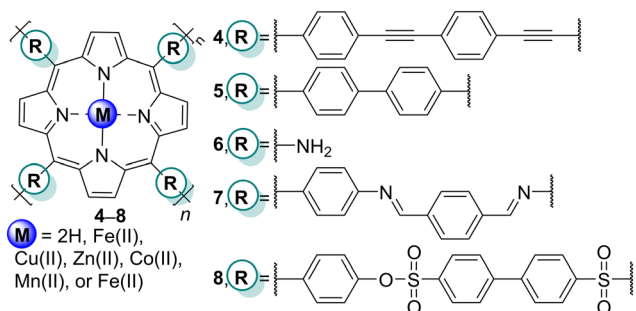| Por | Pollutant | Irradiation time (min) | Light intensity (mW.Cm$^{-2}$) | Irradiation source | Degradation rate (%) | Ref. |
|---|---|---|---|---|---|---|
| Zn1–H$_2$2 | TNT | 180 | 5.1 | UV–vis | 80 | 57 |
| H$_2$3 | MO | 240 | — | Sunlight | 70[a] | 58 |
| | | | | | 16[b] | |
| | | | | | 10[c] | |
| Cu3 | | | | | 28[a] | |
| | | | | | 10[c] | |
| Ag3 | | | | | 25[a] | |
| | | | | | 10[c] | |
| Sn3Cl$_2$ | | | | | 100[a] | |
| | | | | | 60[b] | |
| | | | | | 90[c] | |

[a] pH = 6. [b] pH = 7. [c] pH = 10.

**Fig. 3** Structure of H$_2$6 and polymers Fe4, H$_2$5, H$_2$7, and M8 (M = Cu, Zn, Co, Mn, or Fe).

environment. There are several methods for removing this dye from water, however adsorbents seem to be the best due to their high efficiency, simplicity, and cheapness.[59,60] Thus, the combination of the adsorption of this pollutant from wastewaters with its photodegradation is a trustworthy way to eliminate it. For that reason, Sun and co-workers[61] prepared the polymeric dendrite-like nanostructure Fe4 (Fig. 3) and used it as a photocatalyst to degrade Congo red. According to scanning electron microscopy (SEM), each branch of the dendrite-like nanostructure possesses a diameter size of about 30–80 nm. The chiasma and tangle of the nanostructure formed the final microstructure with a size of about 30 μm. This microporous material showed high selectivity (when compared with MO, methyl violet (MV), methyl red (MR) and rhodamine B (RhB)) and efficiency: 88.3% of the CR dye was decomposed in just 120 s under white light irradiation (Table 2). Despite using *N,N*-dimethylformamide (DMF) in the photocatalytic studies, this material proved to be a good candidate for azo dye photodegradation.

RhB has been used for dyeing cotton, silk, paper, bamboo, and other products and consequently has been found in wastewaters produced by these industries. Cationic RhB dyes are water-soluble and can interact with the negatively charged surface of cell membranes and penetrate cells. For that reason, they are considered more toxic than the anionic ones.

There are several methods to eliminate this pollutant,[62,63] but Zhao and co-workers[64] reported a new one where the porphyrin-based porous organic polymer H$_2$5 (Fig. 3) is used as a photocatalyst for the degradation of RhB and also methylene blue (MB). After verifying that MB was unstable under white light irradiation, the authors proceeded with the photocatalytic studies only for RhB. The commercially available photocatalyst TiO$_2$ (PC-500), *meso*-tetrakis(*p*-aminophenyl)porphyrin (H$_2$6), and polymeric porphyrin H$_2$7 (prepared from the reaction of H$_2$6 and terephthalaldehyde) were used as controls. The experimental results showed that polymer H$_2$5 possesses high photocatalytic activity for RhB: 100% photodegradation after white light irradiation for 80 min (Table 2). The authors proposed that linking porphyrin building blocks in an amorphous way contributes positively to a higher degradation effect, prevents aggregation of the porphyrin molecules (π–π stacking), and ensures the porosity and accessibility of the active sites of the porphyrin molecule. One interesting conclusion of this work was the selectivity of H$_2$5 for MB degradation in the presence of a mixture of both dyes (MB/RhB 1:1).

The presence of dyes like acridine orange (AO) in watercourses negatively affects the quality of aquatic and human lives. In this context, Chen and co-workers[65] reported the photodegradation of AO in an aqueous solution using polymeric metalloporphyrins M8 (M = Cu, Zn, Co, Mn, or Fe) (Fig. 3 and Table 2). It was observed that Co8 was the best photocatalyst under a high-pressure mercury lamp, and the authors assessed its photocatalytic behaviour under an iodine tungsten lamp, or natural sunlight. Polymer Co8 (Fig. 3) revealed a complete photodegradation of AO under natural sunlight irradiation after 3 h. (Table 2). This work showed that polymeric metalloporphyrins could be successfully employed in wastewater treatment using solar light irradiation.

### 4.2. Porphyrins immobilized on polymers

Linking porphyrins to organic polymers can increase their photocatalytic activity and reusability.[66–68] Indeed, several organic

**Table 2** Polymeric porphyrins used for the degradation of several pollutants

| Por | Pollutant | Irradiation time (min) | Irradiation source | Degradation rate (%) | Ref. |
|---|---|---|---|---|---|
| Fe4 | CR | 2 | Visible | 88 | 61 |
| | MO | 4 | | 30 | |
| | MV | | | 10 | |
| | MR | | | 10 | |
| | RhB | | | 0 | |
| H$_2$5 | RhB | 80 | Visible (λ > 420 nm) | 100 | 64 |
| H$_2$6 | | 120 | | 42 | |
| H$_2$7 | | | | 53 | |
| Co8 | AO | 240 | Visible (λ > 420 nm) | 100 | 65 |
| | | 180 | Sunlight | | |
| Fe8 | | 480 | Visible (λ > 420 nm) | | |
| Cu8 | | | | | |
| Mn8 | | | | | |
| Zn8 | | | | | |

This journal is © The Royal Society of Chemistry 2024

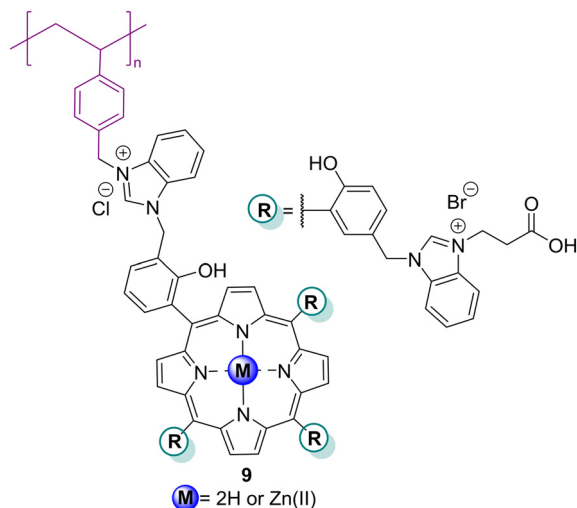*Catal. Sci. Technol.*, 2024, **14**, 2352–2389 | **2355**

**Fig. 4** Structure of polymeric porphyrin derivatives **9** (M = 2H or Zn).

polymers (*e.g.*, poly(*N*-isopropylacrylamide), polyacrylonitrile, polystyrene, *etc.*) incorporating porphyrins, and even self-assembled porphyrin polymers, have been developed for wastewater treatment, namely for the photodegradation of dyes.

Bhagat and co-worker[69] prepared a polymer-supported Brønsted acid-functionalized Zn9 complex tangled with a benzimidazolium moiety (Fig. 4) and assessed its ability as a photocatalyst for the degradation of MO and CR (Table 3) using atmospheric air or $H_2O_2$. After irradiation for 30 min under atmospheric air, a complete degradation of the two dyes was achieved. The catalyst could be reused up to five times without loss of activity.

**4.2.1. Porphyrins supported in polyacrylonitrile fibres.** Qi and co-workers[70] reported the construction of uniform polyacrylonitrile polymer and polyacrylonitrile copolymer nanofibre mat supported metalloporphyrins M10 (M = Zn(II), Cu(II), Ni(II), Co(II), Fe(III), and Pd(II)) and Fe11, respectively by

**Table 3** Porphyrins immobilized on polymers used for the degradation of several pollutants

| Por | Pollutant | Irradiation time (min) | Light source | Light source | Recycle | Ref. |
|---|---|---|---|---|---|---|
| Zn9 | MO | 30 | Visible ($\lambda$ > 400 nm) | 100 | 5 cycles (5% loss) | 69 |
| | | $25^a$ | | | | |
| | CR | 20 | | 85 | | |
| | | $20^a$ | | | | |
| | MR | 30 | | 95 | | |
| | | $30^a$ | | 90 | | |
| Zn10 | Reactive orange | 250 | | 10 | — | 70 |
| Cu10 | | | | 20 | | |
| Ni10 | | | | 20 | | |
| Co10 | | | | 25 | | |
| Pd10 | | | | 15 | | |
| Fe10 | | | | 40 | | |
| Fe11 | | | | 40 | 4 cycles (36% loss) | |
| | Reactive blue | 180 | UV | 100 | — | |
| | Reactive black | | | | | |
| | Reactive red | | | | | |
| | Reactive light yellow | | | 90 | | |
| $H_2$12 | PCP | 360 | Visible ($\lambda$ > 400 nm) | $150.31^b$ | | 71 |
| | TCP | | | $30.51^b$ | | |
| | DCP | | | $46.55^b$ | | |
| $H_2$12 | PCP | | | 35 | | 72 |
| | TCP | | | 15 | | |
| | DCP | | | 0 | | |
| $H_2$13 | PCP | 120 | | 100 | | |
| | TCP | 360 | | | | |
| | DCP | | | 35 | | |
| $H_2$14 | Benzene | — | UV | 95 | | 73 |
| | | | Visible ($\lambda$ > 400 nm) | | | |
| | Toluene | | UV | 90 | | |
| | | | Visible ($\lambda$ > 400 nm) | 80 | | |
| | Ethyl benzene | | UV | 95 | | |
| | | | Visible ($\lambda$ > 400 nm) | 50 | | |
| | Xylene | | UV | 95 | | |
| $H_2$15 | TCP | 360 | Visible ($\lambda$ > 400 nm) | 100 | | 74 |
| $H_2$16 | | | | | | |
| Zn17 | MB | 180 | | 72 | 7 cycles (0% loss) | 75 |
| Zn18 | | 150 | | 75 | 7 cycles (30% loss) | 76 |
| Zn18 | RhB | 240 | | 86 | 5 cycles (5% loss) | 77 |
| Zn19 | | | | 82 | | |
| Zn20 | | | | 73 | | |
| Zn21 | | | | 69 | | |

$^a$ $H_2O_2$. $^b$ mg g$^{-1}$ of Por/material.

**2356** | *Catal. Sci. Technol.*, 2024, **14**, 2352–2389

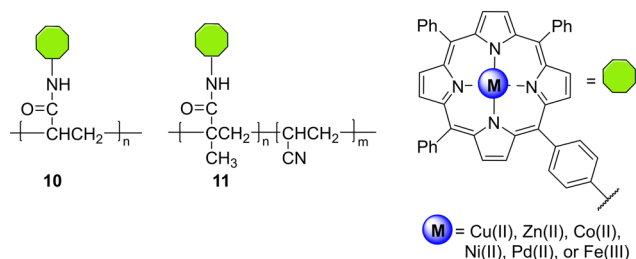This journal is © The Royal Society of Chemistry 2024

**Fig. 5** M10 (M = Zn(II), Cu(II), Ni(II), Co(II), Fe(III), and Pd(II)) and Fe11 supported in a polyacrylonitrile or polyacrylonitrile copolymer nanofibre mat.

electrospinning (Fig. 5 and Table 3). These polymers showed high photocatalytic activity to degrade several azo dyes in an aqueous solution under white light irradiation. The polymer nanofibre mat supported Cu10 and Fe10 were the most effective ones. Using the polymer Fe10 and the copolymer Fe10/nanofibre mat, over 60–80% of the azo dyes were degraded in less than 2 h of irradiation. It is important to mention that the copolymer immobilized Fe11 shows a higher photocatalytic activity. The immobilization of the metalloporphyrins into the nanofibre mats allowed the recovery of the photocatalysts without significant reduction of their photocatalytic activities (e.g., Fe11/nanofibre mat was reused up to four cycles, and photodegradation of 64.5% was still observed in the last cycle).

Lee, Baek, and co-workers[71,72] reported the porphyrin star copolymer H$_2$12 (Fig. 6) that was able to degrade a series of chlorophenols: 2,4-dichlorophenol (2,4-DCP), 2,4,6-trichlorophenol (2,4,6-TCP), and pentachlorophenol (PCP). In 2013, Lee, Baek, and co-workers[73] synthesized the free-base porphyrin star copolymer H$_2$14, and in 2018 the same authors[74] developed two palladium(II) porphyrins coupled to

two different copolymers, H$_2$15 and H$_2$16, in order to evaluate their photocatalytic activity in the degradation of 2,4,6-TCP in water under white light irradiation. Using low energy and extending the absorption wavelength, H$_2$12 could efficiently degrade the chlorophenols in an aqueous solution under white light, reaching removal efficiencies ranging from 30.51 to 150.31 mg g$^{-1}$ of Por/material (Table 3).[71] The same authors[72] compared two different types of porphyrin core star copolymers: the same poly(dimethylaminoethyl acrylate) porphyrin H$_2$12 and H$_2$13, respectively, to efficiently degenerate chlorophenols. Even though they used another block copolymer H$_2$13, the degradation was still more efficient when using H$_2$12, accomplishing a photodegradation rate of 35% and 100% (Table 3), respectively. This difference can be associated with the higher hydrophobicity of H$_2$12 due to the presence of polystyrene polymer in its structure. In this case, the interaction of the hydrophobic contaminants (chlorophenols) with the hydrophobic block (polystyrene) of the material induced a hydrophobic–hydrophobic interaction which could enhance the access to the porphyrin core (photocatalyst), increasing the removal efficiency. The degradation products were identified as hydroquinone and posterior CO$_2$ and H$_2$O.

Baek and co-workers[73] firstly reported that the water-soluble amphiphilic star block copolymers H$_2$14 could efficiently capture toxic organic compounds such as benzene, toluene, ethylbenzene, and xylene (Table 3) from water due to the hydrophobic–hydrophobic interaction with the inner polystyrene block segments and degrade them by the UV-induced photo-oxidation reaction. They also reported the recovery of the star block copolymers by increasing the temperature above their lower critical solution temperature (LCST) where the thermosensitive H$_2$14 forms water insoluble agglomerates.
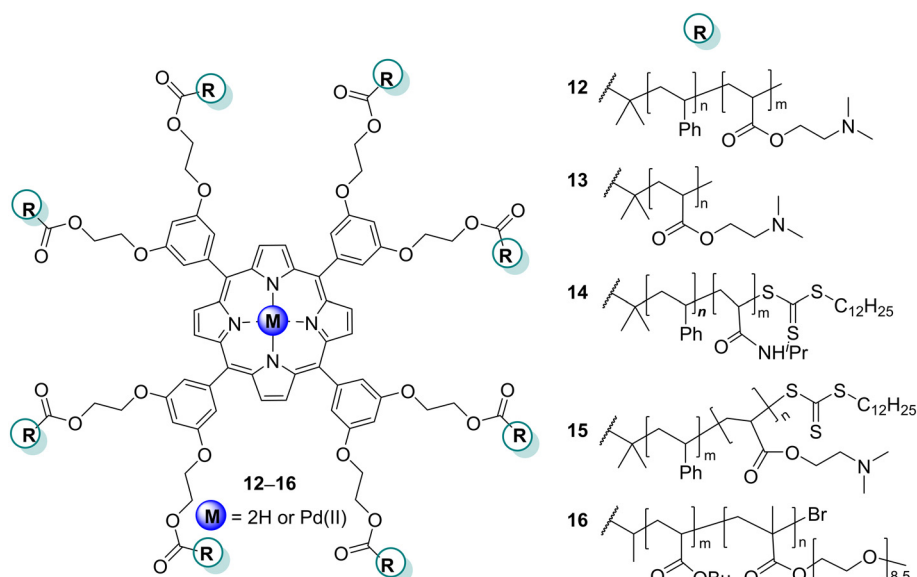


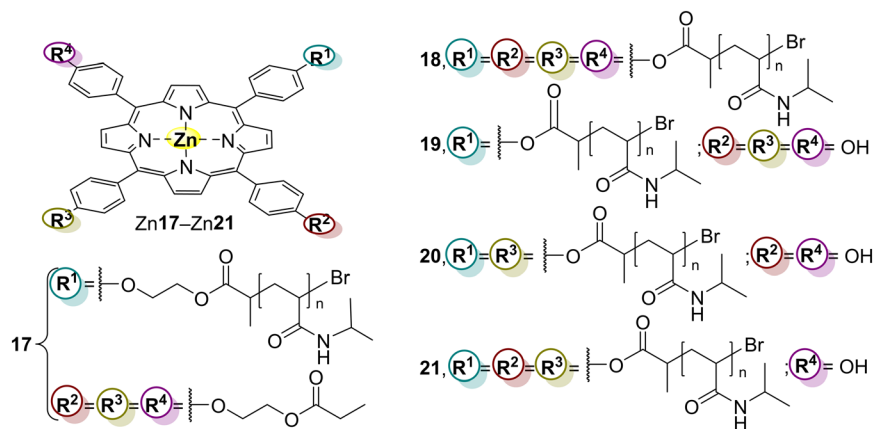**Fig. 6** Free-base and palladium porphyrin star copolymers.

This journal is © The Royal Society of Chemistry 2024

Catal. Sci. Technol., 2024, 14, 2352–2389 | 2357

**Fig. 7** Structures of polymers Zn**17**–Zn**21**.

According to the second study,[74] the amphiphilic porphyrin star block copolymers were also homogenously soluble in water. It was also concluded that the water-soluble star block copolymers with hydrophobic core–shell structures, such as H₂**15** and Pd**16**, were the most effective for the degradation of 2,4,6-TCP in water under white light irradiation when compared with the corresponding homopolymer. The explanation for those results was the effectiveness of the hydrophobic core near the metalloporphyrin in capturing and binding the hydrophobic chlorophenols, contributing to their easier degradation. The authors considered that selecting an inner hydrophobic block to design amphiphilic star block copolymers is vital for the degradation of 2,4,6-TCP in water.

**4.2.2. Porphyrins supported on poly(N-isopropylacrylamide).** Duan and co-workers[75,76] developed polymers **17** and **18** (Fig. 7 and Table 3) containing a Zn(II) porphyrin and evaluated their ability as photocatalysts for the oxidative degradation of MB under white light irradiation. One polymer has a well-defined linear poly(N-isopropylacrylamide) (PAM) (Zn**17**–PAM), and the other is a well-defined star-shaped PAM (Zn**18**–PAM). Both polymers were synthesized *via* atom transfer radical polymerization (ATRP). Polymer Zn**17**–PAM, in the presence of H₂O₂, could degrade 72% of MB when irradiated with white light for 180 min at its lower critical solution temperature (LCST). This photocatalyst could be reused up to 7 times without losing its catalytic activity. The photocatalytic studies using Zn**18**–PAM were made at pH 2 and at the LCST (29 °C) and in the presence of H₂O₂ for 150 min under white light irradiation, where 75% of MB was degraded. This photocatalyst was reusable for up to 7 cycles keeping the photodegradation rate at 70% under the same conditions.

Gao and co-workers[77] reported the synthesis of the Zn(II) porphyrin-based multi-arm star polymers Zn**18**, Zn**19**, Zn**20**, and Zn**21** (Fig. 7 and Table 3), where *n* = 1–4. The polymer used was the same as that reported by Duan and co-workers.[75,76] All porphyrins were prepared *via* ATRP and their ability as photocatalysts to degrade RhB under white light irradiation was assessed. The authors were interested in establishing a relationship between the number of arms at the porphyrin and the respective photocatalytic activity and

stability. Interestingly, as the number of arms increased, the stability and photocatalytic activity also increased. Thus, the best photocatalyst was Zn**18**, which can be recycled up to 5 times without activity loss.

### 4.3. Porphyrins in metal–organic frameworks

Metal–organic frameworks (MOFs) are emerging classes of materials used in photocatalysis, especially those based on metalloporphyrins.[78] Nagaraja and co-workers[79] used the Ni**22** nickel MOF (Fig. 8 and Table 4) in the photodegradation of nitroaromatic compounds under white light for 90 min. When compared with Ni**22** alone, the Ni**22** MOF revealed an enhanced photocatalytic activity (>90% degradation) which may be attributed to a combined catalytic effect. Also, this MOF was recycled and reused for 3 cycles without loss of catalytic activity and structural rigidity.[79] The reusability of the catalysts without loss of stability indicates that they can be applied to treat dye-polluted waters. The degradation products were identified as the respective amino derivatives.

Wang and co-workers[80] synthesized zirconium ultrathin 2D zirconium MOF nanosheets using Ni**22** (Fig. 9 and Table 4) and evaluated their photocatalytic activity against naphthalene-1,5-diol. The authors reported good photocatalytic activity and high photostability of these nanosheets when compared with PCN-222, a well-known zirconium metalloporphyrin MOF. These nanosheets' most increased photocatalytic activity might be due
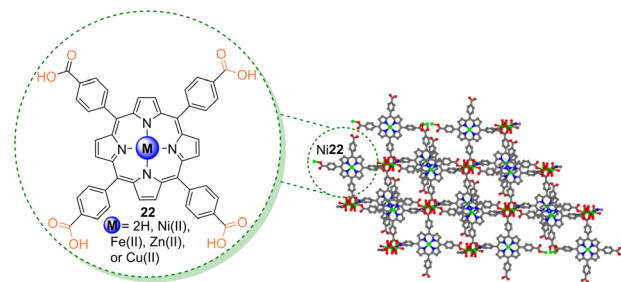


**Fig. 8** Representation of the Ni**22** porphyrin and the Ni**22** nickel MOF structure.[79]

**2358** | *Catal. Sci. Technol.*, 2024, **14**, 2352–2389

This journal is © The Royal Society of Chemistry 2024

**Table 4** Porphyrins in MOFs used for the degradation of several pollutants

| MOF | Por | Pollutant | Irradiation time (min) | Light source | Degradation rate (%) | Recycle | Ref. |
|---|---|---|---|---|---|---|---|
| NiMOF | Ni22 | Nitrobenzene | 90 | Visible ($\lambda$ = 420 nm) | 100 | 3 cycles (5% loss) | 79 |
| | | Nitrotoluene | 60 | | | — | |
| | | Chloronitrobenzene | 105 | | | | |
| | | Bromonitrobenzene | 210 | | | | |
| | | Di-nitrobenzene | 300 | | | | |
| | | Nitronapthalene | 1440 | | 34 | | |
| ZrMOF | | Naphthalene-1,5-diol | 0 | Visible ($\lambda$ > 420 nm) | 100 | | 80 |
| PCN-224 | H$_2$22 | Tetracycline | 90 | | 10[a] | — | 81 |
| | | | | | 50[b] | | |
| | | | | | 98[c] | | |
| | | | 2 | | 100[d] | 5 cycles (5% loss) | |
| | | Ciprofloxacin | 10 | | 90[d] | | |
| | | | 90 | | 90[c] | — | |
| | | | | | 25[b] | | |
| | | | | | 5[a] | | |
| PCN-222 | H$_2$22 | RhB | 120 in the dark + | UV | 100 | 3 cycles (30% loss) | 83 |
| | Ni22 | | 120 min irradiation | | | 3 cycles (10% loss) | |
| | H$_2$22 | Basic violet 14 | | | 99 | — | |
| | Ni22 | | | | 100 | | |
| | H$_2$22 | Crystal violet | | | 56 | | |
| | Ni22 | | | | 70 | | |
| | H$_2$22 | AB | | | 47 | | |
| | Ni22 | | | | 83 | | |
| Ln-MOF | H$_2$22 | Naphthalene-1,5-diol | 20 | Visible $\lambda$ > 420 nm | 60 | — | 84 |
| Cu-MOF | Cu22 | RhB | 360 | | 82[e] | | 85 |
| | | MB | | | 40[f] | | |
| | | CR | | | 89[g] | | |
| | | Tetracycline | | | 71[h] | | |
| | | Norfloxacin | | | 44[f] | | |
| | | Oxytocin | | | 46[f] | | |
| La-MOF | H$_2$22 | MO | 125 | | 16 | | 82 |
| | | | | | 26[i] | | |
| | | MB | | | 24 | | |
| | | | | | 61[i] | | |
| | Fe22 | MO | | | 5 | | |
| | | | | | 55[i] | | |
| | | MB | | | 16 | | |
| | | | | | 93[i] | | |

[a] 6 μM. [b] 500 nm. [c] 150 nm. [d] 300 nm. [e] pH = 3. [f] pH = 9. [g] pH = 7. [h] pH = 5. [i] In the presence of H$_2$O$_2$.
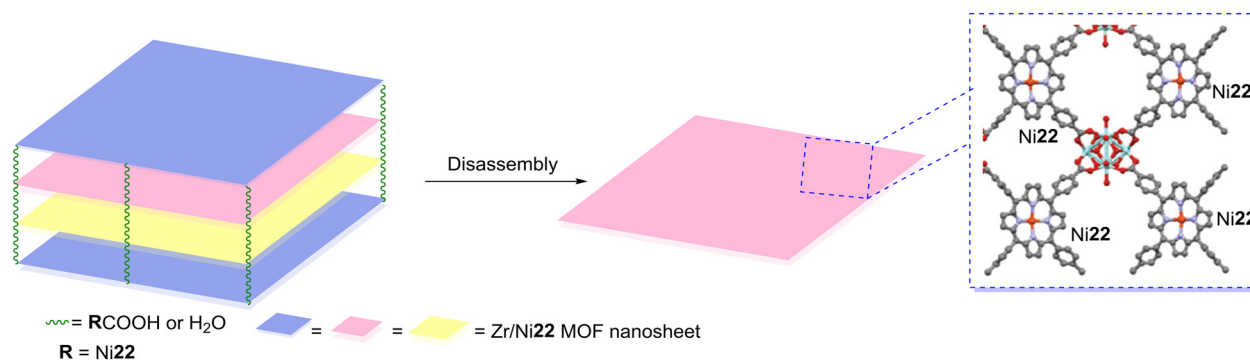


**Fig. 9** Zirconium ultrathin 2D metal–organic framework nanosheets using Ni22. Adapted from ref. 80.

to their nanometre thickness, allowing rapid mass transport and a high percentage of exposed catalytically active surfaces.

More recently, Xue, Wang and co-workers[81] developed a porphyrin MOF (PCN-224), composed of a Zr$_6$O$_4$(OH)$_4$ cluster and the porphyrin ligand H$_2$22 (Table 4), to be used in the photocatalytic degradation, under white light irradiation, of antibiotics such as tetracycline and ciprofloxacin. Three different particle sizes were prepared: 6 μM, 150 nm, 300 nm,

This journal is © The Royal Society of Chemistry 2024

Catal. Sci. Technol., 2024, 14, 2352–2389 | 2359

and 500 nm. The best photocatalyst was found to be 300 nm-PCN-224 followed by 150 nm-PCN-224, 500 nm-PCN-224 and 6 μM-PCN-224. The best photocatalyst could achieve total degradation of tetracycline after 2 min of irradiation and 90% of ciprofloxacin after 10 min of irradiation. No photocatalytic degradation was observed in the absence of light. Also, no significant changes were observed after 5 cycles of photocatalytic activity.

Kumar and co-workers[82] developed a porphyrin $H_2$**22** and Fe**22** La-MOF to be used in the photocatalytic degradation of MO and MB under visible light irradiation. After 125 min of irradiation the $H_2$**22**–La-MOF could degrade 16% of MO and 24% of MB. On the other hand, the Fe**22**–MOF could achieve a photocatalytic rate of 5 and 16% for MO and MB, respectively. These photocatalytic rates could be enhanced after the addition of $H_2O_2$ (Table 4).

B. Zhang, X. Zhang and co-workers[83] prepared a bimetallic porphyrin MOF of PCN-222(Ni/Hf) by inserting Ni(II) in the inner core of $H_2$**22** and coordinating Hf(IV) with the carboxyl groups of the porphyrin. The authors assessed the photocatalytic activity of the MOF for the degradation of four pollutants: RhB, basic violet 14, crystal violet and acid black 210 (AB) – Table 4. The degradation process was not strictly dependent on light since it could reach total degradation of basic violet 14 and RhB after 120 min in the dark. Regarding the degradation of crystal violet and acid black, even under irradiation, it could only reach ~47% and 60% degradation, respectively. These results were much better than those obtained using PCN-222(Hf) (without Ni(II)). The stability of PCN-222(Ni/Hf) is also enhanced when compared with PCN-222(Hf): after three cycles, the photocatalytic activity decreased by only 10% while a reduction of 30% was observed for PCN-222(Hf).

Regarding lanthanides, Huang and co-workers,[84] using the same porphyrin, prepared a series of porphyrin-based 2D MOFs (Ln–$H_2$**22**, Ln = Ce, Sm, Eu, Tb, and Yb) (Fig. 10 and Table 4) with different thicknesses and assessed their ability as photocatalysts for the degradation of naphthalene-1,5-diol in order to establish a metal/thickness–activity relationship. The results showed that the thinner the thickness of the nanosheets, the higher the light harvesting ability and the better the photocatalytic activity. Interestingly, the most effective MOF incorporated Yb, which showed outstanding performance due to the effective energy and electron transfer between $H_2$**22** and $Yb^{3+}$.
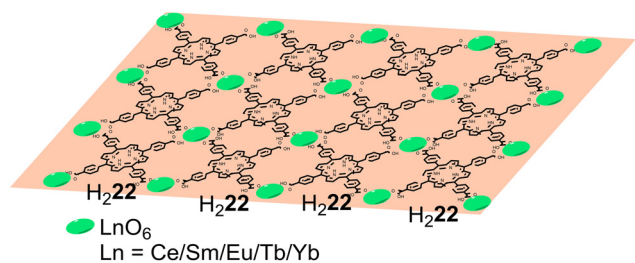


**Fig. 10** Representation of Ln–$H_2$**22** MOF nanosheets.

Zhang and co-workers[85] prepared a Cu**22**-based MOF through a rapid microwave hydrothermal route. The resulting nanosheets displayed excellent crystallinity and were used as photocatalysts for the degradation of Congo red, MB and RhB as well as some antibiotics like tetracycline, norfloxacin, and the hormone oxytocin (Table 4). After adsorption of the pollutants and irradiation with white light ($\lambda > 420$ nm), the Cu**22**-MOF showed good photocatalytic activity reaching the highest photodegradation rates for Congo red (89%) and RhB (81.2%) after 6 h.

# 5. Titanium oxide-supported porphyrins

$TiO_2$-based materials are excellent photocatalysts for the oxidation of pollutants in water. They present several advantages: high photocatalytic efficiency, physical and chemical stability, low cost, and low toxicity. However, bare $TiO_2$ can only be excited by UV light and for that reason, it shows no response to white light.[86] Considering that UV radiation is less than 5% of natural sunlight and that 43% of the solar spectral energy is in the white light spectrum, it is highly desirable to develop $TiO_2$-based photocatalysts that can absorb visible light in order to improve the use of solar light.[86] There are several strategies to increase the light absorption in the visible region, such as doping with noble metals, dye sensitization and even combining $TiO_2$ with other semiconductors. Porphyrin's sensitization is a cheap and efficient method to extend the absorption into the visible region. Despite being a good photocatalyst by itself, the sensitization of $TiO_2$ with porphyrins significantly increases its photocatalytic activity under sunlight and achieves high degradation rates of organic pollutants.[18,87] A brief discussion about the photodegradation of organic contaminants by porphyrins immobilized on $TiO_2$ will be considered in the following examples.

Chang and co-workers[88] and Ji and co-workers[89] prepared several $TiO_2$ materials sensitized with M**3** (Fig. 2): Ni**3**–$TiO_2$, Fe**3**Cl–$TiO_2$, Co**3**–$TiO_2$, Mn**3**–$TiO_2$, and Cu**3**–$TiO_2$ and studied their photoactivity against 2,4-DCP and MO. Chang and co-workers[88] proved that under white light ($\lambda = 419$ nm) irradiation for 4 h, the Ni**3**–$TiO_2$ nanocomposite could degrade 81% of 10 ppm 2,4-DCP. The degradation was time and 2,4-DCP concentration-dependent. This study showed that the synthesized nanohybrid could efficiently eliminate pollutants present in wastewaters using sunlight. On the other hand, Ji and co-workers[89] found that bare $TiO_2$ could only degrade less than 10% of MO even after 180 min of light irradiation. However, the photocatalytic activity of Cu**3** and M**3** (M = Ni(II), Fe(III), Co(II), or Mn(II)) impregnated $TiO_2$ could efficiently be enhanced. Moreover, the Cu**3**–$TiO_2$ composite was the best to degrade MO followed by, in decreasing order, Ni**3**–$TiO_2$, Mn**3**–$TiO_2$, Fe**3**Cl–$TiO_2$, and Co**3**–$TiO_2$. UV light could increase the photocatalytic activity of all photocatalysts, with Cu**3**–$TiO_2$ reaching 98% degradation after 1.5 h.

**2360** | *Catal. Sci. Technol.*, 2024, **14**, 2352–2389

This journal is © The Royal Society of Chemistry 2024

**Table 5** Photodegradation of 4-chlorophenol[91,92]

| Type of microemulsion | Por | Metal complex | Support | Surfactant | Light source | Photodegradation (%) |
|---|---|---|---|---|---|---|
| W/O | — | — | $TiO_2$ | CTAB | UV | 34 |
| O/W | — | — | $TiO_2$ | CTAB | UV | 70 |
| W/O | — | — | $TiO_2$ | CTAB | Visible | 0 |
| O/W | — | — | $TiO_2$ | CTAB | Visible | 0 |
| W/O | Zn3 | — | — | CTAB | UV | 39 |
| O/W | Zn3 | — | — | CTAB | UV | 52 |
| W/O | Zn3 | — | — | CTAB | Visible | 62 |
| O/W | Zn3 | — | — | CTAB | Visible | 26 |
| W/O | — | Ti(IV)-Cit | — | CTAB | UV | 48 |
| O/W | — | Ti(IV)-Cit | — | CTAB | UV | 20 |
| W/O | — | Ti(IV)-Cit | — | CTAB | Visible | 20 |
| O/W | — | Ti(IV)-Cit | — | CTAB | Visible | 20 |
| W/O | Zn3 | — | $TiO_2$ | CTAB | UV | 29 |
| O/W | Zn3 | — | $TiO_2$ | CTAB | UV | 27 |
| W/O | Zn3 | — | $TiO_2$ | CTAB | Visible | 11 |
| O/W | Zn3 | — | $TiO_2$ | CTAB | Visible | 25 |
| O/W | Zn3 | Ti(IV) | — | CTAB | UV | 51 |
| W/O | Zn3 | Ti(IV) | — | — | UV | 75[a] |
| W/O | Zn3 | Ti(IV) | — | — | Visible | 86[a] |

[a] Best results obtained by Madriz and co-workers.[92]

Microemulsions can be used as "reactors" due to their unique properties like ultralow interfacial tension, sizeable interfacial area, thermodynamic stability, and, more importantly, their ability to solubilize otherwise immiscible liquids.[90] Having that in mind, Carrero, Madriz, and co-workers[91,92] reported the use of $TiO_2$, Ti(IV) citrate, and Zn3 (Fig. 2) as photocatalysts in oil-in-water (O/W) and water-in-oil (W/O) microemulsions to degrade 4-chlorophenol (4-CP). According to the authors, $TiO_2$ and titanium(IV) citrate were at the water phase, while Zn3 was in the oil phase due to its hydrophobic character. The surfactant cetyltrimethylammonium bromide (CTAB) has a positively charged head positioned at the water interface, forming an interphase or pseudophase, attracting the negatively charged Ti(IV) citrate complex when present. The photodegradation results are presented in Table 5.

In the experiments, after irradiation of the microemulsions with UV light, it was possible to observe that the 4-CP degradation in O/W (Table 5) was much more effective (70%) than in W/O microemulsions (34%). However, there was no 4-CP degradation in the experiments with the $TiO_2$ suspension under white light irradiation. The higher photodegradation rates in O/W can be explained by the fact that the $TiO_2$ particles act individually and do not form aggregates that can decrease the exposed surface and the photoactivation of the particles. As expected, adding Zn3 did not affect the photodegradation rate given the lack of interaction between $TiO_2$ and Zn3 from their different solubilities. Moreover, the Zn3 microemulsion without $TiO_2$ was irradiated with visible light, showing a higher degradation rate in W/O (62%) than in O/W (26%).[91] On the other hand, when irradiated with UV light, the O/W showed a higher degradation rate (52%) than W/O (39%). The addition of Ti(IV) to Zn3 microemulsion increased the photodegradation rate of 4-CP. A few years later, the same authors[92] used the same porphyrin Zn3, without CTAB, and found that the best

conversion percentage of 4-CP (86%) was obtained using W/O microemulsions of titanium citrate mixed with Zn3 and irradiation with white light for 30 min.

Palmisano and co-workers, Słota and co-workers and Mele and co-workers[93,94] reported the synthesis of a polycrystalline $TiO_2$ impregnated with the free-base porphyrin $H_2$23 or selected metalloporphyrins M23 (M = Cu(II), Fe(III)Cl, or Mn(III)OAc) (Fig. 11), which were used as catalysts for the photodegradation of 4-nitrophenol (4-NP).

According to the first study, the prepared materials $H_2$23 and Cu23 were found to be photostable even after 5 h of light irradiation. Regarding the photocatalytic activity, it is possible to affirm that the $TiO_2$ samples that contain Cu23 are better photocatalysts than the corresponding free-base $H_2$23. The photocatalytic activity under UV light for 2 h of bare $TiO_2$ was compared with that of the synthesized hybrids to establish the role of the central metal in M23 (M = 2H, Cu(II), Fe(III), or Mn(III)).[94] The obtained results showed that different metals can modulate photocatalyst efficiency. The authors also accessed the stability of the prepared materials where it was possible to observe that all the materials were
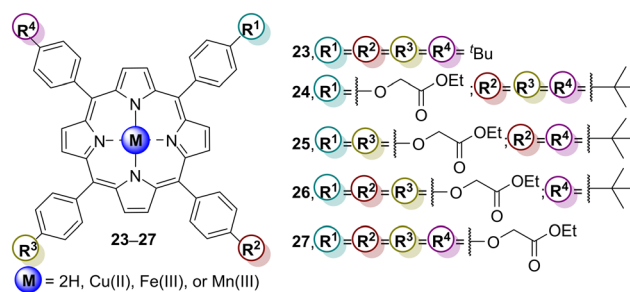


**Fig. 11** Free-base porphyrin $H_2$23, Cu23, Fe23Cl, Mn23OAc and Cu24–Cu27 used to sensitize $TiO_2$.

This journal is © The Royal Society of Chemistry 2024

*Catal. Sci. Technol.*, 2024, **14**, 2352–2389 | **2361**

**Table 6** Porphyrins–TiO$_2$ used for the photodegradation of 4-NP developed by several authors[93–99]

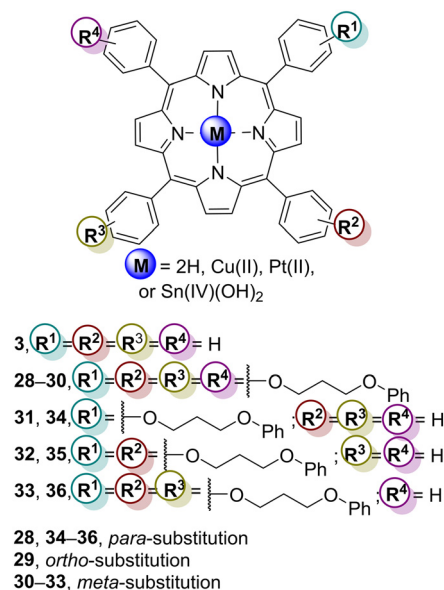| Por | Irradiation time (min) | Light source | Degradation rate (%) | Recycle | Ref. |
|---|---|---|---|---|---|
| H$_2$23 | 300 | Visible ($\lambda$ = 366 nm) | 100 | — | 93 |
| Cu23 | 240 | | | | |
| Cu23 | 120 | | | | 94 |
| Fe23 | 180 | | | | |
| Mn23 | | | | | |
| Cu24 | 60 | White light | | 6 cycles (50% loss) | 95 |
| Cu25 | 55 | | | 6 cycles (45% loss) | |
| Cu26 | 50 | | | 6 cycles (40% loss) | |
| Cu27 | 45 | | | 6 cycles (30% loss) | |
| Cu28 | 400 | Visible ($\lambda$ = 420 nm) | 98 | — | 96 |
| H$_2$28 | | | 90 | | |
| Cu29 | | | 99 | 6 cycles (15% loss) | |
| H$_2$29 | | | 98 | — | |
| Pt28 | 360 | UV–vis | 99 | 6 cycles (10% loss) | 97 |
| Pt29 | | | 97 | — | |
| Pt30 | | | 96 | | |
| Cu30 | 400 | | 90 | | 98 |
| Cu31 | | | 98 | | |
| Cu32 | | | 95 | | |
| Cu33 | | | 100 | | |
| Cu34 | | Visible ($\lambda$ > 420 nm) | 90 | 6 cycles (5% loss) | 99 |
| Cu35 | | | 89 | | |
| Cu36 | | | 87 | | |

stable. For example, Cu23–TiO$_2$ and Fe23Cl–TiO$_2$ were more photoactive than bare TiO$_2$ (anatase), whereas Mn23OAc–TiO$_2$ showed a lower photoreactivity. The metal-free porphyrin H$_2$23 also showed slightly higher photoactivity than the corresponding bare TiO$_2$, indicating that the porphyrin macrocycle is photoactive even in the absence of metal.[94]

Li and co-workers[95] developed four Cu(II) porphyrins (Cu24–Cu27) with one to four peripheral ester groups (Fig. 11) to be used to sensitize TiO$_2$ and to use the composites as photocatalysts for the degradation of 4-NP. The photocatalytic properties of mesoporous TiO$_2$ and Cu24– to Cu27–TiO$_2$ hybrids were evaluated to degrade 4-NP in aqueous media and under white light irradiation. The results showed that the photocatalytic activity order is: Cu27–TiO$_2$ > Cu26–TiO$_2$ > Cu25–TiO$_2$ > Cu24–TiO$_2$ (Table 6). The different number of peripheral groups directly modulates the photocatalytic activity, influencing the electron–hole separation process, and even after 6 cycles, the photocatalytic activity only decreased by 20% for the best photocatalyst. The loss of photodegradation efficiency could be assigned to the *in situ* generated hydroxyl radicals attacking the porphyrin molecules.

A series of studies using TiO$_2$ impregnated with *meso*-tetraphenylporphyrin (TPP–H$_2$3) derivatives bearing 3-phenoxypropyloxy groups at *ortho*-, *meta*- or *para*-positions (Fig. 12 and Table 6) were performed in order to evaluate the photocatalytic activity of the composites in 4-NP degradation.[96,97] The *ortho*, *meta* and *para* tetra-substituted free-base porphyrins H$_2$28–H$_2$30 (Fig. 12) and the corresponding complexes Cu28–Cu30 and Pt28–Pt30 were used in those studies. Later, Li and co-workers[98,99] intended

to assess the influence of the number of *meta*- and *para*-substituents by synthesizing the mono, di, tri, and tetrasubstituted free-base porphyrins H$_2$30–H$_2$33 as well as their Cu(II) derivatives Cu30–Cu33.

The first study[96] was carried out in aqueous media under visible light ($\lambda$ = 420 nm) irradiation. Among the synthesized photocatalysts, Cu29–TiO$_2$ was revealed to be the most efficient in 4-NP degradation, followed by Cu28–TiO$_2$, H$_2$29–TiO$_2$, and H$_2$28–TiO$_2$. TiO$_2$ impregnated with *ortho*-substituted porphyrins (H$_2$29–TiO$_2$ and Cu29–TiO$_2$) exhibited higher photoactivities



**Fig. 12** Free-base, Cu(II), Pt(II), and Sn(IV) porphyrins 28–36.

**2362** | *Catal. Sci. Technol.*, 2024, **14**, 2352–2389

This journal is © The Royal Society of Chemistry 2024

than TiO$_2$ synthesized with *para*-substituted porphyrins (Cu**28**–TiO$_2$ and Pt**28**–TiO$_2$). This can be due to the lower symmetry of the *ortho*-substituted structures, which can lead to a minor extent of aggregation and less important intermolecular π–π interactions. All photocatalysts were stable after irradiation for 5–7 h. In this study, TiO$_2$ impregnated with porphyrins could extend the light absorption efficiency and this depends on the amount of porphyrin loaded into the TiO$_2$ surface. When using the best photocatalyst, almost all 4-NP (99%) was degraded after 400 min of irradiation.

According to Li and co-workers,[97,98] all Pt(II) and Cu(II) porphyrins (Pt**28**–Pt**30** and Cu**30**–Cu**33**, Fig. 12 and Table 6) combined with TiO$_2$ enhanced the photocatalytic efficiency when compared with bare TiO$_2$. Overall, Pt(II) complexes/TiO$_2$ showed better photocatalytic activity in the degradation of 4-NP compared with the Cu(II) porphyrins/TiO$_2$ after 200 min of irradiation. However, when the irradiation time was extended to 300 min, all derivatives induced a complete degradation of the pollutant. Among the *ortho*-, *meta*- and *para*-substituted porphyrins, the *ortho* derivative Pt**29**–TiO$_2$ was the best photocatalyst. Regarding the effect of the number of peripheral *meta*-substitutions on the photocatalysts' efficiency, the best results were obtained with the tetrasubstituted Cu**30** followed by the trisubstituted Cu**33**, disubstituted Cu**32** and monosubstituted Cu**31**.[98] Similarly, Li and co-workers[99] reached the same results for

the *para*-substituted porphyrins, with the trisubstituted Cu**36**–TiO$_2$ being the best catalyst followed by disubstituted Cu**35**–TiO$_2$ and monosubstituted Cu**34**–TiO$_2$ (Fig. 12 and Table 6). To justify those results, the authors[98,99] assumed that the number of substituents does not influence the redox potential of the sensitizers but, instead, it influences the interaction between porphyrins and the porphyrin–TiO$_2$ surface as well as the electron transfer process from the sensitizer to TiO$_2$. Porphyrins with more substituents can adsorb more dissolved oxygen and, consequently, an increased photocatalytic activity is observed. Catalyst recycling studies showed that there is no significant loss of activity after six cycles.

Li and co-workers[100] and Mu and co-workers[101] used the three isomeric Sn(IV) porphyrin derivatives Sn**3**(OH)$_2$ (Fig. 2), Sn**28**(OH)$_2$–Sn**30**(OH)$_2$ (Fig. 12) to prepare the corresponding TiO$_2$–Sn(IV) porphyrin hybrids *via* axial functionalization. The ability of the resulting hybrids to photodegrade 4-NP and MO was then evaluated under visible and UV light. Under white light, the three composites showed higher photocatalytic activity than bare TiO$_2$, with the Sn**28**(OH)$_2$–TiO$_2$ hybrid being the best photocatalyst with a photocatalytic rate of 98.1% after 500 min of light irradiation (Table 7). However, under UV light irradiation, the photocatalytic efficiency of all hybrids was also enhanced when compared with bare TiO$_2$. Regarding the photodegradation efficiencies of 4-NP, an

**Table 7** Porphyrins–TiO$_2$ used for the photodegradation of 4-NP, MO and RhB developed by several authors

| Por | Pollutant | Irradiation time (min) | Light source | Degradation rate (%) | Recycle | Ref. |
|---|---|---|---|---|---|---|
| Sn**28** | 4-NP | 500 | Visible ($\lambda > 400$ nm) | 98.1 | — | 100 |
| | | 450 | UV–vis | 100 | | |
| Sn**29** | | 500 | Visible ($\lambda > 400$) | 90 | | |
| | | 450 | UV–vis | 100 | | |
| Sn**30** | | 500 | Visible ($\lambda > 400$) | | | |
| | | 450 | UV–vis | | | |
| Sn**3** | | 180 | | 90 | 7 cycles (5% loss) | 101 |
| | MO | | | 95 | | |
| Cu**37** | RhB | 30 | | 100 | — | 103 |
| | NP | 60 | | 90 | 6 cycles (5% loss) | |
| Cu**38** | RhB | 30 | | 98 | — | |
| | NP | 60 | | 90 | 6 cycles (40% loss) | |
| Cu**39** | RhB | 30 | | 100 | — | |
| | NP | 60 | | 98 | 6 cycles (5% loss) | |
| Cu**38** | | 160 | | 90 | — | 104 |
| Cu**39** | | 65 | Visible ($\lambda > 350$ nm) | 90 | | 106 |
| Zn**39** | | | | 85 | | |
| Ni**39** | | | | 80 | | |
| Zn**40** | | 180 | UV | 94 | | 107 |
| Cu**40** | | | | 98 | | |
| Co**40** | | | | 94 | | |
| Fe**40**Cl | | | | 93 | | |
| Zn**41** | | | | 95 | | |
| Cu**41** | | | | 98 | 6 cycles (10% loss) | |
| Co**41** | | | | 95 | — | |
| Cu**42** | | 160 | Visible ($\lambda > 350$ nm) | 100 | | 108 |
| | | 120 | UV ($\lambda = 100$–400) | | | |
| Zn**43** | MO | 150 | UV–vis ($\lambda > 100$) | 89 | 6 cycles (10% loss) | 109 |
| Zn**44** | | | | 91 | — | |
| Zn**45** | | | | 84 | | |
| Zn**46** | | | | 73 | | |

efficient degradation is obtained with the peripheral substituents at the *para*-positions as well as the presence of axial ligands, which can prevent π–π interactions and decrease the aggregation of the porphyrin molecules, especially for the most planar Sn28(OH)$_2$.

Moreover, it is important to say that the structure of Sn29(OH)$_2$ (Fig. 12) can have more stressed and stereochemically complicated conformations than others. On the other hand, the substituents of porphyrin Sn28(OH)$_2$ have just a small deviation from planarity, which causes a perfect parallel plane between the porphyrin and the TiO$_2$ surface. This means that Sn28(OH)$_2$ can easily approach the TiO$_2$ surface enabling the initial electron injection process from the porphyrin's excited state into the TiO$_2$ CB leading to an effective photocatalytic effect. As expected, the structure of Sn29(OH)$_2$ makes it inaccessible to the surface of TiO$_2$ and blocks the participation of the porphyrin in the photocatalytic effect. Despite the photocatalytic activity being higher than Co(II) and Zn(II) porphyrins, it is still lower than that of Cu(II) porphyrins, which proves that the presence of different metal ions plays an important role in the photocatalytic process.[102] In the presence of Sn3(OH)$_2$–TiO$_2$ more than 85% degradation was accomplished with 180 min of irradiation. Also, the characterization studies showed an interaction between the hydroxyl groups of Sn3(OH)$_2$ and TiO$_2$. The authors also established the relevance of the O$_2$ concentration. Recycling studies with the photocatalyst Sn3(OH)$_2$–TiO$_2$ showed that it can be reused seven times without loss of activity.[101]

Li and co-workers[103,104] evaluated the effect of the different peripheral substituents in porphyrin derivatives in the photodegradation of the pollutants RhB and 4-NP. They found that among Cu37–TiO$_2$, Cu38–TiO$_2$, and Cu39–TiO$_2$ (Fig. 13), the best photocatalyst for RhB degradation was Cu39–TiO$_2$ (Table 7), but for the degradation of 4-NP it was the second best photocatalyst. Their results confirmed that the impregnation of TiO$_2$ with Cu39 enhanced its photocatalytic activity concerning the degradation of both 4-NP and RhB. The photocatalytic activity of Cu38–TiO$_2$ was assessed regarding the photodegradation of 4-NP in an aqueous solution under white light irradiation with an appropriate amount of H$_2$O$_2$. Under those conditions, a remarkable photocatalytic activity was observed, with almost complete degradation of 4-NP after 160 min of irradiation.

Cu38–TiO$_2$ showed a catalytic efficiency of 86.7% even after 6 cycles. The superior photocatalytic activity of Cu38–TiO$_2$ is probably due to the presence of the heterojunction along with the higher surface, caused by its mesoporous structure. Cu38–TiO$_2$ was also used as a photocatalyst in 4-NP degradation in another work.[105]

Li and co-workers[106] evaluated the photocatalytic activity of the TiO$_2$-based materials Cu39–TiO$_2$, Zn39–TiO$_2$ and Ni39–TiO$_2$ (Fig. 13) in aqueous solution under halogen lamp irradiation and compared it with bare TiO$_2$. All porphyrinic materials revealed enhanced photocatalytic efficiency in the photodegradation of 4-NP, with Cu39–TiO$_2$ being the best photocatalyst followed by Zn39–TiO$_2$ and Ni39–TiO$_2$ (Table 7); bare TiO$_2$ was the least active. This result can be justified by the better combination of the excited potential of the CB of both Cu39 and TiO$_2$. Compared with Cu2–TiO$_2$, the higher catalytic activity of Cu39–TiO$_2$ is probably due to the peripheral OH group that can act as an anchoring group allowing a better interaction between porphyrin and TiO$_2$. This is beneficial to the initial electron injection from the porphyrin excited state to the TiO$_2$ CB, leading to an effective photoactivity.

Vasapollo and co-workers[107] used cardanol, a by-product of the food industry, for the synthesis of the "cardanol-based" free-base porphyrins H$_2$40 and H$_2$41 as well as their Zn(II), Cu(II), Co(II), and Fe(III) complexes (Fig. 13). After their immobilization on TiO$_2$, the materials were tested as sensitizers in 4-NP degradation under UV irradiation for 180 min (Table 7). All metallated complexes (Zn40, Cu40, Co40, Fe40Cl, Zn41, Cu41, Co41, and Fe41Cl) showed a slightly better photocatalytic activity (≈98%) than the free-base derivatives H$_2$40 and H$_2$41 (≈94%). Recycling and stability experiments revealed that all photocatalysts are stable, with the most effective ones being the Cu(II) complexes that could be used for six cycles without loss of activity. The better photoactivity of Cu(II) complexes can be assigned to the Cu(II)–Cu(I) photocatalytic redox cycle. Finally, it was concluded that the oxidizing species responsible for the degradation of 4-NP do not interact with the photocatalyst since the C–C double bond of the cardanol unit appears to be present at the end of the process.

Li and co-workers[108] also reported the synthesis of the free-base H$_2$42 and its Cu(II) complex Cu42 (Fig. 14). These
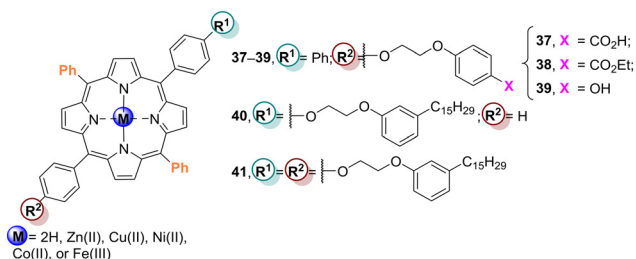


Fig. 13 Free-base and Cu(II) porphyrin derivatives 37–39, cardanol-substituted porphyrins 40 and 41 and porphyrin derivatives 50–52. Used to prepare the Por–TiO$_2$ hybrid materials.
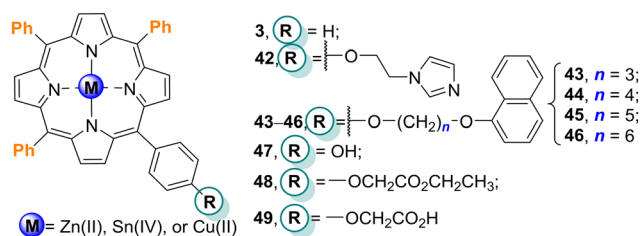


Fig. 14 Free-base porphyrin 42, its Cu(II) complex, Zn(II) porphyrins Zn43–Zn46, M3 and mono(substituted-phenyl)porphyrins 47–49 immobilized on TiO$_2$.

2364 | *Catal. Sci. Technol.*, 2024, **14**, 2352–2389

This journal is © The Royal Society of Chemistry 2024

compounds were used to sensitize $TiO_2$ and the catalytic ability of the resulting hybrids to photodegrade 4-NP was evaluated. The photocatalytic assays were performed in aqueous media under white light and UV irradiation in the presence of $H_2O_2$. The addition of $H_2O_2$ to the photocatalytic system prompted a high photocatalytic activity of $Cu42$–$TiO_2$ after white light irradiation for 160 min (Table 7). An enhanced photocatalytic activity was also observed when irradiated with UV light but only a small increase when $H_2O_2$ was added.

Chen and Shen[109] prepared $TiO_2$ modified with four Zn(II) porphyrins 43–46 (Fig. 14) in order to study the effects of the spacer length of a peripheral substituent on the photodegradation of MO in an aqueous solution under white light. The results showed that all porphyrins enhanced the photocatalytic activity of bare $TiO_2$ with the following order: $Zn44$–$TiO_2$ > $Zn43$–$TiO_2$ > $Zn45$–$TiO_2$ > $Zn46$–$TiO_2$ > bare $TiO_2$. The photocatalytic activity of $Zn44$–$TiO_2$ was much higher than the others (Table 7) because it presented the best match with the CB potential of $TiO_2$. Furthermore, the spacer length of the peripheral substituent can influence the interaction between the Zn(II) porphyrin and $TiO_2$, consequently influencing the initial electron injection process from the porphyrin excited singlet state to the CB of $TiO_2$, essential for an effective photocatalytic effect. The authors performed reusability studies and all the photocatalysts can be reused 6 times without significant loss of activity (10%).

*meso*-(Hydroxyphenyl)porphyrins and their derivatives are frequently used to sensitize $TiO_2$ and the resulting materials typically show high photocatalytic activity.[110–117] For instance, Mu and co-workers[110] used porphyrins $H_247$, $Zn47$ and $Sn47Cl_2$ (Fig. 14) to sensitize $TiO_2$ nanoparticles in order to improve the photocatalytic activity of bare $TiO_2$

nanoparticles. Among the four catalysts ($H_247$, $Zn47$, $Sn47Cl_2$, bare $TiO_2$), the sensitizer $Sn47Cl_2$–$TiO_2$ showed the highest photocatalytic activity, being able to degrade 86% of MO after 180 min irradiation with white light (Table 8). The results also confirmed that the central metal ion in the porphyrin significantly influenced the photocatalytic activity of the hybrid materials.

Li and co-workers[111] immobilized the mono(substituted-phenyl)porphyrins $Cu47$, $Cu48$ and $Cu49$ (bearing hydroxy, ester or carboxy groups, respectively, Fig. 14) on $TiO_2$ and used the resulting hybrids for the photodegradation of 4-NP in aqueous solution under simulated solar irradiation. It was found that porphyrins $Cu47$–$Cu49$ enhanced the catalytic activity of bare $TiO_2$ for 4-NP photodegradation after 300 min of irradiation with a xenon lamp (35% with bare $TiO_2$ and almost complete degradation using the hybrids) – Table 8. $Cu49$–$TiO_2$ was the best photocatalyst followed by $Cu47$–$TiO_2$, $Cu48$–$TiO_2$, and bare $TiO_2$. Also, the authors concluded that a larger polarity of the substituent groups and a stronger interaction between $Cu47$–$Cu49$ and $TiO_2$ accelerate the electron injection process and improve the electron–hole separation. $Cu49$ has the largest polarity and its impregnation on $TiO_2$ afforded the highest photocatalytic activity. Therefore, the polarity of the porphyrin substituents is also an important factor to be considered in the photodegradation of organic pollutants. The photodegradation results confirmed that the impregnation of $TiO_2$ with $Cu47$, $Cu48$, and $Cu49$ increased the photodegradation of 4-NP and RhB. It is important to highlight that the different peripheral substituents in the porphyrin macrocycle led to different catalytic activities; porphyrins containing –OH or –COOH groups ($Cu47$ and $Cu49$) were the best ones for the degradation of 4-NP and RhB. These results can be justified by the strong interaction of these groups with the surface of $TiO_2$.

**Table 8** *meso*-(Hydroxyphenyl) porphyrins–$TiO_2$ used for the photodegradation of 4-NP and MO

| Por | Pollutant | Irradiation time (min) | Light source | Degradation rate (%) | Recycle | Ref. |
|---|---|---|---|---|---|---|
| $Sn47Cl$ | MO | 180 | Visible ($\lambda > 320$ nm) | 86 | — | 110 |
| $Zn47$ | | | | 50 | | |
| $H_247$ | | | | 60 | | |
| $Cu47$ | 4-NP | 300 | UV–vis ($\lambda = 380$–780 nm) | 100 | | 111 |
| | | 60 | UV–vis ($\lambda = 340$–780) nm | 90 | | 112 |
| $Cu48$ | | 300 | UV–vis ($\lambda = 380$–780 nm) | | | 111 |
| | | 60 | UV–vis ($\lambda = 340$–780 nm) | 95 | | 112 |
| $Cu49$ | | 300 | UV–vis ($\lambda = 380$–780 nm) | 100 | | 111 |
| | | 60 | UV–vis ($\lambda = 340$–780 nm) | | | 112 |
| $H_250$ | | | Visible $\lambda > 350$ nm | N.E. | | 113 |
| $Cu50$ | | | | 96 | | |
| $Co50$ | | | | 81 | | |
| $Zn50$ | | | | 86 | | |
| $Cu51$ | | 300 | | 100 | | 114 |
| $Cu52$ | | 45 | | | 6 cycles (15% loss) | 115 |
| $Co52$ | | 75 | | | 6 cycles (22% loss) | |
| $Zn52$ | | | | | 6 cycles (19% loss) | |
| $Cu53$ | | 60 | | 97 | — | 116 |
| | | 40 | | 100 | 6 cycles (10% loss) | |
| **$Cu54$** | | 60 | | | — | 117 |
| | | 30 | | | 6 cycles (10% loss) | |

N.E. – not evaluated.

This journal is © The Royal Society of Chemistry 2024

*Catal. Sci. Technol.*, 2024, **14**, 2352–2389 | **2365**

Later, the same authors compared the photodegradation efficiency of porphyrins Cu47–Cu49 (Fig. 14) immobilized on "home-prepared" and commercial $TiO_2$ (p-$TiO_2$ and c-$TiO_2$, respectively).[112] The results showed that the commercial c-$TiO_2$ caused 84.9% degradation of 4-NP in aqueous solution under metal halide lamp irradiation for 60 min. However, under the same experimental conditions, the "home-prepared" p-$TiO_2$ just exhibited a photodegradation rate of 43.6%. All Cu47–$TiO_2$ hybrids showed higher photocatalytic activity than p-$TiO_2$ in the following order: Cu49–c-$TiO_2$ ≈ Cu49–p-$TiO_2$ > Cu47–c-$TiO_2$ ≈ Cu48–p-$TiO_2$ > Cu47–p-$TiO_2$ > c-$TiO_2$ > Cu48–c-$TiO_2$ > p-$TiO_2$. It is well known that the surface area along with the hydroxylation level of $TiO_2$ could affect the interaction of the sensitizer and $TiO_2$, which, in turn, improves the photocatalytic activity. Moreover, the anchoring group also plays an important role which could explain the higher activity of Cu49; the carboxy group could accelerate the electron transfer from the porphyrin to $TiO_2$. The formation of porphyrin dimers Cu47–Cu47, Cu48–Cu48, and Cu49–Cu49 on the lower and less hydroxylated surface area of c-$TiO_2$ was also detected. It is important to highlight that regardless of the porphyrin chosen to sensitize $TiO_2$, the monosubstituted porphyrin structure is more beneficial for increasing photodegradation than the dimeric structures.

In order to understand the influence of the metal ion in 5,15-bis(4-hydroxyphenyl)porphyrins in the photodegradation of 4-NP, Li and co-workers[113] immobilized the free-base $H_2$50 along with the metallated porphyrins Cu50, Zn50, and Co50 (Fig. 15) on the surface of $TiO_2$. The four porphyrins and the corresponding $TiO_2$ composites were then evaluated as photocatalysts to degrade 4-NP. The impregnation of porphyrins M50 (M = 2H, Cu(II), Zn(II), or Co(II)) did not influence the particle size of $TiO_2$ but increased its photocatalytic activity. The four photocatalysts enhanced the photoactivity in the following order: Cu50–$TiO_2$ (95.8%) > Zn50–$TiO_2$ (85.6%) > Co50–$TiO_2$ (80.8%) > Cu3–$TiO_2$ (66.8%) > bare $TiO_2$ (60%) after irradiation for 60 min (Table 8). These results showed that the metal ion plays, effectively, an important role in the photodegradation efficiency. Also, the

OH anchoring group of the metalloporphyrin is a factor that improves its efficiency as a photocatalyst. Moreover, the results of photoluminescence showed that the three photocatalysts M50 (M = Cu(II), Zn(II), or Co(II)) could increase the separation efficiency of the photoinduced electron and hole. The highest photocatalytic activity was observed with the Cu50–$TiO_2$ hybrid.

Hu and co-workers[114] synthesized the dicarboxylic acid Cu51 (Fig. 15 and Table 8), impregnated it on $TiO_2$ and evaluated the photocatalytic activity of the resulting composite on the degradation of 4-NP in aqueous media under xenon lamp irradiation. The results showed that the Cu51–$TiO_2$ composite's photoactivity was enhanced when compared with bare $TiO_2$ due to the interaction between the carboxy group of the porphyrin and the hydroxyls anchored in the $TiO_2$ surface.

As already mentioned, the metalloporphyrins with carboxy groups exhibit higher photocatalytic activity due to the strong interactions between the –COOH groups and $TiO_2$. Also, the role of the central metal is revealed to be crucial, and for that reason, Li and co-workers[115] studied the influence of different metals on the photocatalytic activity. Cu52–$TiO_2$ is still the most efficient photocatalyst, followed by Co52–$TiO_2$, Zn52–$TiO_2$ (Fig. 15), and bare $TiO_2$. The Cu(II) ions can easily accept electrons to reach a steady state, causing the isolation of electron holes when compared with Co(II) and Zn(II) in M52–$TiO_2$. All the metalloporphyrin composites could be recycled 6 times with a maximum loss of 22% (Table 8) in the photodegradation efficiency.

The two porphyrinic mesoporous materials Cu53–$TiO_2$ and Cu54–$TiO_2$ (Fig. 16) are efficient photocatalysts for the degradation of 4-NP (Table 8), but the highest efficiency was observed for Cu54–$TiO_2$.[116,117] The chemical interaction between the carboxy groups of Cu54 and $TiO_2$ is stronger than the physical interaction of the ester groups of Cu53 with $TiO_2$.[116] As the interaction strength increases, the electron transfer efficiency also increases, leading to a better photocatalytic effect. According to the authors, the electron transfer occurs through space, not through the linker group that connects the porphyrin core to the anchoring group.
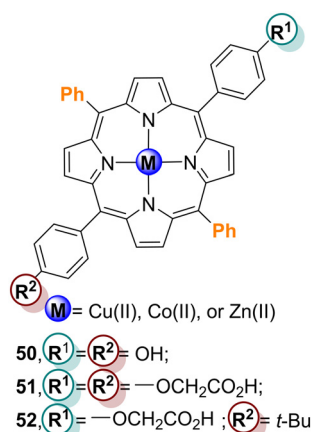

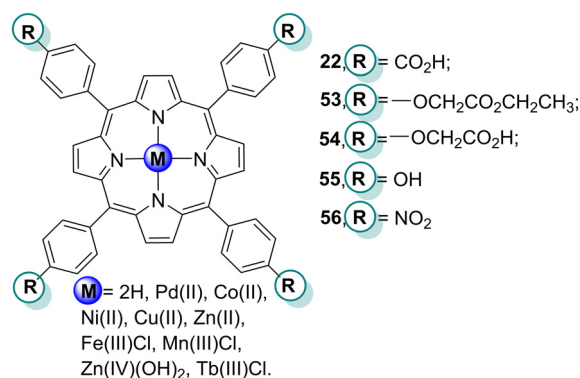
**Fig. 15** Porphyrin derivatives 50–52.



**Fig. 16** meso-Tetra(substituted-phenyl)porphyrin derivatives 22, 53–57.

**2366** | Catal. Sci. Technol., 2024, **14**, 2352–2389

This journal is © The Royal Society of Chemistry 2024

Moreover, when considering the steric constraint of porphyrins, Cu54 bonds to the $TiO_2$ surface by two carboxy groups, with a certain planar deviation, whereas Cu54 places vertical to the surface of $TiO_2$. As a result, the photocatalytic efficiency is higher for Cu54–$TiO_2$ than for Cu53–$TiO_2$. Moreover, the efficiency is maintained at 90% after six cycles.

Tasseroul and co-workers[118] designed xerogels based on $TiO_2$ modified with the free-base *meso*-tetrakis(4-carboxyphenyl)porphyrin $H_2$22 and its Ni(II) complex Ni22 (Fig. 16) in order to assess their potential to degrade 4-NP (Table 9). An improvement of the photocatalytic activity was observed for the xerogels dried for 10 days, with this effect being more pronounced with Ni22. The high specific surface area of the xerogels allowed the adsorption of 4-NP to be increased and, consequently, the reaction rate to increase.

To degrade MB, Viana and co-workers[119] modified $TiO_2$ nanoparticles with $H_2$22 (Fig. 16) and Mn22Cl (Fig. 16). The carboxylic group, which is chemically linked to the $TiO_2$ nanoparticle, enhances the electronic coupling between the porphyrin and the semiconductor. In the case of the free base $H_2$22, the porphyrins could be anchored to $TiO_2$ by one or two of the carboxylic groups that appear to be perpendicular to the $TiO_2$ surface but Mn22Cl was anchored in a non-

perpendicular way to $TiO_2$, suggesting that the filling of the $TiO_2$ pores by these molecules occurs, leading to a reduction of the catalyst surface area, in the case of Mn22Cl, decreasing its photocatalytic activity when compared with $H_2$22.

Shi and co-workers[120] modified $TiO_2$ with $H_2$22 or $H_2$56 (Fig. 16) and used the composites to degrade acid chrome blue K in aqueous media under visible-light irradiation. The results revealed that both $H_2$22–$TiO_2$ and $H_2$56–$TiO_2$ could efficiently degrade this dye in 15 min under natural sunlight (94.0% and 96.1% degradation, respectively, Table 9).

The presence of pharmaceuticals in the environment, from wastewater of the pharmaceutical industry, excreted by patients on drug therapy, and drugs flushed down the toilet, is worrying.[121] Famotidine, a histamine H2 receptor antagonist used to prevent peptic ulcers,[122] can be considered a wastewater pollutant if not destroyed properly. Nolan and co-workers[123] prepared a hybrid composed of $TiO_2$ modified with $H_2$22 and assessed its capability as a catalyst in the photodegradation of this drug using both visible and solar light irradiation. After reusing the photocatalyst, it could maintain 67% of the original photocatalytic activity. A careful analysis of the photodegradation products of famotidine using the $H_2$22–$TiO_2$ composite revealed that it did not lead to complete

**Table 9** Tetracarboxylic porphyrins M22, $H_2$56 and Zn64 immobilized on $TiO_2$ for the photodegradation of several pollutants

| Por | Pollutant | Irradiation time (min) | Light source | Degradation rate (%) | Recycle | Ref. |
|---|---|---|---|---|---|---|
| $H_2$22 | 4-NP | 360 | Visible ($\lambda$ > 350 nm) | $0^a$ | — | 118 |
|  |  |  |  | $30^b$ |  |  |
| Ni22 |  |  |  | $42^b$ |  |  |
| $H_2$22 | MB | 180 | UV ($\lambda$ = 254 nm) | 74 |  | 119 |
| Mn22Cl |  |  |  | 30 |  |  |
| $H_2$22 | Acid chrome blue K | 15 | Visible ($\lambda$ > 400 nm) | 94 |  | 120 |
| $H_2$56 |  | 60 |  | 96 |  |  |
| $H_2$22 | Famotidine | 180 |  | 100 | 1 cycle (33% loss) | 123 |
|  |  | 30 | Natural sunlight | 90 | — |  |
|  | Tamsulosin | 180 | Visible ($\lambda$ > 400 nm) | 20 |  |  |
|  | Solifenacin |  |  | 25 |  |  |
| $H_2$22 | Oxolinic acid |  | Sunlight simulator | 60 |  | 124 |
| Zn22 |  |  |  | 52 |  |  |
| Cu22 |  |  |  | 68 |  |  |
| Sn2 |  |  |  | 50 |  |  |
| $H_2$22 | Oxytetracycline |  |  | 60 |  |  |
| Zn22 |  |  |  | 35 |  |  |
| Cu22 |  |  |  | 62 |  |  |
| Sn2 |  |  |  | 60 |  |  |
| $H_2$22 | Atrazine | 60 | Visible ($\lambda$ > 420 nm) | 25 |  | 126 |
| Fe22Cl |  |  |  | 57 |  |  |
| Cu22 |  |  |  | 82 |  |  |
| Zn22 |  |  |  | 40 |  |  |
| $H_2$22 | MB | 30 |  | $98^c$ |  | 128 |
|  |  |  |  | $59^d$ |  |  |
| Cu22 |  |  |  | $91^c$ |  |  |
|  |  |  |  | $50^d$ |  |  |
| $H_2$22 |  | 60 |  | $100^c$ |  | 129 |
| Cu22 |  | 400 |  | $90^c$ |  | 130 |
| $H_2$22 |  | 80 |  | 70 | 10 cycles (10% loss) | 135 |
| Zn64 |  |  |  | 84 |  |  |
| Fe22 |  | 120 | UV–visible ($\lambda$ > 100 nm) | $85^e$ | 5 cycles (10% loss) | 136 |
|  |  |  |  | 68 |  |  |

$^a$ Dried in 3 days. $^b$ Dried in 10 days. $^c$ 80 mg of photocatalyst. $^d$ 20 mg of photocatalyst. $^e$ Presence of SA.

This journal is © The Royal Society of Chemistry 2024

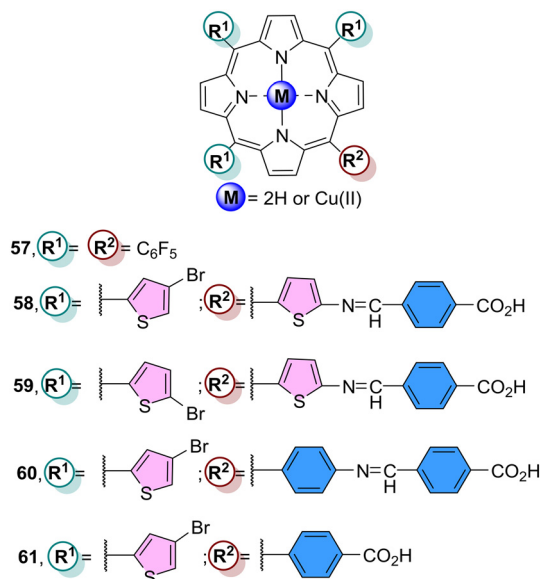*Catal. Sci. Technol.*, 2024, **14**, 2352–2389 | **2367**

**Fig. 17** Free-base fluorinated H$_2$57 and Cu(II) derivatives Cu58–Cu61.

mineralization of the drug, but instead generated a range of degradation products, mainly the *S*-oxide of famotidine. The optimized conditions used to degrade famotidine were also used to degrade other pharmaceuticals (tamsulosin and solifenacin) but without success. It was concluded that the H$_2$22–TiO$_2$ composite is substrate specific.

D'Urso and co-workers[124] studied the ability of TiO$_2$ modified with cationic porphyrins M2 (M = 2H, Zn(II), and Sn(IV)(OH)$_2$) (Fig. 2) and anionic porphyrins H$_2$22, Zn22, and Cu22 (Fig. 16 and Table 9) to degrade oxolinic acid and oxytetracycline, two antibiotics used in aquaculture.[125] These pharmaceuticals are photodegraded in the presence of bare TiO$_2$ but it would be important to enhance its catalytic activity using porphyrins. Preliminary studies indicated that porphyrin H$_2$22 was the best $^1O_2$ generator while Cu22 could

not generate $^1O_2$. All cationic porphyrins exhibited similar results. Despite these results, the Cu22–TiO$_2$ composite was considered the best photocatalyst among the hybrid materials, being slightly specific for oxolinic acid. Sn2(OH)$_2$ was chosen for immobilization on TiO$_2$ due to the presence of the hydroxyl axial ligands, but it did not show significant results in the photodegradation of both pharmaceuticals.

In 2009, Chovelon and co-workers[126] used porphyrins H$_2$22, Fe22Cl, Cu22, and Zn22 (Fig. 16) supported on TiO$_2$ to degrade atrazine[127] in aqueous solution under white light irradiation. Atrazine was only degraded after the addition of H$_2$O$_2$ and the best results were obtained with Cu22–TiO$_2$, which achieved 82% degradation after 1 h of irradiation. The photodegradation rates with the remaining composites were much lower: Fe22Cl (57%), Zn22 (40%) and H$_2$22 (25%) – Table 9. The authors could identify a series of intermediates after a first allylic oxidation.

Later, Zheng and co-workers[128] also used modified TiO$_2$ with H$_2$22 and Cu22 (Fig. 16 and Table 9) to degrade MB under white light. The best photocatalyst was also Cu22–TiO$_2$, with a MB photodegradation rate of 59.3% upon 40 min of irradiation (20 mg amount of photocatalyst). This efficiency could be increase to 92% with the increase on the amount of photocatalyst to 80 mg. Wang and co-workers also confirmed that H$_2$22–TiO$_2$ and Cu22–TiO$_2$ can efficiently degrade MB under white light irradiation.[129,130] Their studies on the photodegradation of MB revealed that the sensitization of TiO$_2$ with H$_2$22 and Cu22 enhances its photoactivity and provides good photocatalysts for wastewater treatment.

TiO$_2$ nanoparticles modified with H$_2$57 (Fig. 17) were prepared and used as photocatalysts for photodegradation of MB by Tsai and co-workers.[131] The photocatalytic activity of H$_2$57–TiO$_2$ was assessed by performing MB degradation in aqueous media under white light. The absorption spectrum of the H$_2$57–TiO$_2$ nanoparticle was extended to 300–500 nm, which greatly enhanced the photocatalytic activity when

**Table 10** Several porphyrins immobilized on TiO$_2$ for the degradation of several pollutants[131–134,137–139]

| Por | Pollutant | Irradiation time (min) | Light source | Degradation rate (%) | Recycle | Ref. |
|---|---|---|---|---|---|---|
| H$_2$57 | MB | 60 | Natural sunlight | 90 | — | 131 |
| Cu58 | 4-NP | 120 | Visible (λ > 420) | 100 | | 132 |
| Cu59 | | 45 | | | 5 cycles (30% loss) | |
| | MB | 50 | | | | |
| | RhB | 120 | | | | |
| Cu60 | 4-NP | | | 80 | — | |
| Cu61 | | | | 60 | | |
| Fe62Cl | | 180 | Natural sunlight | 100$^a$ | 3 cycles (10% loss) | 133 |
| H$_2$63 | MB | 60 | UV | 30 | — | 134 |
| | | | Visible (λ > 400) | 60 | | |
| Fe63Cl | | | UV | 85 | | |
| | | | Visible (λ > 400) | 0 | | |
| H$_2$65 | Acid black 1 | 120 | Natural sunlight | 100 | | 137 |
| H$_2$66 | α-Terpinene | 40 | Visible light (λ > 410 nm) | | 4 cycles (6% loss) | 138 |
| H$_2$67 | 4-NP | 480 | UV–vis | 52$^b$ | 4 cycles (20% loss) | 139 |
| | | | | 55$^c$ | 4 cycles (25% loss) | |
| | | | | 61$^d$ | 4 cycles (10% loss) | |

$^a$ In the presence of H$_2$O$_2$ and TEOA. $^b$ 0.001 molar ratio content. $^c$ 0.003 molar ratio content. $^d$ 0.006 molar ratio content.

**2368** | *Catal. Sci. Technol.*, 2024, **14**, 2352–2389

This journal is © The Royal Society of Chemistry 2024

compared with bare $TiO_2$ reaching 90% degradation of MB after 60 min of solar irradiation (Table 10).

In 2016, Halder and Bhavana[132] studied the role of conformation and the effect of the substituents in the *meso*-positions of porphyrins derivatives Cu58, Cu59, Cu60, and Cu61 (Fig. 17 and Table 10) adsorbed on $TiO_2$ in the photocatalytic degradation of 4-NP, RhB and MB. The activity of Cu59–$TiO_2$ is significantly higher than that of Cu58–$TiO_2$ and higher than both Cu60–$TiO_2$ and Cu61–$TiO_2$. For instance, the time required to degrade 4-NP with Cu59–$TiO_2$ is 45 min while 2 h are necessary when Cu58–$TiO_2$ is used. With Cu60–$TiO_2$ and Cu61–$TiO_2$ a complete degradation of 4-NP is not achieved in 2 h. Similar results were obtained for RhB and MB. The differences observed in the photocatalytic activity of these compounds were explained considering the position of the substituents and their conformations. The best photocatalyst (Cu59–$TiO_2$) was found to be stable under the experimental conditions and its efficacy was maintained after five cycles.

The photocatalytic activity of hemin anchored $TiO_2$ (Fe62Cl–$TiO_2$, Fig. 18 and Table 10) was investigated by ArunaKumari and Devi[133] through the degradation of 4-NP in aqueous solution under solar light irradiation but with the assistance of an appropriate amount of triethanolamine (used as an electron donor). The structural characterization of the catalyst confirmed that the chemisorption of the hemin molecules on the surface of $TiO_2$ is through O=C–O–Ti bonds which can not only enhance the extent of adsorption but also act as electron transfer channels that facilitate the electron transfer process. The photocatalyst can be reused 3 times without loss of activity. Pal and co-workers[134] investigated the potential application of hematoporphyrin-functionalized titania nanohybrids ($H_2$63–$TiO_2$ and Fe63Cl–$TiO_2$) (Fig. 18 and Table 10) for the photodegradation of MB in aqueous solution under visible and UV light. Under UV light, Fe63Cl–$TiO_2$ shows higher photocatalytic activity due to the cooperative functions of Fe63Cl and $TiO_2$ in generating reactive species. On the other hand, $H_2$63–$TiO_2$ shows higher photocatalytic activity under

white light due to the absence of Fe(III) ions that obstruct the electron transfer from the porphyrin macrocycle to $TiO_2$.

In 2020, Son and co-workers[135] reported the synthesis of the porphyrin–squaraine-based sensitizer Zn64 (Fig. 19) that shows broad absorption in the visible and NIR regions, an essential feature in photocatalytic studies. This panchromatic porphyrin derivative was then immobilized on $TiO_2$ and the resulting composite was used as a catalyst for the photodegradation of MB. The photocatalytic studies were performed under white light irradiation and the results were compared with bare $TiO_2$ and $H_2$22–$TiO_2$ (a well-established good photocatalyst). After 80 min of irradiation, Zn64–$TiO_2$ exhibited the highest photocatalytic activity (~80%) followed by $H_2$22–$TiO_2$ (~70%) > $TiO_2$ (~20%). As predicted, the fast and efficient activity of Zn64 is due to its broad absorption ability. The addition of $H_2O_2$ slightly improved the photocatalytic activity. The photocatalyst can be reused up to 10 cycles without significant loss of activity.

In 2015, Yao and co-workers[136] bonded porphyrin Fe22Cl to $TiO_2$ particles using 2-hydroxy-5-sulfosalicylic acid (SSA) or salicylic acid (SA) as a bridging molecule (Fig. 20A and B). These materials were then used as photocatalysts in the photodegradation of MB. The main objective was to check the influence of the bridge between the porphyrin and the $TiO_2$ support on the photocatalytic activity. The photocatalytic activity of both derivatives Fe22Cl–SSA–$TiO_2$ and Fe22Cl–SA–$TiO_2$ was evaluated under white light. Adsorption studies showed that Fe22Cl–SSA–$TiO_2$ and Fe22Cl–SA–$TiO_2$ present a higher capacity to adsorb MB than bare $TiO_2$. The FT-IR results showed that the Fe22Cl molecules, rather than being adsorbed onto the surface of $TiO_2$, are linked to $TiO_2$ through stable π-conjugated chemical bonds (Fig. 20A and B). The Fe22Cl–SSA–$TiO_2$ hybrid showed the best photocatalytic activity (99.3%) under visible light when compared with Fe22Cl–SA–$TiO_2$ (85.2%), Fe22Cl–$TiO_2$ (68.9%) and $TiO_2$ (30.7%). Even after being recycled 5 times, the best photocatalyst could degrade *ca.* 90% of MB. However, a slight decrease of photoactivity was observed when SA was used, suggesting that the bridge between the porphyrin and $TiO_2$ was weaker. Moreover, the degradation efficiency of MB with Fe22Cl–$TiO_2$ seems to decrease rapidly after recycling, which
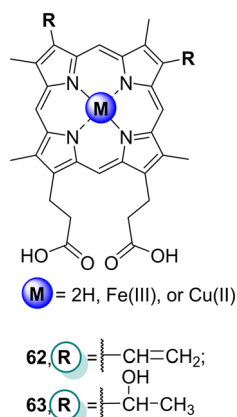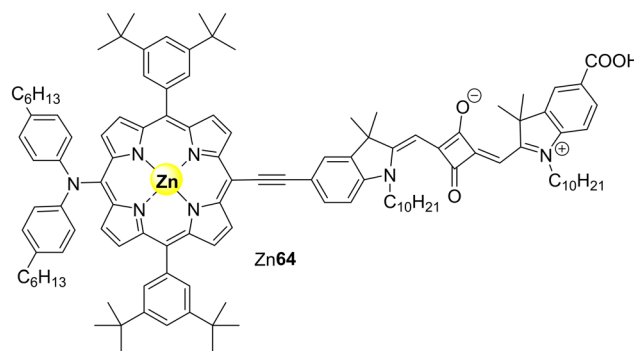


**Fig. 18** Structures of porphyrins **62** and **63**.



**Fig. 19** Structure of the porphyrin–squaraine-based panchromatic sensitizer (Zn64) immobilized on $TiO_2$.

This journal is © The Royal Society of Chemistry 2024

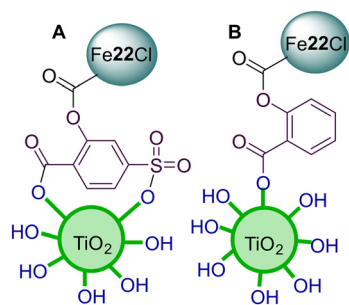*Catal. Sci. Technol.*, 2024, **14**, 2352–2389 | **2369**

**Fig. 20** Representation of TiO$_2$ modified with porphyrin Fe**22**Cl using 2-hydroxy-5-sulfosalicylic acid (A) or salicylic acid (B) bridging molecules.



**Fig. 22** Representation of the porphyrin-based hybrid silica-titania photocatalyst **67**.

could be due to a bleaching process that is suppressed when SSA is used. The authors suggested that there is a break of the aromatic rings of MB, which was further degraded to CO$_2$ and H$_2$O.

In 2017, Sobral and co-workers[137] prepared and used composite H$_2$**65**–TiO$_2$ (Fig. 21) for the photodegradation of acid black 1 under direct sunlight. The authors found that the photocatalytic activity of bare TiO$_2$ was efficiently improved with its sensitization with H$_2$**65**; the photocatalyst H$_2$**65**–TiO$_2$ could efficiently degrade 90.1% of acid black 1 after 90 min of direct sunlight irradiation, reaching a complete degradation after 120 min.

In 2012, Cai and co-workers[138] developed TiO$_2$ microspheres modified with porphyrin H$_2$**66** (Fig. 21). To sensitize TiO$_2$ microspheres with H$_2$**66** the authors used allyl bromide and 3-mercaptopropyltrimethoxysilane (MPS) as linkers and studied the capacity of the photocatalyst in α-terpinene degradation under visible light irradiation. The structural characterization of this material revealed that H$_2$**66**–MPS was chemisorbed on the surface of TiO$_2$ through a Si–O–Ti bond (Fig. 21). Regarding the photodegradation assays, when compared with bare TiO$_2$, the presence of the H$_2$**66**–linker–TiO$_2$ greatly enhanced the degradation of α-terpinene under white light. The photocatalyst was reused four times with high efficiency (7% loss).
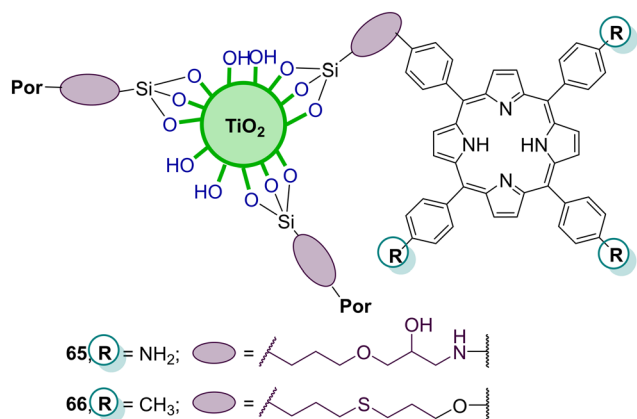
Mahy and co-workers[139] modified TiO$_2$ with three different ratios of a sylilated *meso*-tetrakis(4-aminophenyl) porphyrin derivative (H$_2$**67**–Si) and evaluated the activity of the resulting hybrids H$_2$**67**–Si–TiO$_2$ (Fig. 22) on the photocatalytic degradation of 4-NP under white light. The hybrid materials proved to be efficient photocatalysts and an improvement in photoactivity is observed when the amount of porphyrin improves.

After 24 h of testing, the photodegradation rate remains constant and no leaching was revealed. However, in the recycling tests, a decrease of photoactivity towards bare TiO$_2$ activity was observed due to bond breaking between H$_2$**67**–Si and TiO$_2$. Remarkably, H$_2$**67**–Si–TiO$_2$ was revealed to be nearly 6 times more photoactive than commercial Evonik P25 for 4-NP degradation under white light.

## 5.1. Other titanium oxide supports

**5.1.1. Titanate nanotubes.** In 2011, Kang and co-workers[140] studied the effects of anchoring modes on the properties of titanate nanotubes (TiNTs) modified with two porphyrins: Zn**3** and Zn**47** (Fig. 14). Both Zn**3**–TiNTs and Zn**47**–TiNTs are capable of MO degradation under white light irradiation (Table 11). In fact, the greater the amount of Zn**3** or Zn**47** loaded into TiO$_2$, the higher the photocatalytic activity. The structural characterization of the hybrids showed that Zn**47** was bonded mainly on the outer surfaces of the TiNTs through hydrogen bonds while Zn**3** was physically adsorbed into the pore channels of the TiNTs *via* a capillary process. The different anchoring modes influence the separation of photogenerated electrons and holes and the stability of the Zn**47**/Zn**3** coupled TiNTs. The anchoring mode of Zn**3** on the TiNTs allows an efficient photoinduced electron transfer which consequently confers a photocatalytic activity seven times higher than that of Zn**47**–TiNTs after 30 min of irradiation.

In 2013, Wan and co-workers[141] studied the photocatalytic degradation of some organic dyes with H$_2$**22** (Fig. 16)



**Fig. 21** Representation of H$_2$**65**–TiO$_2$ and H$_2$**66**–TiO$_2$.

**2370** | *Catal. Sci. Technol.*, 2024, **14**, 2352–2389

This journal is © The Royal Society of Chemistry 2024

**Table 11** Porphyrins immobilized on titanate tubes for the degradation of MO and MB

| Por | Pollutant | Irradiation time (min) | Light source | Degradation rate (%) | Recycle | Ref. |
|---|---|---|---|---|---|---|
| Zn3 | MO | 30 | Visible ($\lambda > 370$ nm) | 80 | | 140 |
| Zn47 | | 60 | | 30 | | |
| $H_2$22 | MB | 180 | | 99 | | 141 |
| Zn22 | | 50 | Visible ($\lambda > 420$ nm) | 100 | 5 cycles (10% loss) | 142 |
| Cu22 | | 40 | Visible ($\lambda > 390$ nm) | | — | 143 |
| Fe22Cl | | 120 | | 85 | 5 cycles (5% loss) | 144 |

modified TiNTs. Within one year apart, Zheng and co-workers,[142] and Wan and co-workers[143,144] modified TiNTs with metallated porphyrins to obtain Zn22–TiNTs, Fe22Cl–TiNTs and Cu22–TiNTs, respectively, to be used as catalysts in the photodegradation of MB (Table 11).

According to Wan and co-workers,[141] a degradation rate of 99.4% was achieved after white light irradiation for 3 h using 5% of $H_2$22 loaded into $TiO_2$ nanotubes. Photocatalytic studies showed that the best composite was also efficient in the photodegradation of other organic pollutants, namely RhB.

On the other hand, the studies reported by Zheng and co-workers,[142] and Wan and co-workers[143,144] revealed that the photocatalysts Fe22Cl–TiNTs, Cu22–TiNTs and Zn22–TiNTs have good activity for MB degradation (higher than 90%) under white light irradiation (Table 11). Moreover, the unique cooperative effect caused by the high surface area, along with the strong adsorption ability and low gap energy, makes Fe22Cl–TiNTs and Zn22–TiNTs good photocatalysts.

**5.1.2. BaTiO₃.** Devi and Nithya[145] modified $BaTiO_3$ with hemin (Fe62Cl, Fig. 18) and evaluated the photocatalytic activity of the resulting material in the degradation of 4-CP under solar light irradiation, compared with bare $BaTiO_3$. After irradiation for 150 min, a 91.8% degradation of 4-CP was observed using Fe62Cl–$BaTiO_3$ while only 13.4% degradation was achieved with $BaTiO_3$. A complete (100%) photodecomposition of 4-CP was observed after irradiation for 60 min using the photocatalyst Fe62Cl–$BaTiO_3$ and $H_2O_2$. Trapping experiments with TBA and EDTA allowed identifying the main active species in the oxidative degradation process as hydroxyl free radicals and electron holes ($h^+$).

# 6. Silica-supported porphyrins

Silica has excellent optical properties, exceptional adsorption and ability of selective separation of chemicals. Moreover, its large surface area, along with its good mechanical and thermal properties, makes silica a good material for active phase-support in catalysis.[146] Several types of silica structures can be used for supporting dyes (namely porphyrins) and the resulting hybrids have been frequently used as photocatalysts in water pollutant degradation. The role of those types of silica (nano)structures in photocatalysis is discussed in the following examples.

## 6.1. SiO₂ modified with porphyrins

Regarding $SiO_2$ hybrids, Cai and co-workers[147] reported the fabrication of silica microspheres functionalized with free-base porphyrin units. The hybrids $H_2$68 and $H_2$69 (Fig. 23) were used as catalysts for the photodegradation of naphthalene-1,5-diol (Table 12) in water and illumination with an iodine tungsten lamp. Hybrid $H_2$69 revealed much higher activity than $SiO_2$ alone or the porphyrin $H_2$68. After irradiation for 50 min, the degradation rate was 92.7% with hybrid $H_2$69 but only 42.9% in the presence of the unsupported porphyrin. The enhanced catalytic performance of hybrid $H_2$69 can be related to the presence of sulfonic groups. The authors also evaluated the reusability of microspheres $H_2$69 and found that their catalytic performance has slightly decreased after being reused five times.

Lee and co-workers[148] reported the preparation of two photocatalysts consisting of a Sn(IV) porphyrin derivative Sn3(OH)$_2$ supported on silica and the amino-$C_{60}$ derivative 70 also supported on silica (Fig. 24) and evaluated the influence of the two sensitizers on the photodegradation of a range of phenolic pharmaceutical compounds (Table 12) frequently found as water pollutants. Both photosensitizers were activated under white light to generate $^1O_2$. The study demonstrated that Sn3(OH)$_2$ allowed more effective oxidation of the pharmaceuticals than 70. However, a decrease in the
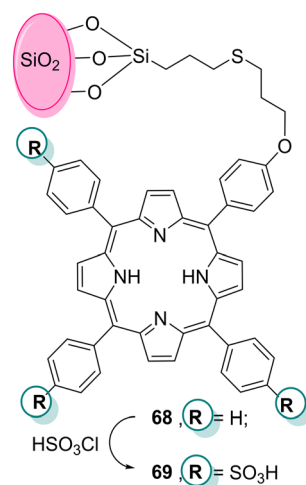


**Fig. 23** Representation of SiO₂–porphyrin microspheres **68** and **69**.

This journal is © The Royal Society of Chemistry 2024

*Catal. Sci. Technol.*, 2024, **14**, 2352–2389 | **2371**

**Table 12** SiO$_2$ modified with porphyrins for the degradation of several pollutants

| Por | Pollutant | Irradiation time (min) | Light source | Degradation rate (%) | Recycle | Ref. |
|---|---|---|---|---|---|---|
| H$_2$68 | Naphthalene-1,5-diol | 50 | Visible light ($\lambda > 410$ nm) | 43 | — | 147 |
| H$_2$69 | | | | 93 | 5 cycles (5% loss) | |
| Sn3(OH)$_2$ | Naproxen | 120 | Visible light ($\lambda > 400$ nm) | 30 | — | 148 |
| | Trimethoprim | | | 40 | | |
| | Atorvastatin | | | 70 | | |
| | Tolmetin | | | 75 | | |
| | Losartan | | | 100 | | |
| | Propanolol | | | | | |
| | Cimetidine | | | | | |
| | Ranitidine | | | | | |
| | Caffeine | | Fluorescent lamp (visible light) | 0 | | |
| | Acetaminophen | | | | | |
| | Amoxicillin | | | | | |
| | Naproxen | | | 50 | | |
| | Trimethoprim | | | 60 | | |
| | Atorvastatin | | | 70 | | |
| | Tolmetin | | | 90 | | |
| | Losartan | | | 100 | | |
| | Propanolol | | | | | |
| | Cimetidine | | | | | |
| | Ranitidine | | | | | |
| Fe22Cl | Phenol | 90 | Visible light ($\lambda > 400$ nm) | 95 | | 150 |
| Cu71 (X = PF$_6^-$) | 2,6-DBP | | Visible light ($\lambda = 350$–800 nm) | 80 | | 151 |
| Cu71 (X = ClO$_4^-$) | | 50 | | 64 | | |
| Cu72 (X = PF$_6^-$) | | | | 55 | | |
| Cu74 (X = ClO$_4^-$) | | 50 | | 61 | | |
| H$_2$57 | Metoprolol | 720 | Simulated solar irradiation | 90 | | 152 |
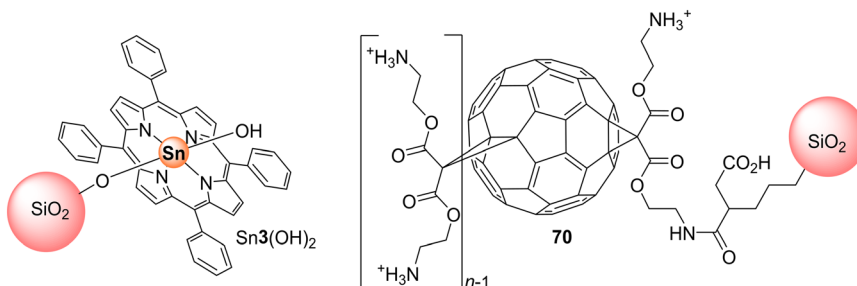


**Fig. 24** Representation of the photocatalysts Sn3(OH)$_2$–SiO$_2$ and aminoC$_{60}$–SiO$_2$ **70** used for the degradation of phenolic pharmaceuticals.

activity of Sn3(OH)$_2$–SiO$_2$ was observed during the recycling tests due to a self-destructive reaction *via* $^1$O$_2$ induced oxidation of the porphyrin macrocycle. On the other hand, the photocatalytic activity of the aminoC$_{60}$–SiO$_2$ **70** did not decrease when it was reused for five cycles.

In 1993, Bauer and co-workers[149] reported that a simple photo-Fenton reaction (Fe$^{2+}$, H$_2$O$_2$ and light) was adequate to increase the photodegradation of the wastewater pollutant 4-CP when compared with the same reaction in the dark. More recently, Diaz-Uribe and co-workers[150] produced a catalyst composed of *meso*-tetrakis(4-carboxyphenyl)porphyrin iron(III) (Fe22Cl) (Fig. 16) adsorbed on silica and evaluated its efficiency in the oxidation of phenol assisted by white light. In this study, the phenol concentration was reduced from 100 mg L$^{-1}$ to *ca.* 5 mg L$^{-1}$ after 90 min of white light irradiation *via* oxidation through the photo-Fenton reaction.

Hydroquinone, catechol, and *p*-benzoquinone were identified as intermediate oxidation products but the chain reaction proceeds until the formation of short chain acids that are finally transformed into carbon dioxide and water. The main ROS responsible for the degradation of phenol was OH$^{\bullet-}$ and its presence during the photooxidation process was corroborated by chemical trapping with terephthalic acid. The study was carried out at four pH values (1.8, 2.4, 2.8, and 3.2), but it was found that the highest rate constant (3.6 ± 0.2 × 10$^{-2}$ min$^{-1}$) and the highest yield of the photooxidation process occurred at pH 2.8.

Setsune and co-workers[151] synthesized the copper(I) complexes of an $N^{21},N^{22}$-etheno bridged octaethylporphyrin (Cu71 (X = PF$_6^-$ or ClO$_4^-$)) and the copper(I) complex of $N^{21}$, $N^{22}$-etheno bridged *meso*-tetraphenylporphyrin (Cu72) with different counter ions (*e.g.*, PF$_6^-$ and ClO$^-$) (Fig. 25 and

**2372** | *Catal. Sci. Technol.*, 2024, **14**, 2352–2389

This journal is © The Royal Society of Chemistry 2024
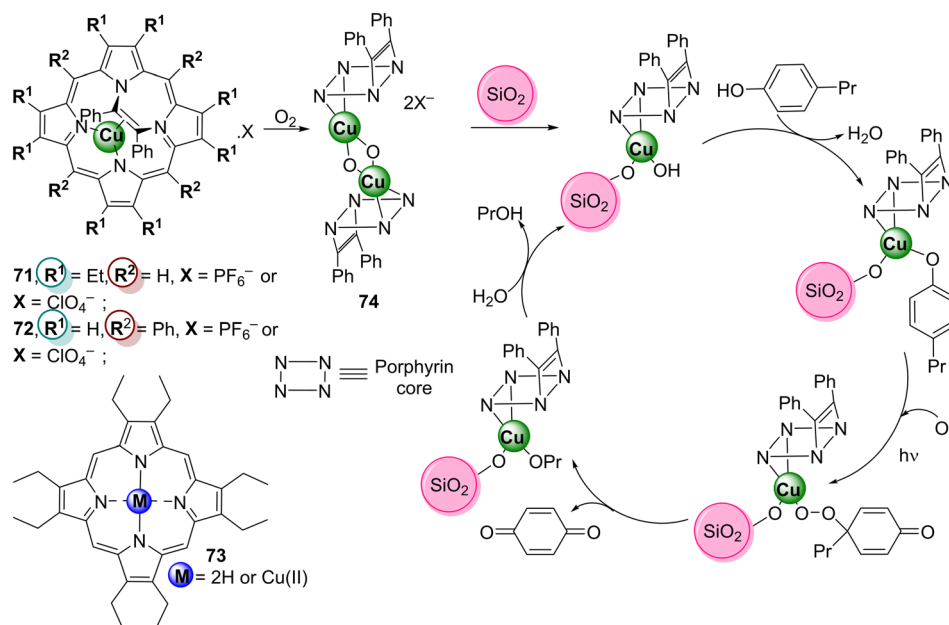
**Fig. 25** Copper(I) complexes of the $N^{21},N^{22}$-etheno bridged porphyrins **71** and **72**, and the proposed mechanism of the photodegradation of 4-propylphenol catalysed by these complexes immobilized on silica gel.

Table 12). These complexes were also immobilized on silica gel and used as catalysts for the photooxidation of phenols (2,6-di-$t$-butylphenol (2,6-DBP) and 4-propylphenol) both under homogeneous and heterogeneous conditions. A plausible mechanism for the heterogeneous photooxidation of 4-propylphenol is shown in Fig. 25.

For the homogenous catalysis, an acetonitrile solution of 2,6-DBP and Cu**71** (X = $PF_6^-$) was irradiated with white light for 90 min. The only detected oxidation product was 2,6-di-$tert$-butyl-1,4-benzoquinone, formed in 80% yield (determined by $^1$H NMR). On the other hand, Cu**71** (X = $ClO_4^-$) achieved a conversion rate of 64% after 50 min of irradiation; without photoirradiation, only 7% of 2,6-DBP was modified. The efficiency of Cu**72** was not very different from the one of OEP derivative Cu**71** (X = $ClO_4^-$). The $N^{21},N^{22}$-etheno bridge porphyrin derivatives could afford higher phenol conversion than the free-base H$_2$**73** and the tetradentate Cu**73** complex. This could be due to their relative photostabilities since a Pd complex of $N^{21},N^{22}$-etheno bridge porphyrin was reported to be more photostable than the free-base porphyrin.[153,154] The di(μ-hydroxo)dicopper(II) diporphyrin Cu**74** (obtained by air-oxidation of complex Cu**71** (X = $PF_6^-$)) was found to have a similar reactivity in photooxidizing 2,6-DBP (61%) as Cu**71** (X = $PF_6^-$), which indicated that derivative Cu**71** (X = $PF_6^-$) acts in the photodegradation reaction through the formation of complex Cu**74**. Regarding the heterogenous catalysis, the phenol derivative was degraded within 60 min of irradiation with white light when incubated with Cu**71** (X = $PF_6^-$). Also, this compound was immediately oxidized into a complex Cu**74**-type which proved to be essential for the photoreaction process. It is important to highlight that, contrary to the homogenous catalysis, the photooxidation of phenol

derivatives using Cu**71** (X = $PF_6^-$) was faster than with its respective free-base in the heterogeneous one. The final composites could be easily recovered and reused up to three times without loss of activity.

Metoprolol is a well-known prescribed β-blocker that is not entirely removed from water in sewage treatment plants. For that reason, Simões and co-workers[152] studied the photocatalytic activity of the free-base H$_2$**57** as a photosensitizer, under homogeneous and heterogeneous conditions, in metoprolol degradation. The promising results led to the study of H$_2$**57** immobilized on 3-aminopropyl silica (Fig. 26).

Under homogeneous conditions and with simulated solar radiation, H$_2$**57** was found to be efficient in the photodegradation of metoprolol, with *ca.* 90% degradation after 12 h. Similarly, the use of the heterogeneous catalyst H$_2$**57**–silica
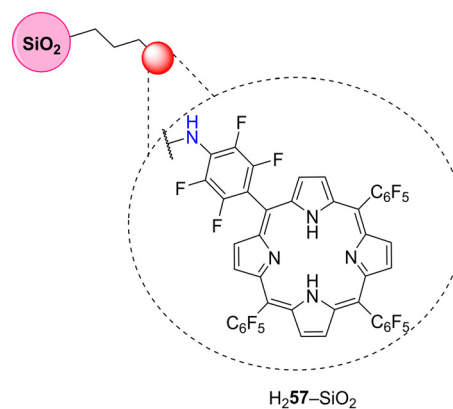


**Fig. 26** Representation of the H$_2$**57**–silica photocatalyst (more *para*-F atoms may be substituted).

This journal is © The Royal Society of Chemistry 2024

*Catal. Sci. Technol.*, 2024, **14**, 2352–2389 | **2373**

**Review**
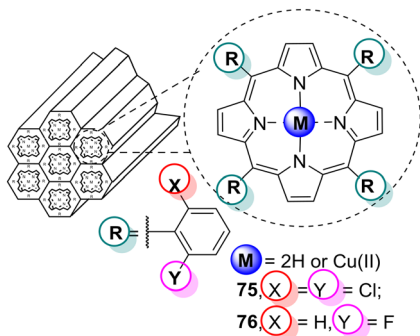
**Fig. 27** Representation of MCM-41 immobilized porphyrins **75** and **76**.



**Fig. 28** ZnO microrods modified by a porphyrin heteroaggregate.

allowed 60% degradation of metoprolol after irradiation for 12 h. Despite the decrease in the photodegradation efficiency, the use of the immobilized porphyrin allows its easy recovery. Studies performed in a sample from the secondary effluent of a wastewater treatment plant fortified with metoprolol revealed that the efficiency of $H_2$**57**–silica was not decreased by the complex matrix of the effluent. It was confirmed that singlet oxygen was the main component responsible for the photodegradation of metoprolol.

### 6.2. MCM-41 silica modified with porphyrins

Pereira and co-workers[155] reported the preparation of MCM-41 with encapsulated porphyrins M**75** (M = 2H or Cu(II)) and M**76** (M = 2H or Cu(II)) (Fig. 27) in a ship-in-a-bottle way, and the resulting materials were used to degrade 2,4,6-trimethylphenol and two pesticides: fenamiphos and diuron. These pesticides are considered potential groundwater contaminants and it is necessary to find efficient and economical ways to eliminate them. The four immobilized porphyrins M**75** (M = 2H or Cu(II)) and M**76** (M = 2H or Cu(II)) @MCM-41 were evaluated as photocatalysts for the degradation of 2,4,6-trimethylphenol under polychromatic light (300–460 nm). The best results were obtained with the photocatalyst $H_2$**76**@MCM-41, achieving a degradation of 80%. The studies were extended to the degradation of fenamiphos and diuron in an aqueous solution. The degradation of both pollutants was possible in the presence of $O_2$ under white light irradiation using $H_2$**76**@MCM-41 as a photocatalyst, which was recovered by filtration and reused with no significant decrease of its catalytic activity.

## 7. Immobilized porphyrins on a diversity of supports

### 7.1. Self-assembly of supramolecular materials

Bhosale and co-workers[156] developed a photocatalyst based on a supramolecular nanostructure induced by arginine and the free-base *meso*-tetrakis(4-carboxyphenyl)porphyrin ($H_2$**22**, Fig. 8) that can degrade RhB. In the presence of L-/D-arginine, $H_2$**22** forms one-dimensional, self-assembled supramolecular nanobelts with a well-defined morphology that shows an
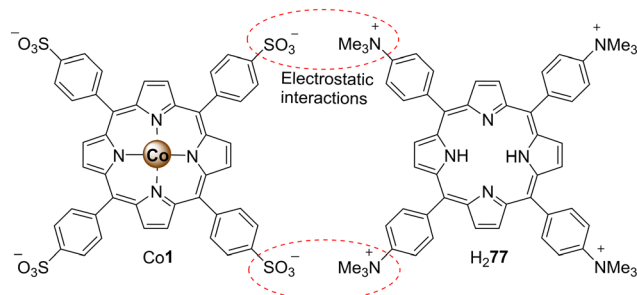
enhanced photocatalytic performance with a maximum RhB degradation up to 90% (when compared with only 15% degradation induced by the $H_2$**22** monomer) after 3 h under white light irradiation.

### 7.2. Porphyrin–ZnO composites

Zinc oxide is an efficient photocatalyst. In fact, it has been reported[157–159] that ZnO can achieve more significant photocatalytic activity than $TiO_2$, the most used inorganic material in catalysis. When modified with porphyrin derivatives, the photocatalytic activity of ZnO is substantially improved, as shown in the next examples concerning the degradation of RhB, MB, MO, and 4-NP.

Kang and co-workers[160] reported the formation of an inorganic–organic material composed of ZnO microrods and nano-heteroaggregates containing the anionic and cationic porphyrins Co**1** and $H_2$**77** (Fig. 28). The modified ZnO microrods that revealed a photocatalytic activity higher than those of the porphyrin monomers and pure ZnO prompted a total photodegradation of RhB in water, at room temperature, after white light irradiation ($\lambda \geq 420$ nm) for 60 min (Table 13).

Li and co-workers[161] reported the synthesis of an organic–inorganic photocatalyst made of Cu**78** (Fig. 29) impregnated onto the surface of ZnO. The photocatalytic activity of Cu**78**–ZnO was evaluated in the photodegradation of RhB under either UV–vis ($\lambda = 380$–780 nm) or visible ($\lambda \geq 420$ nm) lights. When irradiated with white light, 63% of RhB was photodegraded with Cu**78**–ZnO after 210 min (Table 13), but only 23% of RhB was degraded using ZnO (ZnO does not absorb white light). The photocatalyst's reusability was evaluated, and a decrease in the catalytic efficiency from 95% to 83% was observed after five cycles, indicating a slow reduction of the photocatalytic activity.

Mele and co-workers[162] accomplished the synthesis of composite nanomaterials based on ZnO impregnated with a lipophilic tetrasubstituted porphyrin bearing hydrogenated cardanol units ($H_2$**79** and Cu**79**) (Fig. 29). The FTIR analysis showed that non-covalent interactions occur between $H_2$**79** and the ZnO support. Sunlight irradiation for 30 min was sufficient to achieve almost complete decomposition (98%) of RhB in the presence of both photocatalysts ($H_2$**79**–ZnO and Cu**79**–ZnO) – Table 13. These results indicate that these hybrids may be used to eliminate pollutants efficiently from

**2374** | *Catal. Sci. Technol.*, 2024, **14**, 2352–2389

This journal is © The Royal Society of Chemistry 2024

**Table 13**  Porphyrin–ZnO composites for the degradation of several pollutants

| Por | Pollutant | Irradiation time (min) | Light source | Degradation rate (%) | Recycle | Ref. |
|---|---|---|---|---|---|---|
| Co1/H$_2$77 | RhB | 60 | Visible ($\lambda \geq 420$ nm) | 100 | — | 160 |
| Cu78 | | 210 | | 63 | | 161 |
| | | 36 | UV–vis ($\lambda = 380$–780 nm) | 95 | 5 cycles (12% loss) | |
| H$_2$78 | | 30 | Sunlight | 98 | 4 cycles (15% loss) | 162 |
| H$_2$79 | | | | | | |
| H$_2$63 | MB | 60 | Visible light ($\lambda > 395$ nm) | 55 | — | 37 |
| | | | | 80[a] | | |
| | | | | 17[b] | | |
| H$_2$63 | | | UV | 25 | | |
| | | | | 90[a] | | |
| | | | | 100[b] | | |
| H$_2$62 | | 50 | Solar | 85 | 4 cycles (0% loss) | 163 |
| | RhB | 80 | | | | |
| | Eosin yellow | | | | | |
| Fe62Cl | 4-NP | 120 | UV | 99 | — | 164 |
| | | 180 | Solar | 99[c] | | |
| Sn22Cl$_2$ | MO | 240 | Visible light ($\lambda > 400$ nm) | 85 | | 165 |

[a] In the presence of Cu(II) ions. [b] In the presence of Fe(III) ions. [c] In the presence of triethanolamine.

water under ambient conditions. The photocatalysts' reusability was assessed, and it was observed that after four cycles, their photodegradation efficiency was kept above 83%.

As already mentioned, MB is extensively used in the dye industry that can produce hazardous environmental effects in aquatic and human beings.[166,167] To remove it from water, Pal and co-workers,[37] and more recently Thomas and co-worker,[163] reported the formation of light-harvesting nanohybrids composed of ZnO nanorods incorporating organic pigments, namely hematoporphyrin (H$_2$63) (ref. 37) and protoporphyrin IX (H$_2$62) (ref. 163) (Fig. 18 and Table 13).

Pal and co-workers[37] showed that the photoactivation of H$_2$63–ZnO nanohybrids with white light leads to the formation of reactive oxygen species and consequently to the photodegradation of MB. Overall, this work[37] revealed that



**Fig. 29**  Porphyrin derivatives used to prepare Cu78–ZnO, H$_2$79–ZnO and Cu79–ZnO hybrids.

this nanohybrid is an effective material for wastewater treatment. Moreover, in another work, they used the nanohybrids Cu62–ZnO and Fe62Cl–ZnO for the photodegradation of MB under white light in the presence of naturally abundant Cu(II) and Fe(III) ions and discovered that these ions could enhance or retard, respectively, the photodegradation of MB. In the presence of Cu(II) ions, 80% degradation of MB was achieved while only 17% degradation was observed in the presence of Fe(III) ions; these results may be correlated with the additional structural stability of the porphyrin macrocycle metallated with Cu(II).[37]

The photocatalyst composed of protoporphyrin IX–ZnO nanorods (H$_2$62–ZnO, Fig. 18) was also reported by Thomas and co-workers.[163] The photocatalytic activity of the prepared nanorods was evaluated for several pollutants, such as MB, RhB, and eosin yellow, achieving >80% degradation after 50 or 80 min of solar light irradiation (Table 13). The photocatalyst was found to be stable and reusable for four cycles, and the photocatalytic activity was retained. It is noteworthy that the spectroscopic results revealed that H$_2$62 was chemisorbed to the ZnO surface through O=C–O–Zn bonds. It becomes important to highlight that H$_2$62 was not the best photocatalyst despite having a good photocatalytic activity. The best was perylene-3,4,9,10-tetracarboxylic dianhydride–ZnO followed by fluorescein–ZnO and phosphotungstic acid–ZnO.[163]

Due to its high stability, 4-NP is a water-soluble highly toxic and hazardous pollutant. Once dissolved in water, its removal by conventional methods is extremely difficult.[168–170] However, Devi and co-workers[164] reported the preparation of a ZnO-based photocatalyst able to degrade 4-NP under UV and solar light irradiation. According to the authors, almost total degradation of 4-NP occurs after 120 min under UV light irradiation in the presence of ZnO modified with hemin (chloro(protoporphyrinato)iron(III)) (Fe62Cl, Fig. 18 and Table 13) and H$_2$O$_2$. On the other hand, the same
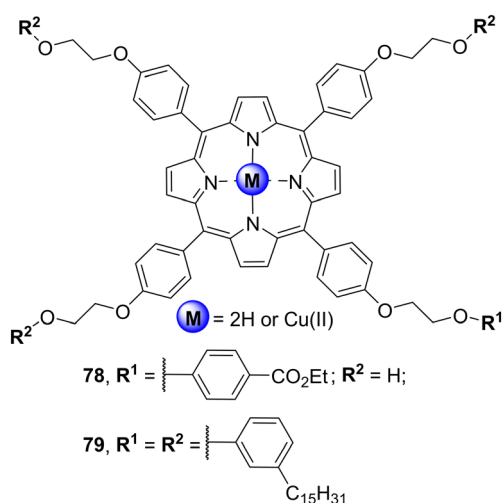
This journal is © The Royal Society of Chemistry 2024

*Catal. Sci. Technol.*, 2024, **14**, 2352–2389 | **2375**

degradation rate is achieved after 180 min with triethanolamine as an electron donor under solar light irradiation. The presence of electron donors enhances the efficiency of the degradation process by regenerating neutral hemin from its oxidized form. The neutral hemin can then absorb white light, undergo excitation, and promote a new cyclic process.[164]

MO, due to its toxicity in water, is frequently used in photodegradation studies.[171] Rahimi and co-workers[165] reported the photodegradation of 85% of MO using ZnO nanorods with tin(IV) porphyrin derivative Sn22Cl$_2$ after white light irradiation for 240 min. It was found that $O_2^{\bullet-}$ is the principal species responsible for the photodegradation of MO.

### 7.3. CdS nanocomposites

Cadmium sulphide CdS nanocomposites[172,173] are an emerging class of materials used in photocatalysis. Various research groups[174] used the free-base H$_2$22 (Fig. 30) to prepare CdS nanocomposites used to degrade RhB. It is important to highlight that the photodegradation of RhB with H$_2$22–CdS was more efficient under solar light irradiation than with UV light. The photocatalyst was reused five times without loss of its stability.[174]

### 7.4. Porphyrin–polyoxometalate hybrid materials

Polyoxometalates (POMs) are inorganic metal oxide clusters with remarkable properties. They already have been applied in photocatalysis, electrochemistry, photochromic materials, among others.[175,176] Their possible recuperation and reusability make them appealing photocatalysts for the oxidation of organic compounds.[175–177] In 2014, Rabbani and co-workers[178] reported the synthesis of an organic–inorganic framework where H$_2$3 (Fig. 2) was immobilized on the surface of the polyoxometalate
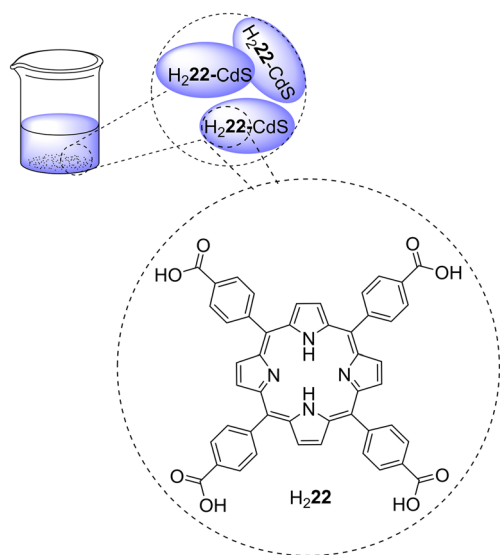
H$_3$PMo$_{12}$O$_{40}$. The photocatalytic activity of the hybrid material H$_2$3–H$_3$PMo$_{12}$O$_{40}$ regarding the photodegradation of MB in water under white light irradiation was evaluated and the results confirmed that its efficiency for MB degradation is higher than bare H$_3$PMo$_{12}$O$_{40}$. These hybrid materials are, thus, a good alternative for MB photodegradation in an aqueous medium.

### 7.5. Porphyrin–Bi$_2$MoO$_6$ composites

The photocatalytic performance of Bi$_2$MoO$_6$ for water splitting and degradation of organic compounds under visible-light irradiation is well known.[179] However, Bi$_2$MoO$_6$ only absorbs white light in the 420–500 nm region. To extend its absorption range to use the sunlight fully, Zhang and co-workers[180] introduced different amounts of Cu22 (Fig. 8) into Bi$_2$MoO$_6$ and studied its influence in the photodegradation of RhB. As expected, the resulting composite Cu22/Bi$_2$MoO$_6$ revealed enhanced photocatalytic activity, which can be attributed to the broadened absorption spectrum as well as the increased charge separation rate in the composite. It is important to highlight that the amount of Cu22 loaded into Bi$_2$MoO$_6$ is an important factor for the photocatalytic activity of the composite since above a certain fraction of porphyrin/Bi$_2$MoO$_6$ a decrease of the photocatalytic activity was observed. This result can be explained by the fact that more active reaction sites on the surface of Bi$_2$MoO$_6$ become occupied. The photocatalyst can be reused for five cycles without loss of activity.

### 7.6. Porphyrin–bismuth ferrite hybrids

Condorelli and co-workers[181] functionalized multiferroic bismuth ferrite (BFO) with porphyrin H$_2$22 (Fig. 8) and the resulting hybrid showed an enhanced photocatalytic activity for the degradation of MB and RhB when compared with bare BFO. The photocatalytic studies were performed in water under simulated solar light irradiation. This hybrid was reused up to four cycles without loss of activity.

### 7.7. Magnetic nanoparticles

Kim and co-workers[182] reported the use of water-soluble magnetic nanoparticles functionalized with a Pt(II) 5,15-bis(carboxyphenyl)porphyrin (Pt80, Fig. 31 and 32) as a
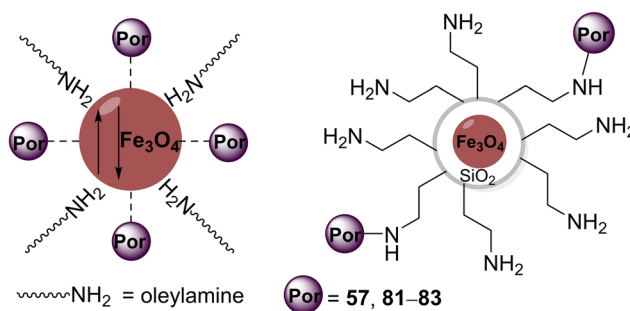


**Fig. 30** Representation of CdS nanocomposites modified with H$_2$22 for the photodegradation of dyes.



**Fig. 31** Representation of magnetic nanoparticles–porphyrin hybrids used in this sub-section.

2376 | Catal. Sci. Technol., 2024, 14, 2352–2389

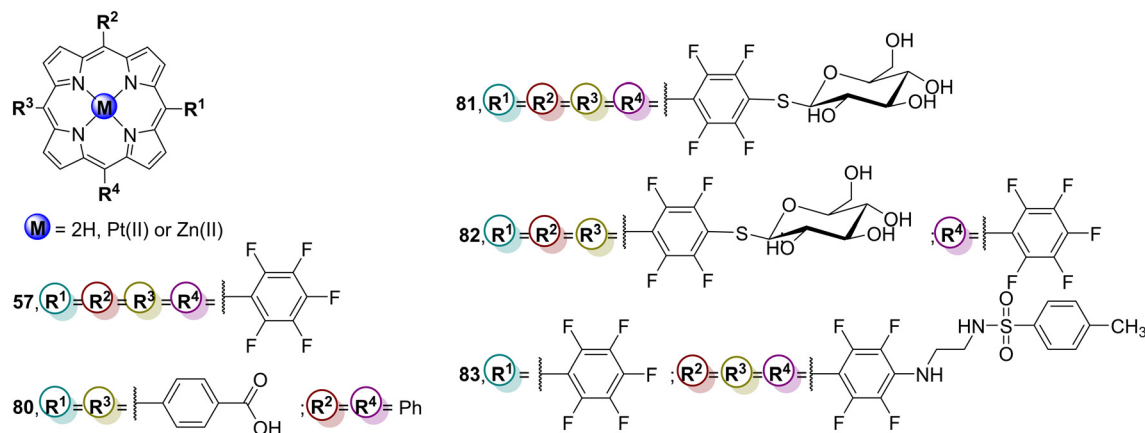This journal is © The Royal Society of Chemistry 2024

**Fig. 32** Representation of the silica magnetic nanoparticles functionalized with $H_2$57, Pt80 $H_2$81, $H_2$82 and Zn83.

catalyst for the photodegradation of 2,4,6-TCP in aqueous media under white light irradiation. After immobilization on the magnetic nanoparticles, porphyrin Pt80 maintains its optical and functional properties along with a high singlet oxygen quantum yield. When irradiated with white light, the excited nanoparticles convert $^3O_2$ into $^1O_2$ and other ROS that are responsible for the degradation of 2,4,6-TCP. Despite their high solubility in water, the magnetic property of the microstructure allows its recovery and reuse up to seven cycles by applying a magnetic field.

Tomé and co-workers[183] developed silica core–shell magnetic nanoparticles (NP) functionalized with three different porphyrins, $H_2$57, $H_2$81, and $H_2$82 (Fig. 32) and assessed their ability as photocatalysts for the degradation of 17β-estradiol. All non-immobilized porphyrins ($H_2$57, $H_2$81, and $H_2$82) could achieve complete degradation of 17β-estradiol after 8 h of white light irradiation. However, when immobilized in magnetic nanoparticles, $H_2$82–NP could induce a complete degradation of the hormone, whereas $H_2$57–NP and $H_2$81–NP could only achieve 50% degradation after the same time of irradiation.

In 2021, Simões and co-workers[184] developed a silica coated nanomagnet porphyrin hybrid and compared the ability of the Zn83–nanomagnet hybrid (Fig. 32) as a photocatalyst for the degradation MO with that of non-immobilized porphyrins $H_2$83 and Zn83. The photocatalytic assays were performed under white light irradiation in the presence of hydrogen peroxide. After 270 min of irradiation, complete degradation of the pollutant was achieved by using

non-immobilized Zn83 or the Zn83–nanomagnet hybrid. In the absence of $H_2O_2$, 60% of MO was degraded when the Zn83–nanomagnet was used, whereas only 10% degradation was observed with the non-immobilized Zn83 and $H_2$83.

### 7.8. Metal-free graphite-like carbon nitride (g-C$_3$N$_4$)

Regarding this type of support, Liu and co-workers[28] published a review exploring the ability of graphitic carbon nitride modified with porphyrins, phthalocyanines or other similar dyes as photocatalysts for $H_2$ evolution, $CO_2$ reduction and pollutant degradation. Also, Raizada and co-workers[185] reviewed the removal of contaminants from wastewater through photocatalysis by non-noble metals doped on this support. Concerning this last application, they mentioned the work of Zhu and co-workers[186] where the hybridization of graphite-like carbon nitride (g-C$_3$N$_4$) with Cu22 (Fig. 8) is explored in the photodegradation of phenol under white light (Table 14). The Cu22 molecules are easily assembled on the surface of g-C$_3$N$_4$ nanosheets through covalent bond and intermolecular interactions, such as electrostatic interaction and π–π stacking interactions between Cu22 and the graphene nanosheets. When compared with pure g-C$_3$N$_4$, Cu22–g-C$_3$N$_4$ showed higher photocatalytic activity under white light irradiation. The enhancement of the photocatalytic activity derives from the efficient electron transfer process from the photoexcited Cu22 molecules to g-C$_3$N$_4$.

**Table 14** Porphyrin–metal-free graphite-like carbon nitride (g-C$_3$N$_4$) for the degradation of several pollutants

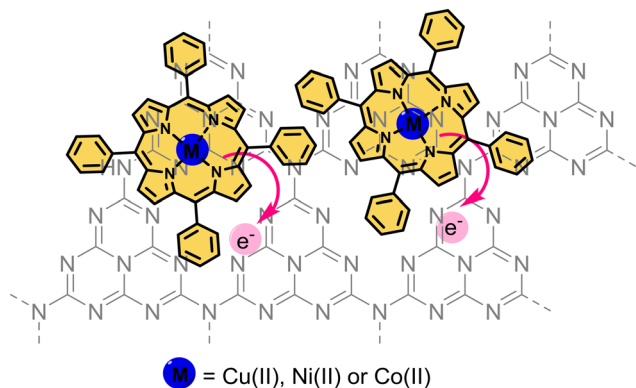| Por | Pollutant | Irradiation time (min) | Light source | Degradation rate (%) | Recycle | Ref. |
|---|---|---|---|---|---|---|
| Cu22 | Phenol | 480 | Visible ($\lambda$ > 420 nm) | 25 | — | 186 |
| $H_2$22 | RhB | 60 | Visible ($\lambda$ > 380 nm) | 100 | 4 cycles (0% loss) | 187 |
| Cu3 | | 90 | Visible ($\lambda$ > 420 nm) | 69 | — | 188 |
| Ni3 | | | | 93 | | |
| Co3 | | | | 100 | | |
| Fe22 | | 120 | | 98 | | 189 |

This journal is © The Royal Society of Chemistry 2024

*Catal. Sci. Technol.*, 2024, **14**, 2352–2389 | **2377**

**Fig. 33** Representation of the hybrid structures of Cu3–, Ni3–, and Co3–g-C$_3$N$_4$.

Cai and co-workers[187] adsorbed the metal-free porphyrin H$_2$22 (Fig. 8) on g-C$_3$N$_4$ (through π–π stacking interactions) and the resulting hybrid revealed a doubled photocatalytic activity for RhB degradation (Table 14) when compared with bare g-C$_3$N$_4$. The immobilization of the porphyrin on g-C$_3$N$_4$ broadened its absorption spectrum and improved its photocatalytic activity.

Zhu and co-workers[188] developed a series of Cu3, Ni3, and Co3 modified g-C$_3$N$_4$ (Fig. 33) in order to assess the photocatalytic degradation of RhB. Co3–g-C$_3$N$_4$ exhibited the highest photocatalytic efficiency reaching a total degradation (99.8%) after 90 min of irradiation, followed by Ni3–g-C$_3$N$_4$, Cu3–g-C$_3$N$_4$, and pristine g-C$_3$N$_4$. The addition of metalloporphyrins, particularly Co3, is favourable for the interfacial charge transfer process, by minimizing the electron–hole recombination, enhancing the photodegradation efficiency of RhB.

Moreover, Li and co-workers[189] constructed a visible light-driven PCN-222 g-C$_3$N$_4$ heterojunction using Fe22 (Fig. 8) to decompose RhB and ofloxacin. The composite 1.0 wt% PCN-222–g-C$_3$N$_4$ showed the best photocatalytic activity for ofloxacin and RhB degradation under white light irradiation. The photocatalytic activity of this composite was ca. 3 times higher than that of pristine g-C$_3$N$_4$, reaching ~98% after irradiation for 120 min. This enhanced photocatalytic activity was attributed to the extended light response range, fast generation, efficient separation of the photogenerated carrier and enhanced adsorption capacity of organic contaminants. The prepared PCN-222–g-C$_3$N$_4$ photocatalyst exhibited excellent recyclability and can be reused four times without activity loss.

### 7.9. Layered hydroxides

Recently, Liu and co-workers[190] constructed an organic–inorganic hybrid palladium porphyrin/NiFe-LDH (Pd22/NiFe-LDH and H$_2$22/NiFe-LDH) (Fig. 16) and evaluated its ability as a photocatalyst for the degradation of tetracycline under white light irradiation. The results showed that Pd22/NiFe-LDH is more efficient, achieving a degradation rate of 91% when compared to H$_2$22/NiFe-LDH (74%) and bare NiFe-LDH
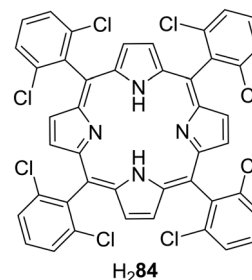


**Fig. 34** Porphyrin H$_2$84 bearing 2,6-dichlorophenyl groups.

(67%). This enhanced photocatalytic activity is due to the higher production of O$_2$$^{·-}$ and HO$^·$.

### 7.10. Lignin

Calvete, Pereira and co-workers[191] described the photocatalytic degradation of trimethoprim and sulfamethoxazole, highly prescribed antibiotics, using a white mercury lamp, air as an oxidant and a photocatalyst based on the encapsulation of stable *meso*-tetra(2,6-dichlorophenyl) porphyrin (H$_2$84) (Fig. 34) into acetylated lignin nanoparticles. The authors could achieve almost compete degradation (99 ± 1%) of trimethoprim and sulfamethoxazole after 120 min and 240 min, respectively. The combination of these antibiotics is usually known as cotrimoxazole (also an antibiotic) and for that reason the authors also accessed the ability of this nanoparticle for its photodegradation. After 120 min of irradiation, it was possible to achieve the same photocatalytic rate. It is important to mention that there was no degradation in the dark or just in the presence of the lignin nanoparticles (without porphyrin) for these antibiotics. The photocatalyst could be reused up to 10 times without significant loss of activity (~5% loss).

### 7.11. Agarose

Hou and co-workers[192] developed a Tb-porphyrin (Tb22Cl) (Fig. 16) aerogel using agarose as a building block for the photocatalytic degradation of RhB. After 75 min under visible light irradiation ($\lambda > 420$ nm), it was possible to achieve 61% of degradation.

## 8. Immobilized porphyrins on modified inorganic supports

### 8.1. TiO$_2$–Zr-MOF

In 2017, Feng and co-workers[193] developed an efficient catalyst composed of a zirconium-based porphyrin–MOF PCN-222 immobilized onto the surface of TiO$_2$ nanoparticles *via* 4-mercaptopyridine, which is axially bonded to the metal centre of porphyrin Zn22 (Fig. 35). The composite was effective for RhB degradation under white light irradiation due to the synergistic effect of its components, being able to degrade 75% of RhB after irradiation for 270 min. Fluorescence spectroscopy studies confirmed that the enhanced photocatalytic activity resulted from the electron
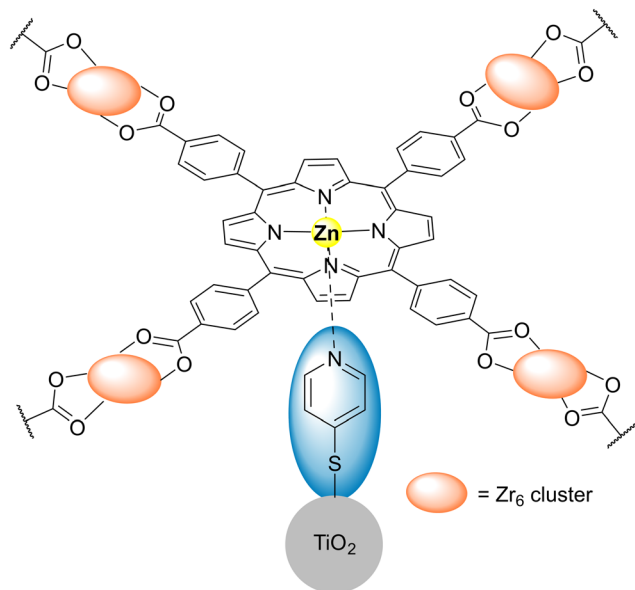
2378 | Catal. Sci. Technol., 2024, 14, 2352–2389

This journal is © The Royal Society of Chemistry 2024

Fig. 35 Representation of zirconium-based porphyrin Zn**22**–MOF PCN-222 immobilized onto TiO$_2$ nanoparticles *via* 4-mercaptopyridine.

transfer from PCN-222 to TiO$_2$ and efficient charge separation. Moreover, the composite showed excellent stability and recyclability.

### 8.2. Doped TiO$_2$

Huang and co-workers[194] modified La-doped TiO$_2$ with Cu**85** (Fig. 36) and assessed its ability as a photocatalyst for MO degradation. Under white light, the photocatalytic activity of La-TiO$_2$ is higher than bare TiO$_2$ and it increases with the sensitization by Cu**85**.

In another study,[195] it was observed that the maximum degradation of 4-NP was obtained when the free-base H$_2$**23** (Fig. 11) was used with TiO$_2$ doped with Fe(III). This catalyst showed an enhanced photocatalytic activity compared with TiO$_2$ or Fe–TiO$_2$, causing a complete degradation of 4-NP after irradiation for 45 min. Finally, the photocatalyst can be recycled at least three times without loss of activity.

The photocatalytic activity of micro and nanostructures of TiO$_2$ impregnated with complexes of metalloporphyrin M**23** (M = Mn(III), Fe(III), Ni(II), and Cu(II)) (Fig. 11) under UV light irradiation was also evaluated.[196] The highest photocatalytic activity was achieved with impregnated micro-TiO$_2$ catalysts, which indicates an improvement of the electron transfer process between the sensitizer and TiO$_2$ compared with the nano-crystalline structure. Cu**23** revealed excellent performance when used in the micro-anatase composite.[196]

Rahimi and co-workers[197] used the free-base porphyrin H$_2$**22** to sensitize vanadium-doped TiO$_2$. Two photocatalysts were prepared: one containing an ester-like linkage formed between a carboxyl group of H$_2$**22** and a hydroxyl group of the TiO$_2$ surface (H$_2$**22**–V-TiO$_2$) and the other an amide bond (H$_2$**22**-CO–NHR-V-TiO$_2$) (Fig. 37). These materials were used as catalysts for the photodegradation of MO in an aqueous
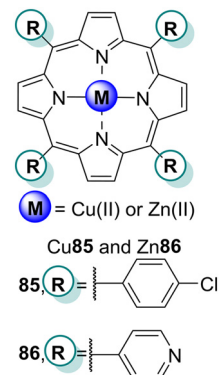


Fig. 36 Structure of the porphyrin **85** immobilized on La-doped TiO$_2$ and porphyrin used to prepare triad hybrid multilayers on quartz surfaces **86**.

solution under visible light irradiation. The photocatalytic activity of H$_2$**8**–V-TiO$_2$ was much higher than that of H$_2$**8**-CO–NHR-V-TiO$_2$ with rates of 95% and 62%, respectively, after irradiation for 180 min.

Yao and co-workers[198] modified nitrogen doped TiO$_2$ powder with metalloporphyrins Co**3**, Ni**3**, Co**55**, and Ni**55** (Fig. 2 and 16) and evaluated the photocatalytic ability of the resulting materials to degrade MB. Nitrogen-doped anatase powder (N-TiO$_2$) modified by each of the four metalloporphyrins exhibited higher degradation efficiency than the unmodified N-TiO$_2$. The results showed that Co**3**–N-TiO$_2$ and Co**55**–N-TiO$_2$ exhibited higher degradation efficiency than the corresponding nickel complexes Ni**3** and Ni**55**–N-TiO$_2$, with Co**3**–N-TiO$_2$ being the best photocatalyst with 94.1% degradation of MB after 180 min irradiation with white light. Additionally, the composites were reused up to four times without significant loss of activity.

Rahimi and co-workers,[199] and Abou-Gamra and co-workers[200] also used H$_2$**22** (Fig. 16) on Co-doped TiO$_2$ and regular TiO$_2$ and assessed the ability of the composites to degrade MB and RhB. The results using H$_2$**22**–Co-TiO$_2$ (ref. 199) and H$_2$**22**–TiO$_2$ (ref. 200) showed that these materials are more efficient than bare Co-TiO$_2$ and TiO$_2$, respectively, for the degradation of MB and RhB under white light. The sensitization of metal-doped TiO$_2$ enhances the photocatalytic activity due to the formation of O=C–O–Ti bonds that can function as an electron transfer channel, accelerating the electron injection to the CB of TiO$_2$. Moreover, the composites can directly use sunlight, allowing their use in wastewater treatment.

Rabbani and co-workers[201] synthesized an Ag-doped mesoporous TiO$_2$ (Ag-TiO$_2$) powder modified with Zn**22** (Fig. 16) and the composite was used to degrade 4-NP and MB. The results revealed that Zn**22**–Ag-TiO$_2$ has a higher activity than Ag-TiO$_2$ under white light but a lower activity under UV light irradiation. The higher activity of Ag-TiO$_2$ under UV light can be justified by the high band gap, being only activated under UV light. The presence of porphyrin molecules on its surface (Zn**22**–Ag-TiO$_2$) leads to a decrease

This journal is © The Royal Society of Chemistry 2024

*Catal. Sci. Technol.*, 2024, **14**, 2352–2389 | **2379**

of active sites for UV light absorption. Regarding the reusability of Zn**22**–Ag-TiO₂, it was verified that there were no significant changes in their photocatalytic activity for four cycles.

Rahimi and co-workers[202] used fluorine-doped TiO₂ (F-TiO₂) nanoparticles modified with H₂**22** or Zn**22** (Fig. 16) to photodegrade RhB. The photocatalytic assays were done under UV and white light irradiation. The results showed that, under white light, Zn**22**–F-TiO₂ and H₂**22**–F-TiO₂ are better catalysts than bare F-TiO₂. The O=C–O–Ti bonds formed between Zn**22** or H₂**22** and TiO₂ act as an electron transfer channel and accelerate the electron injection to the CB of F-TiO₂.

### 8.3. TiO₂–organic polymers

Considering that photocatalysts resulting from the association of porphyrins with either TiO₂ or organic polymers are very effective for the photodegradation of organic pollutants, in 2012, Qi and co-workers[203] prepared a fibrous polymer mat-supported Fe**3**Cl–TiO₂ and used it in the photodegradation of azo dyes. The photocatalyst could degrade MO and other azo dyes in up to 98.5% in 5 h. Even after four cycles, the degradation rate remains at 87.0%. These results could contribute to preparing a membrane photo-reactor for continuous wastewater treatment.

In 2016, Cantarella and co-workers[204] embedded TiO₂ modified with H₂**22** (Fig. 16) in poly(methyl methacrylate) (PMMA), aiming to obtain a photocatalyst with no need for recovery after water treatment. The photocatalyst was used in MB degradation and even after 8 cycles, its ability to degrade MB did not decrease. These PMMA materials are stable, cheap and can be prepared by simple methods and, thus, are considered a potential tool for removing organic pollutants from wastewater.

Qi and co-workers[205] supported a porphyrin-polyacrylonitrile fibre mat (Fig. 38) in TiO₂ and the resulting material (Fe**87**–PANC–TiO₂ mat) was used as a photocatalyst for methyl red degradation in an aqueous solution under white light. A *ca.* 75% methyl red degradation after irradiation for 120 min was reported. The photocatalyst could be recovered and reused up to 3 times but with a loss of 10% activity after each cycle.
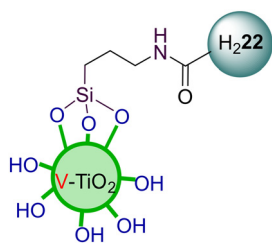
### 8.4. TiO₂–SiO₂

Charge-transfer catalysts of TiO₂–SiO₂, particularly Pt-modified TiO₂–SiO₂ catalysts,[206] have higher activity than bare TiO₂. Either TiO₂ or SiO₂ is widely used as an inorganic support for photocatalytic activity. However, their limitations require the immobilization of a photoactive molecule on the support. Using a TiO₂–SiO₂ composite modified with a photoactive porphyrin molecule enhances the photocatalytic activity. For that reason, Cai and co-workers[207] prepared TiO₂–SiO₂ modified with Zn(ɪɪ) carboxyphenyl porphyrins with different *para*-substituents to be used as photocatalysts for α-terpinene degradation. The photodegradation of α-terpinene with Zn**88**–, Zn**89**–, and Zn**90**–TiO₂–SiO₂ (Fig. 39) revealed that their photocatalytic activity was much higher than that of bare TiO₂–SiO₂ under white light irradiation. After irradiation for 50 min, the best photocatalyst was Zn**89**–TiO₂–SiO₂ (95.6% degradation), followed by Zn**90**–TiO₂–SiO₂ (84.1%) and Zn**88**–TiO₂–SiO₂ (76.9%).

Qian and co-workers,[208] using the layer-by-layer method, constructed triad hybrid multilayers on quartz surfaces formed by zinc *meso*-tetra(4-pyridyl)porphyrin (Zn**86**) (Fig. 35) and pyridine-functionalized TiO₂ (TiO₂-Py) nanoparticles connected by Pd(ɪɪ) ions. The photocatalytic activity of the nanocomposites for the degradation of MO was assessed in aqueous media under irradiation with visible light ($\lambda > 420$ nm) at room temperature. After 48 h, the photocatalyst could degrade 50% of MO, but a complete degradation was achieved only after 8 days. When reused, the photocatalytic activity decreased by about 10%.

### 8.5. Surface-modified TiO₂ nanoparticles

Roques-Carmes and co-workers[209] coupled porphyrin derivatives H₂**91** and chlorin H₂**92** to surface-modified TiO₂ nanoparticles (Fig. 40) and the photodegradation of MB and MO was used to assess the photocatalytic efficiency of the prepared catalysts under simulated solar and visible light. Porphyrin H₂**91** and chlorin H₂**92** serve as visible–light antennas, thus extending the photoresponse of the hybridized TiO₂ nanoparticles towards the visible light region.
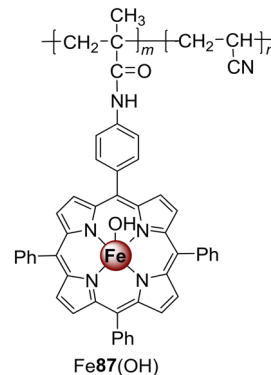


**Fig. 37** Representation of vanadium doped TiO₂ modified with H₂**22** using a 3-aminopropylsilane bridging unit.



**Fig. 38** Fe**87**(OH) supported in a polyacrylonitrile fibre mat.

**2380** | *Catal. Sci. Technol.*, 2024, **14**, 2352–2389

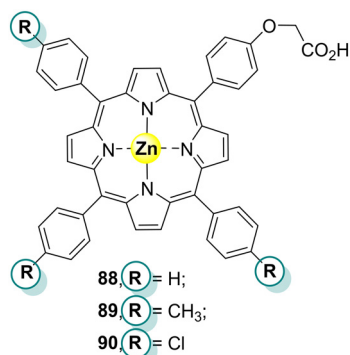This journal is © The Royal Society of Chemistry 2024

**Fig. 39** Zn(II) porphyrins immobilized on TiO$_2$–SiO$_2$.

Enhanced photocatalytic efficiency towards the degradation of MB and MO was observed for the (3-aminopropyl) triethoxysilane (APTES)-modified nanosystems, especially for TiO$_2$–APTES–H$_2$**92** that lead to 91% degradation of MO under visible light irradiation. Similar nanoparticles prepared using SiO$_2$ instead of TiO$_2$ revealed low photocatalytic activity when compared with those with TiO$_2$.

### 8.6. TiO$_2$ nanotubes–reduced graphene oxide

Wan and co-workers[210] fabricated ternary composites of TiO$_2$ nanotubes (TiNT) with reduced graphene oxide (rGO) and porphyrin H$_2$**22** and assessed their capability as photocatalysts for the degradation of MB under white light. The experimental results showed more than 92% of MB degradation, about 4.3 times higher than the pure TiNT. The authors suggest a mechanism in which rGO acts as the adsorbent, electron acceptor, and transporter to increase the separation of the electron–hole pairs, accelerating the decomposition of organic pollutants. In turn, porphyrin has a critical role in capturing photons and expanding the absorption wavelength to the visible light region.

The same authors also reported the formation of a similar porphyrin/rGO–TiNT nanocomposite but using Cu**22**.[211] In this case, experimental results showed a photodegradation of more than 95% MB, which is about 5 times higher than that of the pure TiNT.

### 8.7. TiO$_2$–graphene

Rahimi and co-workers[212] prepared a TiO$_2$–graphene nanocomposite pillared with porphyrin Sn**3**(OH)$_2$ (Fig. 41) and used this material as a photocatalyst to degrade MO in an aqueous solution under white light irradiation. This pillared graphene–TiO$_2$–Sn**3**(OH)$_2$ allowed the complete photocatalytic degradation of MO in 180 min. It was determined that the OH radical is the main active species responsible for the degradation of MO.

### 8.8. TiO$_2$–MOF

Lü, Zhu and co-workers[213] published a series of 2D M**22** (M = Cu(II), Zn(II), Co(II), and Mn(II))–MOFs/TiO$_2$ (Fig. 16) binary nanocomposites and their ability as photocatalysts for the
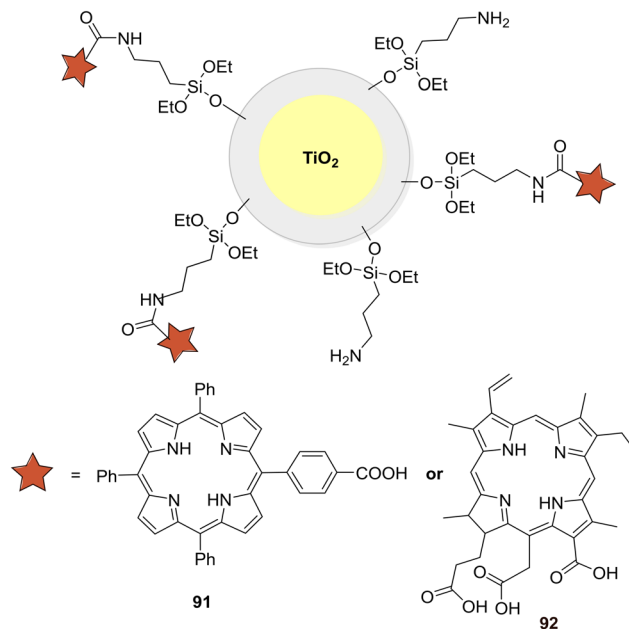


**Fig. 40** Representation of the TiO$_2$–APTES–PS NPs.

degradation of RhB under visible light irradiation. After 30 min of irradiation, the best photocatalyst was Cu**22**–MOF/ TiO$_2$ (97%) followed by Zn**22**–MOF/TiO$_2$ (88%), Co**22**–MOF/ TiO$_2$ (65%) and Mn**22**–MOF/TiO$_2$ (57%).

### 8.9. Fe$_3$O$_4$@ZrO$_2$

Ghafuri and co-workers[214] synthesized a mixture of inorganic supports of Fe$_3$O$_4$@ZrO$_2$ derivatized with H$_2$**22**, Zn**22**, and Co**22** as well as the free-base porphyrin H$_2$**93**, and its metal complexes Zn**93** and Co**93** (Fig. 42). The photocatalytic properties of materials with carboxy porphyrins H$_2$**22**–, Zn**22**–, Co**22**–Fe$_3$O$_4$@ZrO$_2$ and 2-naphthyl esters, H$_2$**93**, Zn**93**, and Co**93**–Fe$_3$O$_4$@ZrO$_2$ for the degradation of MB were evaluated and compared. The results showed that carboxy and 2-naphthyl benzoate derivatives lead to different degradation rates, as shown in Fig. 42.

The results of the photodegradation of MB allowed us to conclude that: a) the presence of a porphyrin increases the
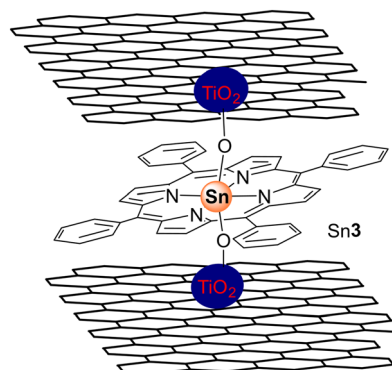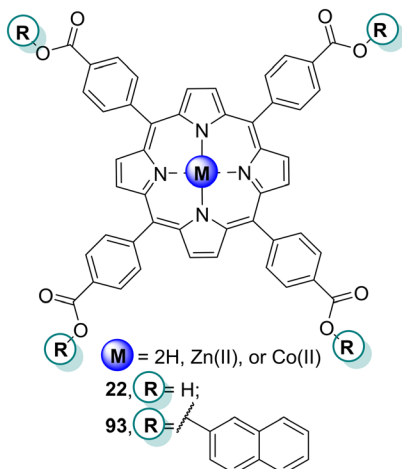


**Fig. 41** Representation of Sn**3** functionalized pillared graphene–TiO$_2$.

This journal is © The Royal Society of Chemistry 2024

*Catal. Sci. Technol.*, 2024, **14**, 2352–2389 | **2381**

| Catalyst | MB degradation rate (%) |
|---|---|
| No catalyst | 10 |
| $Fe_3O_4@ZrO_2$ | 24 |
| $H_2$**22**–$Fe_3O_4@ZrO_2$ | 60 |
| Zn**22**–$Fe_3O_4@ZrO_2$ | 95 |
| Co**22**–$Fe_3O_4@ZrO_2$ | 98 |
| $H_2$**93**–$Fe_3O_4@ZrO_2$ | 57 |
| Zn**93**–$Fe_3O_4@ZrO_2$ | 65 |
| Co**93**–$Fe_3O_4@ZrO_2$ | 73 |

M = 2H, Zn(II), or Co(II)
**22**, R = H;
**93**, R =

**Fig. 42** Porphyrins used to sensitize $Fe_3O_4@ZrO_2$ and the MB photodegradation rates under white light irradiation for 3 h.

activity of the inorganic support; b) carboxy porphyrin derivatives are more active than the corresponding 2-naphthyl esters; c) Zn(II) and Co(II) porphyrins are more active than the corresponding free-base porphyrins; d) Co(II) porphyrins are more active than Zn(II) porphyrins.

### 8.10. SiO₂–ZnO

Sobral and co-workers[215] reported the chemical modification of the inorganic support SiO₂–ZnO (prepared by mixing 70% SiO₂ and 30% ZnO) with *meso*-tetrakis(*p*-aminophenyl) porphyrin ($H_2$**65**) using 3-glycidoxypropyltrimethoxysilane as a coupling agent. This material (Fig. 43) was used as a catalyst for the photodegradation of naphthol black blue under direct sunlight and white light. A 60% degradation of naphthol black blue was achieved with both types of light but at 120 and 180 min of irradiation time, respectively. Moreover, the catalyst was found to be reusable.

### 8.11. SiO₂ (quartz)–MOF

Mn**22**–MOF (Fig. 44) with catalytically active sites was built upon functionalized quartz glass surfaces using a layer-by-layer self-assembly method.[216] With a porous reticular structure, the Mn**22**–MOF films, in the presence of $H_2O_2$, could efficiently degrade 90% of MB under visible-light irradiation for 180 min.
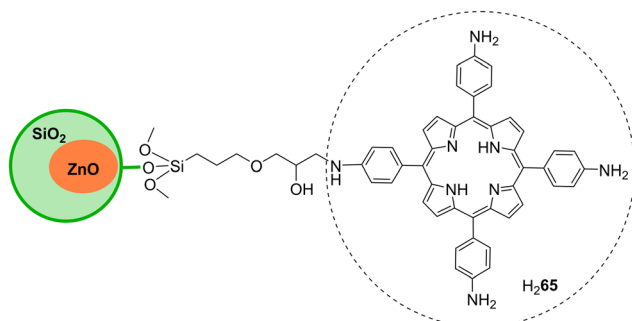
**Fig. 43** Representation of $H_2$**65** immobilized on SiO₂–ZnO.

The catalyst is easily recovered, and after being reused five times, it can still degrade over 85% of MB.

### 8.12. Reduced graphene oxide–Ag nanoparticles

Sun and co-workers[217] reported the preparation of organic/ inorganic ternary nanohybrids constituted by a Sn(IV) porphyrin (Sn**62**Cl₂), Ag nanoparticles, and reduced graphene oxide (Fig. 45). The nanohybrids revealed superior catalytic activity for the degradation of RhB under white light, reaching 42% degradation in 3 h. Moreover, the ternary nanohybrid was also an active catalyst for reducing 4-NP to 4-aminophenol by NaBH₄: 97% of 4-NP was reduced within 17 min.

More recently, La, Nguyen and co-workers[218] developed the same hybrid (*g*-C₃N₄/Ag nanoparticles) using the porphyrin $H_2$**22** (Fig. 16). The authors evaluated the ability of the hybrid in the photocatalytic degradation of RhB after exposure to sunlight. The authors could achieve a maximum of 97% degradation of RhB using $H_2$**22**-*g*-C₃N₄/Ag which was better than using bare *g*-C₃N₄/Ag (79%) and $H_2$**22** (89%). The incorporation of $H_2$**22** in the hybrid allowed its recovery and reusability for four times with a 12% loss of activity. The authors identified $O_2^{\bullet-}$ and HO$^\bullet$ as the species responsible for the photodegradation mechanism.

### 8.13. S or P and N co-doped graphene quantum dots

In 2016, Mahyari and co-workers[219] explored the properties of Fe(III) *meso*-tetra(4-sulfonatophenyl)porphyrin (Fe**1**Cl) (Fig. 2) supported on S and N co-doped graphene quantum dots (GQDs) as a recyclable heterogeneous photocatalyst for aerobic oxidation of benzyl alcohols under white light irradiation. The synthesized photocatalyst revealed high conversion rates and selectivity for the oxidation of benzyl alcohols to the corresponding aldehydes in water at room temperature. This study provided a promising efficient photocatalyst, recyclable up to 5 cycles without activity loss,
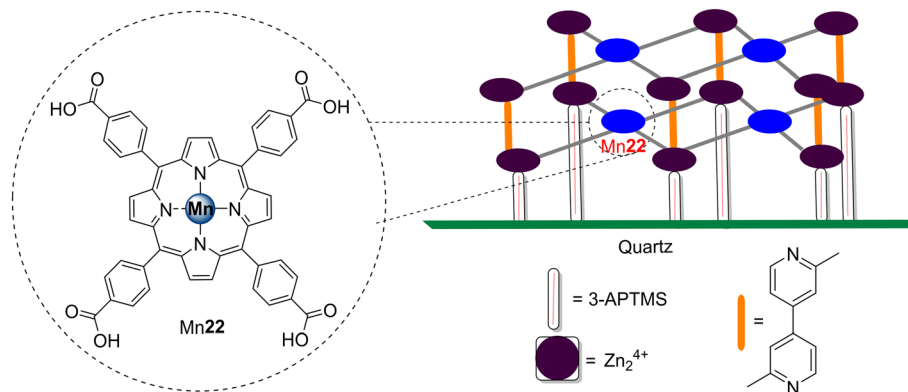
**Fig. 44**  Mn**22**–MOF films immobilized on quartz glass.

to be used in wastewater treatment. The same authors[220] extended this study to P and N co-doped graphene quantum dots modified with cobalt(II) porphyrin **1** (Co**1**). The composite also showed high performance and recyclability as



**Fig. 45**  Representation of Sn**62**Cl$_2$, AgNPs, on rGO.

a heterogeneous photocatalyst in the aerobic oxidation of benzyl alcohols under white light irradiation.

### 8.14. BiVO$_4$–graphene nanocomposites

Rahimi and co-workers[221] prepared a composite of BiVO$_4$–graphene impregnated with porphyrin H$_2$**22** (Fig. 16) and evaluated its ability as a photocatalyst to degrade MO in aqueous solution under white light irradiation. The introduction of graphene in the BiVO$_4$ composite enhanced its photocatalytic activity up to 2 times. Incorporation of porphyrin H$_2$**22** allowed the photocatalytic activity of the resulting nanocomposite to be improved under white light irradiation. After the photosensitization with porphyrin, the photocatalytic activity of the resulting H$_2$**22**–BiVO$_4$–graphene nanocomposite increased 3.5 times and allowed the degradation of 78%, 87%, and 97% of MO at 30 min, 60 min, and 150 min of irradiation, respectively.

### 8.15. Bi$_2$WO$_6$–reduced graphene oxide

Bismuth tungstate-based materials (Bi$_2$WO$_6$) have been widely used as photocatalysts in environmental, energy, and biological fields, including water treatment, air purification, and inactivation of bacteria.[222,223]

Huang and co-workers[224] constructed a ternary H$_2$**22**/rGO/Bi$_2$WO$_6$ Z-scheme heterojunction and evaluated its photocatalytic activity. The composite revealed enhanced photocatalytic activity towards the degradation of the antibiotic tetracycline under white light (removal of 83.6%) when compared with pure Bi$_2$WO$_6$, rGO/Bi$_2$WO$_6$, and H$_2$**22**/Bi$_2$WO$_6$. Recycling experiments with the composite showed that the tetracycline removal efficiency remained 79.3% after five cycles.

## 9. Summary and outlook

This work outlines the significant advances in the photocatalytic oxidation of water pollutants using simple porphyrin derivatives as well as porphyrins linked to a range of organic or inorganic materials, namely polymers, fibres, carbon nanostructures, ZnO, SiO$_2$, and TiO$_2$ (or mixtures of these supports), under UV, visible, and/or solar light irradiation. The presence of different
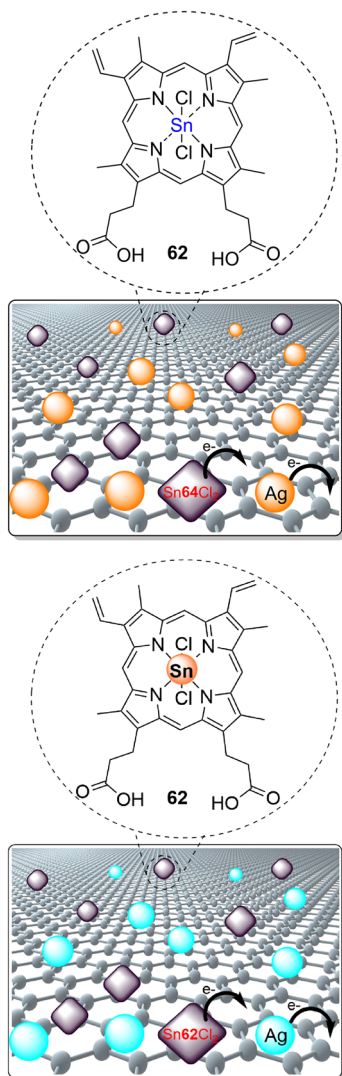
This journal is © The Royal Society of Chemistry 2024

Catal. Sci. Technol., 2024, **14**, 2352–2389 | **2383**

metals in the porphyrin core resulted in different photocatalytic activities, with the highest degradation rates being achieved with Cu(II) porphyrin derivatives.

Moreover, by sensitizing $TiO_2$ or $SiO_2$ supports with porphyrins, the photocatalytic activity was greatly enhanced due to the reduction of the material's band gap and the absorption of visible light. This sensitization could be made through covalent or non-covalent interactions. It is important to highlight that the photocatalytic mechanism is based on the excitation of the porphyrin followed by electron transfer to the CB of the support. The photogenerated holes and the excited electrons can react with $O_2$ or $H_2O$ to form reactive oxygen species, which will degrade the pollutant. In some cases, the addition of $H_2O_2$ is necessary to obtain high rates of pollutant degradation.

The light source (UV, visible, or solar light) is also an important parameter. When solar/white light is used, the support can also be excited along with the porphyrin, but only a small or no excitation of the porphyrin moiety occurs with UV light. The use of solar light is considered a huge advantage in photocatalysis since it reduces costs and takes advantage of all solar spectrum. It is also important to mention that almost all photocatalysts discussed here are reusable, with no significant loss of activity in most cases, and in some cases, the photocatalyst is specific for a selected pollutant. While the presented photocatalytic studies highlighted in this review are promising, there is a noticeable absence of research on identifying the degradation products.

This review shows that the scientific community is closer to finding effective methods for the degradation of pollutants that are difficult to remove from water. However, scale-up studies with the photocatalysts' production and practical applications (in the field) of this technology are (urgently) needed.

## Abbreviations

| | |
|---|---|
| 2,4,6-TCP | 2,4,6-Trichlorophenol |
| 2,4,6-TNT | 2,4,6-Trinitrotoluene |
| 2,4-DCP | 2,4-Dichlorophenol |
| 2,6-DBP | 2,6-Di-*t*-butylphenol |
| 4-CP | 4-Chlorophenol |
| 4-NP | 4-Nitrophenol |
| AO | Acridine orange |
| ATRP | Atom transfer radical polymerization |
| BFO | Bismuth ferrite |
| CdS | Cadmium sulphide |
| CB | Conduction band |
| CEES | 2-Chloroethyl ethyl sulfoxide |
| CEESO | 2-Chloroethyl ethyl sulfoxide |
| CTAB | Cetyltrimethylammonium bromide |
| DMF | Dimethylformamide |
| GO | Graphene oxide |
| LCST | Lower critical solution temperature |
| MB | Methylene blue |
| MO | Methyl orange |
| MOF | Metal–organic framework |

| | |
|---|---|
| NIR | Near-infrared |
| PAM | Poly(*N*-isopropylacrylamide) |
| PAN | Polyacrylonitrile |
| PCP | pentachlorophenol |
| PMMA | Poly(methyl methacrylate) |
| POM | Polyoxometalate |
| Por | Porphyrin |
| RhB | Rhodamine B |
| ROS | Reactive oxygen species |
| SA | Salicylic acid |
| SSA | 2-Hydroxy-5-sulfosalicylic acid |
| TiNT | Titanate nanotube |
| TPP | *meso*-Tetraphenylporphyrin |
| UV | Ultra-violet |
| VB | Valence band |

## Conflicts of interest

There are no conflicts of interest to declare.

## Acknowledgements

## References

1 T. Phani Madhavi, M. Srimurali and K. Nagendra Prasad, *J. Environ. Res. Dev.*, 2014, **8**, 890–894.
2 J. Shortle, *Water Econ. Policy*, 2017, **03**, 1771004.
3 H. Safardoust-Hojaghan and M. Salavati-Niasari, *J. Cleaner Prod.*, 2017, **148**, 31–36.
4 A. Tewari, A. Dubey and P. Singh, *J. Environ. Res. Dev.*, 2012, **6**, 609–615.
5 X. Zhou, Y. Li and Y. Zhao, *RSC Adv.*, 2014, **4**, 15620–15629.
6 V. K. Gupta, I. Ali, T. A. Saleh, A. Nayak and S. Agarwal, *RSC Adv.*, 2012, **2**, 6380.
7 J. Schütz, E. Rydin and B. J. Huser, *Lake Reservoir Manage.*, 2017, **33**, 152–162.
8 X. Yan Xue, R. Cheng, L. Shi, Z. Ma and X. Zheng, *Environ. Chem. Lett.*, 2017, **15**, 23–27.

**2384** | *Catal. Sci. Technol.*, 2024, **14**, 2352–2389

This journal is © The Royal Society of Chemistry 2024

9 J. M. Dickhout, J. Moreno, P. M. Biesheuvel, L. Boels, R. G. H. Lammertink and W. M. de Vos, *J. Colloid Interface Sci.*, 2017, **487**, 523–534.

10 M. Herraiz-Carboné, S. Cotillas, E. Lacasa, C. Sainz de Baranda, E. Riquelme, P. Cañizares, M. A. Rodrigo and C. Sáez, *Sci. Total Environ.*, 2021, **797**, 149150.

11 W. Trösch, *Technology Guide: Principles - Applications - Trends*, 2009, pp. 394–397.

12 F. Petronella, A. Truppi, C. Ingrosso, T. Placido, M. Striccoli, M. L. Curri, A. Agostiano and R. Comparelli, *Catal. Today*, 2017, **281**, 85–100.

13 H. Rajbongshi and D. Kalita, *J. Nanosci. Nanotechnol.*, 2020, **20**, 5885–5895.

14 R. K. Vital, N. K. V. Saibaba, K. B. Shaik and R. Gopinath, *J. Biorem. Biodegrad.*, 2016, **7**, 1000317.

15 D. Pathania, S. Sharma and P. Singh, *Arabian J. Chem.*, 2017, **10**, S1445–S1451.

16 P. Fageria, S. Gangopadhyay and S. Pande, *RSC Adv.*, 2014, **4**, 24962–24972.

17 Y. Li, T. Li, J. Tian, X. Wang and H. Cui, *Part. Part. Syst. Charact.*, 2017, **34**, 1700127.

18 B. Cabir, M. Yurderi, N. Caner, M. S. Agirtas, M. Zahmakiran and M. Kaya, *Mater. Sci. Eng. B: Solid-State Mater. Adv. Technol.*, 2017, **224**, 9–17.

19 K. P. Priyanka, S. Sankararaman, K. M. Balakrishna and T. Varghese, *J. Alloys Compd.*, 2017, **720**, 541–549.

20 A. Rey, P. García-Muñoz, M. D. Hernández-Alonso, E. Mena, S. García-Rodríguez and F. J. Beltrán, *Appl. Catal., B*, 2014, **154–155**, 274–284.

21 J. Sun, L. Qiao, S. Sun and G. Wang, *J. Hazard. Mater.*, 2008, **155**, 312–319.

22 Z. Wu, X. Liu, C. Yu, F. Li, W. Zhou and L. Wei, *Sci. Total Environ.*, 2021, **796**, 148941.

23 L. Fernández, V. I. Esteves, Â. Cunha, R. J. Schneider and J. P. C. Tomé, *J. Porphyrins Phthalocyanines*, 2016, **20**, 150–166.

24 C. Melis, L. Colombo and A. Mattoni, *J. Phys. Chem. C*, 2011, **115**, 18208–18212.

25 Q. An, F. Zhang, J. Zhang, W. Tang, Z. Wang, L. Li, Z. Xu, F. Teng and Y. Wang, *Sol. Energy Mater. Sol. Cells*, 2013, **118**, 30–35.

26 D. Zeng, C. Yu, Q. Fan, J. Zeng, L. Wei, Z. Li, K. Yang and H. Ji, *Chem. Eng. J.*, 2020, **391**, 123607.

27 G. Guo, H. Guo, F. Wang, L. J. France, W. Yang, Z. Mei and Y. Yu, *Green Energy Environ.*, 2020, **5**, 114–120.

28 N. Zhang, L. Wen, J. Yan and Y. Liu, *Chem. Pap.*, 2020, **74**, 389–406.

29 D. Chen, D. Yang, J. Geng, J. Zhu and Z. Jiang, *Appl. Surf. Sci.*, 2008, **255**, 2879–2884.

30 Z. Mesgari and J. Saien, *Sep. Purif. Technol.*, 2017, **185**, 129–139.

31 L. R. Milgrom, *The Colours of Life*, Oxford University Press, Oxford, UK, 1997.

32 J. E. Falk, *Porphyrins and Metalloporphyrins: A new edition based on the original volume*, Elsevier Scientific Pub, Liverpool, 1975.

33 X. Huang, K. Nakanishi and N. Berova, *Chirality*, 2000, **12**, 237–255.

34 G. I. Vargas-Zúñiga and J. L. Sessler, in *Advances in Inorganic Chemistry*, Elsevier Inc., 1st edn, 2018, vol. 71, pp. 327–377.

35 Z. Xu and S. Swavey, *Dalton Trans.*, 2011, **40**, 7319.

36 B. B. Beyene and C. H. Hung, *Coord. Chem. Rev.*, 2020, **410**, 213234.

37 P. Kar, S. Sardar, E. Alarousu, J. Sun, Z. S. Seddigi, S. A. Ahmed, E. Y. Danish, O. F. Mohammed and S. K. Pal, *Chem. – Eur. J.*, 2014, **20**, 10475–10483.

38 K. M. Smith, R. Guilard and K. Kadish, *The Porphyrin Handbook. Applications: Past, Present and Future*, Academic Press, New York, 2000, vol. 1–10.

39 Q. Liu, Y. Ding, Y. Yang, L. Zhang, L. Sun, P. Chen and C. Gao, *Mater. Sci. Eng., C*, 2016, **59**, 445–453.

40 S. R. D. Gamelas, A. T. P. C. Gomes, N. M. M. Moura, M. A. F. Faustino, J. A. S. Cavaleiro, C. Lodeiro, M. I. S. Veríssimo, T. Fernandes, A. L. Daniel-da-Silva, M. T. S. R. Gomes and M. G. P. M. S. Neves, *Molecules*, 2018, **23**, 1–15.

41 C. I. V. Ramos, N. M. M. Moura, S. M. F. Santos, M. A. Faustino, J. P. C. Tomé, F. M. L. Amado and M. G. P. M. S. Neves, *Int. J. Mass Spectrom.*, 2015, **392**, 164–172.

42 K. B. Ferenz and A. U. Steinbicker, *J. Pharmacol. Exp. Ther.*, 2019, **369**, 300–310.

43 S. M. G. Pires, M. M. Q. Simões, I. C. M. S. Santos, S. L. H. Rebelo, M. M. Pereira, M. G. P. M. S. Neves and J. a. S. Cavaleiro, *Appl. Catal., B*, 2012, **439–440**, 51–56.

44 C. M. B. Carvalho, T. J. Brocksom and K. T. de Oliveira, *Chem. Soc. Rev.*, 2013, **42**, 3302.

45 V. Almeida-Marrero, J. A. González-Delgado and T. Torres, *Macroheterocycles*, 2019, **12**, 8–16.

46 S. R. D. Gamelas, J. M. D. Calmeiro, A. T. P. C. Gomes, M. A. F. Faustino, M. G. P. M. S. Neves, A. Almeida, J. P. C. Tomé and L. M. O. Lourenço, *Dyes Pigm.*, 2020, **181**, 108476.

47 C. P. S. Ribeiro, S. R. D. Gamelas, M. A. F. Faustino, A. T. P. C. Gomes, J. P. C. Tomé, A. Almeida and L. M. O. Lourenço, *Photodiagn. Photodyn. Ther.*, 2020, **31**, 101788.

48 S. R. G. Fernandes, R. Fernandes, B. Sarmento, P. M. R. Pereira and J. P. C. Tomé, *Org. Biomol. Chem.*, 2019, **17**, 2579–2593.

49 C. Costentin, H. Dridi and J.-M. Savéant, *J. Am. Chem. Soc.*, 2015, **137**, 13535–13544.

50 R.-M. Ion, in *Phthalocyanines and Some Current Applications*, ed. Y. Ylmaz, InTech Open, London, 2017, vol. 9, pp. 189–221.

51 S. N. Ahmed and W. Haider, *Nanotechnology*, 2018, **29**, 342001.

52 J. K. Challis, M. L. Hanson, K. J. Friesen and C. S. Wong, *Environ. Sci.: Process. Impacts*, 2014, **16**, 672–696.

53 C. Schweitzer and R. Schmidt, *Chem. Rev.*, 2003, **103**, 1685–1758.

54 S. Mathai, T. A. Smith and K. P. Ghiggino, *Photochem. Photobiol. Sci.*, 2007, **6**, 995–1002.

55 A. A. Buglak, M. A. Filatov, M. A. Hussain and M. Sugimoto, *J. Photochem. Photobiol., A*, 2020, **403**, 112833.

56 K.-S. Ju and R. E. Parales, *Microbiol. Mol. Biol. Rev.*, 2010, **74**, 250–272.

This journal is © The Royal Society of Chemistry 2024

*Catal. Sci. Technol.*, 2024, **14**, 2352–2389 | **2385**

57 W. M. Hikal and H. J. Harmon, *Polyhedron*, 2009, **28**, 113–120.

58 S. D. Gokakakar and A. v. Salker, *Indian J. Chem. Technol.*, 2009, **16**, 492–498.

59 M. Z. H. b. Zakaria, N. S. A. Zauzi, R. Baini, N. M. Sutan and M. R. Rahman, *IOP Conf. Ser.: Mater. Sci. Eng.*, 2017, **216**, 012003.

60 K. Hunger, P. Mischke, W. Rieper and S. Zhang, in *Ullmann's Encyclopedia of Industrial Chemistry*, Wiley-VCH Verlag GmbH & Co. KGaA, Weinheim, Germany, 2017, pp. 1–24.

61 Z. Xiao, Y. Zhou, X. Xin, Q. Zhang, L. Zhang, R. Wang and D. Sun, *Macromol. Chem. Phys.*, 2016, **217**, 599–604.

62 N. Bordoloi, M. D. Dey, R. Mukhopadhyay and R. Kataki, *Water Sci. Technol.*, 2018, **77**, 638–646.

63 D. K. Surendran, M. M. Xavier, V. P. Viswanathan and S. Mathew, *Environ. Sci. Pollut. Res.*, 2017, **24**, 15360–15368.

64 M. Li, H. Zhao and Z. Y. Lu, *Microporous Mesoporous Mater.*, 2020, **292**, 109774.

65 H. Chen, X. Jin, K. Zhu and R. Yang, *Water Res.*, 2002, **36**, 4106–4112.

66 G. Panzarasa and G. Soliveri, *Appl. Sci.*, 2019, **9**, 1266.

67 B. Muktha, G. Madras, T. N. Guru Row, U. Scherf and S. Patil, *J. Phys. Chem. B*, 2007, **111**, 7994–7998.

68 Y. B. Zhou and Z. P. Zhan, *Chem. - Asian J.*, 2018, **13**, 9–19.

69 V. B. Khajone and P. R. Bhagat, *Res. Chem. Intermed.*, 2020, **46**, 783–802.

70 L. Shao, G. Xing, W. Lv, H. Yu, M. Qiu, X.-M. Zhang and C. Qi, *Polym. Int.*, 2013, **62**, 289–294.

71 J. W. Choi, S. G. Chung, K. Y. Cho, K. Y. Baek, S. W. Hong, D. J. Kim and S. H. Lee, *Water, Air, Soil Pollut.*, 2012, **223**, 1437–1441.

72 S. G. Chung, Y. S. Chang, J. W. Choi, K. Y. Baek, S. W. Hong, S. T. Yun and S. H. Lee, *Chem. Eng. J.*, 2013, **215–216**, 921–928.

73 K. Y. Cho, J. W. Choi, S. H. Lee, S. S. Hwang and K. Y. Baek, *Polym. Chem.*, 2013, **4**, 2400–2405.

74 K. Y. Cho, H. J. Kim, X. H. Do, J. Y. Seo, J. W. Choi, S. H. Lee, H. G. Yoon, S. S. Hwang and K. Y. Baek, *Res. Chem. Intermed.*, 2018, **44**, 4663–4684.

75 N. Qiu, Y. Li, S. Han, T. Satoh, T. Kakuchi and Q. Duan, *J. Appl. Polym. Sci.*, 2014, **131**, 1–8.

76 N. Qiu, Y. Li, S. Han, G. Cui, T. Satoh, T. Kakuchi and Q. Duan, *J. Photochem. Photobiol., A*, 2014, **283**, 38–44.

77 Y. Ruan and B. Gao, *J. Mol. Struct.*, 2020, **1210**, 128050.

78 Y. Li, H. Xu, S. Ouyang and J. Ye, *Phys. Chem. Chem. Phys.*, 2016, **18**, 7563–7572.

79 M. S. Deenadayalan, N. Sharma, P. K. Verma and C. M. Nagaraja, *Inorg. Chem.*, 2016, **55**, 5320–5327.

80 T. He, B. Ni, S. Zhang, Y. Gong, H. Wang, L. Gu, J. Zhuang, W. Hu and X. Wang, *Small*, 2018, **14**, 10–15.

81 Y. Zong, S. Ma, J. Gao, M. Xu, J. Xue and M. Wang, *ACS Omega*, 2021, **6**, 17228–17238.

82 C. Shi, Z. Zhao, L. Zhao, A. Kushwaha, A. Kumar, J. Wang, Y. Pan, M. Muddassir and Q. Lan, *Inorg. Chem. Commun.*, 2023, **154**, 110920.

83 N. Wang, S. Liu, Z. Sun, Y. Han, J. Xu, Y. Xu, J. Wu, H. Meng, B. Zhang and X. Zhang, *Nanotechnology*, 2021, **32**, 465705.

84 Z. W. Jiang, Y. C. Zou, T. T. Zhao, S. J. Zhen, Y. F. Li and C. Z. Huang, *Angew. Chem., Int. Ed.*, 2020, **59**, 3300–3306.

85 S. Zhao, S. Li, Z. Zhao, Y. Su, Y. Long, Z. Zheng, D. Cui, Y. Liu, C. Wang, X. Zhang and Z. Zhang, *Environ. Sci. Pollut. Res.*, 2020, **27**, 39186–39197.

86 V. Likodimos, *Appl. Catal., B*, 2018, **230**, 269–303.

87 S. Gorduk, O. Avciata and U. Avciata, *Inorg. Chim. Acta*, 2018, **471**, 137–147.

88 M. Y. Chang, Y. H. Hsieh, T. C. Cheng, K. S. Yao, M. C. Wei and C. Y. Chang, *Thin Solid Films*, 2009, **517**, 3888–3891.

89 X.-T. Zhou, H.-B. Ji and X.-J. Huang, *Molecules*, 2012, **17**, 1149–1158.

90 M. A. Malik, M. Y. Wani and M. A. Hashim, *Arabian J. Chem.*, 2012, **5**, 397–417.

91 L. Madriz, H. Carrero, J. Herrera, A. Cabrera, N. Canudas and L. Fernández, *Top. Catal.*, 2011, **54**, 236–243.

92 L. Madriz, H. Carrero, O. Núñez, R. Vargas and J. Herrera, *Quim. Nova*, 2016, **33**, 1714–1719.

93 G. Mele, R. Del Sole, G. Vasapollo, E. García-López, L. Palmisano and M. Schiavello, *J. Catal.*, 2003, **217**, 334–342.

94 G. Mele, R. del Sole, G. Vasapollo, E. García-López, L. Palmisano, L. Jun, R. Słota and G. Dyrda, *Res. Chem. Intermed.*, 2007, **33**, 433–448.

95 X. Liu, M. Yu, Z. Zhang, X. Zhao and J. Li, *Res. Chem. Intermed.*, 2016, **42**, 5197–5208.

96 C. Wang, J. Li, G. Mele, G. M. Yang, F. X. Zhang, L. Palmisano and G. Vasapollo, *Appl. Catal., B*, 2007, **76**, 218–226.

97 M. Y. Duan, J. Li, M. Li, Z. Q. Zhang and C. Wang, *Appl. Surf. Sci.*, 2012, **258**, 5499–5504.

98 C. Wang, J. Li, G. Mele, M. Duan, X. Lü, L. Palmisano, G. Vasapollo and F. Zhang, *Dyes Pigm.*, 2010, **84**, 183–189.

99 X. F. Lü, J. Li, C. Wang, M. Y. Duan, Y. Luo, G. P. Yao and J. L. Wang, *Appl. Surf. Sci.*, 2010, **257**, 795–801.

100 M. Duan, J. Li, G. Mele, C. Wang, X. Lü, G. Vasapollo and F. Zhang, *J. Phys. Chem. C*, 2010, **114**, 7857–7862.

101 J. Zhang, L. Zhang, X. Li, S.-Z. Kang and J. Mu, *J. Dispersion Sci. Technol.*, 2011, **32**, 943–947.

102 P. Pichat, *Photocatalysis and Water Purification: From Fundamentals to Recent Applications*, 2013.

103 M. Yu, J. Li, W. Sun, M. Jiang and F. Zhang, *J. Mater. Sci.*, 2014, **49**, 5519–5528.

104 W. J. Sun, J. Li, G. P. Yao, M. Jiang and F. X. Zhang, *Catal. Commun.*, 2011, **16**, 90–93.

105 M. M. Yu, C. Wang, J. Li, L. Yuan and W. J. Sun, *Appl. Surf. Sci.*, 2015, **342**, 47–54.

106 W. Sun, J. Li, G. Yao, F. Zhang and J.-L. Wang, *Appl. Surf. Sci.*, 2011, **258**, 940–945.

107 G. Vasapollo, G. Mele, R. Del Sole, I. Pio, J. Li and S. E. Mazzetto, *Molecules*, 2011, **16**, 5769–5784.

108 G. P. Yao, J. Li, Y. Luo and W. J. Sun, *J. Mol. Catal. A: Chem.*, 2012, **361–362**, 29–35.

**2386** | *Catal. Sci. Technol.*, 2024, **14**, 2352–2389

This journal is © The Royal Society of Chemistry 2024

109  S. Chen and F. Shen, *J. Inclusion Phenom. Macrocyclic Chem.*, 2017, **88**, 229–238.

110  C. Huang, Y. Lv, Q. Zhou, S. Kang, X. Li and J. Mu, *Ceram. Int.*, 2014, **40**, 7093–7098.

111  X. F. Lü, W. J. Sun, J. Li, W. X. Xu and F. X. Zhang, *Spectrochim. Acta, Part A*, 2013, **111**, 161–168.

112  X. Lü, H. Qian, G. Mele, A. de Riccardis, R. Zhao, J. Chen, H. Wu and N. Hu, *Catal. Today*, 2017, **281**, 45–52.

113  W. Sun, J. Li, X. Lü and F. Zhang, *Res. Chem. Intermed.*, 2013, **39**, 1447–1457.

114  X. Lü, N. Hu, J. Li, H. Ma, K. Du and R. Zhao, *Res. Chem. Intermed.*, 2014, **40**, 1911–1922.

115  X. Zhao, X. Liu, M. Yu, C. Wang and J. Li, *Dyes Pigm.*, 2017, **136**, 648–656.

116  X. Q. Su, J. Li, Z. Q. Zhang, M. M. Yu and L. Yuan, *J. Alloys Compd.*, 2015, **626**, 252–259.

117  C. Dang, Q. Zhang, M. Xu, X. Ruan, P. Xu, J. Yan and J. Li, *Inorg. Nano-Met. Chem.*, 2017, **47**, 783–787.

118  L. Tasseroul, S. D. Lambert, D. Eskenazi, M. Amoura, C. A. Páez, S. Hiligsmann, P. Thonart and B. Heinrichs, *J. Photochem. Photobiol., A*, 2013, **272**, 90–99.

119  C. P. M. de Oliveira, A. L. A. Lage, D. C. da S. Martins, N. D. S. Mohallem and M. M. Viana, *Surf. Interfaces*, 2020, **21**, 100774.

120  D. Li, W. Dong, S. Sun, Z. Shi and S. Feng, *J. Phys. Chem. C*, 2008, **112**, 14878–14882.

121  K. Kümmerer and K. Kümmerer, *Pharmaceuticals in the Environment*, Royal Society of Chemistry, Cambridge, 2015.

122  A. S. Taha, C. McCloskey, R. Prasad and V. Bezlyak, *Lancet*, 2009, **374**, 119–125.

123  S. Murphy, C. Saurel, A. Morrissey, J. Tobin, M. Oelgemöller and K. Nolan, *Appl. Catal., B*, 2012, **119–120**, 156–165.

124  M. Gaeta, G. Sanfilippo, A. Fraix, G. Sortino, M. Barcellona, G. Oliveri Conti, M. E. Fragalà, M. Ferrante, R. Purrello and A. D'Urso, *Int. J. Mol. Sci.*, 2020, **21**, 3775.

125  G. Rigos and G. M. Troisi, *Rev. Fish Biol. Fish.*, 2005, **15**, 53–73.

126  G. Granados-Oliveros, E. A. Páez-Mozo, F. M. Ortega, C. Ferronato and J. M. Chovelon, *Appl. Catal., B*, 2009, **89**, 448–454.

127  H. He, Y. Liu, S. You, J. Liu, H. Xiao and Z. Tu, *Int. J. Environ. Res. Public Health*, 2019, **16**, 5129.

128  J. M. Wan, Z. Z. Wu, H. G. Wang and X. M. Zheng, *Adv. Mater. Res.*, 2012, **441**, 544–548.

129  H. Wang, D. Zhou, Z. Wu, J. Wan, X. Zheng, L. Yu and D. L. Phillips, *Mater. Res. Bull.*, 2014, **57**, 311–319.

130  H. Wang, D. Zhou, S. Shen, J. Wan, X. Zheng, L. Yu and D. Lee Phillips, *RSC Adv.*, 2014, **4**, 28978–28986.

131  C.-C. Huang, P. S. Parasuraman, H.-C. Tsai, J.-J. Jhu and T. Imae, *RSC Adv.*, 2014, **4**, 6540.

132  S. Halder and P. Bhavana, *J. Mol. Struct.*, 2016, **1120**, 62–69.

133  M. L. ArunaKumari and L. Gomathi Devi, *Environ. Sci.: Water Res. Technol.*, 2015, **1**, 177–187.

134  S. Sardar, S. Sarkar, M. T. Z. Myint, S. Al-Harthi, J. Dutta and S. K. Pal, *Phys. Chem. Chem. Phys.*, 2013, **15**, 18562.

135  R. Satish Kumar, K. S. Min, S. H. Lee, N. Mergu and Y. A. Son, *J. Photochem. Photobiol., A*, 2020, **397**, 112595.

136  B. Yao, C. Peng, W. Zhang, Q. Zhang, J. Niu and J. Zhao, *Appl. Catal., B*, 2015, **174–175**, 77–84.

137  B. Krishnakumar, A. Balakrishna, C. T. Arranja, C. M. F. Dias and A. J. F. N. Sobral, *Spectrochim. Acta, Part A*, 2017, **176**, 134–141.

138  J.-H. Cai, J.-W. Huang, H.-C. Yu and L.-N. Ji, *Int. J. Photoenergy*, 2012, **2012**, 1–10.

139  J. G. Mahy, C. A. Paez, C. Carcel, C. Bied, A. S. Tatton, C. Damblon, B. Heinrichs, M. Wong Chi Man and S. D. Lambert, *J. Photochem. Photobiol., A*, 2019, **373**, 66–76.

140  X. Li, L. Liu, S. Z. Kang, J. Mu and G. Li, *Appl. Surf. Sci.*, 2011, **257**, 5950–5956.

141  M. Wei, J. Wan, Z. Hu, B. Wang and Z. Peng, *RSC Adv.*, 2015, **5**, 58184–58190.

142  H. G. Wang, Y. Fu, T. Han, J. M. Wan and X. M. Zheng, *RSC Adv.*, 2015, **5**, 33570–33578.

143  M. Wei, J. Wan, Z. Hu, Z. Peng and B. Wang, *J. Mater. Sci.: Mater. Electron.*, 2016, **27**, 4026–4034.

144  M. Wei, J. Wan, Z. Hu, Z. Peng, B. Wang and H. Wang, *Appl. Surf. Sci.*, 2017, **391**, 267–274.

145  L. Gomathi Devi and P. M. Nithya, *Inorg. Chem. Front.*, 2018, **5**, 127–138.

146  N. N. Ilkhechi and B. K. Kaleji, *Silicon*, 2017, **9**, 943–948.

147  J. H. Cai, J. W. Huang, H. C. Yu and L. N. Ji, *J. Taiwan Inst. Chem. Eng.*, 2012, **43**, 958–964.

148  H. Kim, W. Kim, Y. MacKeyev, G. S. Lee, H. J. Kim, T. Tachikawa, S. Hong, S. Lee, J. Kim, L. J. Wilson, T. Majima, P. J. J. Alvarez, W. Choi and J. Lee, *Environ. Sci. Pollut. Res.*, 2012, **46**, 9606–9613.

149  G. Ruppert, R. Bauer and G. Heisler, *J. Photochem. Photobiol., A*, 1993, **73**, 75–78.

150  C. E. Diaz-Uribe, W. A. L. Vallejo and J. Miranda, *J. Photochem. Photobiol., A*, 2014, **294**, 75–80.

151  Y. Takao, F. Matsumoto, K. Moriwaki, T. Mizuno, T. Ohno and J.-I. Setsune, *J. Porphyrins Phthalocyanines*, 2015, **19**, 786–793.

152  C. M. B. Neves, O. M. S. Filipe, N. Mota, S. A. O. Santos, A. J. D. Silvestre, E. B. H. Santos, M. G. P. M. S. Neves and M. M. Q. Simões, *J. Hazard. Mater.*, 2019, **370**, 13–23.

153  Y. Takao, T. Ohno, K. Moriwaki, F. Matsumoto and J. Setsune, *J. Porphyrins Phthalocyanines*, 2010, **14**, 64–68.

154  Y. Takao, T. Takeda, S. Tanikawa and J. Setsune, *J. Porphyrins Phthalocyanines*, 2003, **7**, 521–525.

155  M. Silva, M. E. Azenha, M. M. Pereira, H. D. Burrows, M. Sarakha, C. Forano, M. F. Ribeiro and A. Fernandes, *Appl. Catal., B*, 2010, **100**, 1–9.

156  D. D. La, S. v. Bhosale, L. A. Jones and S. v. Bhosale, *Photochem. Photobiol. Sci.*, 2017, **16**, 151–154.

157  X. Chen, Z. Wu, D. Liu and Z. Gao, *Nanoscale Res. Lett.*, 2017, **12**, 4–13.

158  K. M. Lee, C. W. Lai, K. S. Ngai and J. C. Juan, *Water Res.*, 2016, **88**, 428–448.

This journal is © The Royal Society of Chemistry 2024

*Catal. Sci. Technol.*, 2024, **14**, 2352–2389 | 2387

159 F. Chen, C. Yu, L. Wei, Q. Fan, F. Ma, J. Zeng, J. Yi, K. Yang and H. Ji, *Sci. Total Environ.*, 2020, **706**, 136026.

160 X. Li, Y. Cheng, S. Kang and J. Mu, *Appl. Surf. Sci.*, 2010, **256**, 6705–6709.

161 W. Sun, J. Li, G. Mele, Z. Zhang and F. Zhang, *J. Mol. Catal. A: Chem.*, 2013, **366**, 84–91.

162 V. G. P. Ribeiro, A. M. P. Marcelo, K. T. da Silva, F. L. F. da Silva, J. P. F. Mota, J. P. C. do Nascimento, A. S. B. Sombra, C. da Silva Clemente, G. Mele, L. Carbone and S. E. Mazzetto, *Materials*, 2017, **10**, 1–16.

163 S. Radhika, *J. Environ. Chem. Eng.*, 2017, **5**, 4239–4250.

164 L. G. Devi, M. L. ArunaKumari, B. G. Anitha, R. Shyamala and G. Poornima, *Surf. Interfaces*, 2016, **1–3**, 52–58.

165 R. Rahimi, M. Yaghoubi-Berijani, S. Zargari, M. Rabbani and S. Shariatinia, *Res. Chem. Intermed.*, 2016, **42**, 4697–4714.

166 M. Shaban, M. R. Abukhadra, A. A. P. Khan and B. M. Jibali, *J. Taiwan Inst. Chem. Eng.*, 2017, **82**, 102–116.

167 M. Berrios, M. A. Martín and A. Martín, *J. Ind. Eng. Chem.*, 2012, **18**, 780–784.

168 K. Chakraborty, S. Ibrahim, P. Das, S. Ghosh and T. Pal, in *AIP conference proceedings*, 2017, vol. 050077, p. 050077.

169 K. Chakraborty, S. Chakrabarty, T. Pal and S. Ghosh, *New J. Chem.*, 2017, **41**, 4662–4671.

170 M. Ahmaruzzaman, *Adv. Colloid Interface Sci.*, 2008, **143**, 48–67.

171 T. Chen, Y. Zheng, J. Lin and G. Chen, *J. Am. Soc. Mass Spectrom.*, 2008, **19**, 997–1003.

172 F. Liu, X. Shao, J. Wang, S. Yang, H. Li, X. Meng, X. Liu and M. Wang, *J. Alloys Compd.*, 2013, **551**, 327–332.

173 X. Liu, Z. Fang, X. Zhang, W. Zhang, X. Wei and B. Geng, *Cryst. Growth Des.*, 2009, **9**, 197–202.

174 Q. Liu, R. Zhu, Y. Jiang, Q. Jia, S. Yang, Q. Shao, D. Wang and P. Cui, *Mater. Sci. Eng. B: Solid-State Mater. Adv. Technol.*, 2014, **188**, 106–113.

175 R. Sivakumar, J. Thomas and M. Yoon, *J. Photochem. Photobiol., C*, 2012, **13**, 277–298.

176 Y. Li, M. Liu and L. Chen, *J. Mater. Chem. A*, 2017, **5**, 13757–13762.

177 C. Chen, P. Lei and J. Zhao, *Environ. Sci. Technol.*, 2004, **38**, 329–337.

178 R. Rahimi, F. Rafiee and M. Rabbani, *Proceedings of The 18th International Electronic Conference on Synthetic Organic Chemistry*, 2014, p. b017.

179 H. Yu, L. Jiang, H. Wang, B. Huang, X. Yuan, J. Huang, J. Zhang and G. Zeng, *Small*, 2019, **15**, 1–30.

180 Z. Zhang, H. Huang, S. Sun, J. Xu and N. Zhang, *J. Porphyrins Phthalocyanines*, 2018, **22**, 469–474.

181 C. Tudisco, L. Pulvirenti, P. Cool and G. G. Condorelli, *Dalton Trans.*, 2020, **49**, 8652–8660.

182 K. H. Choi, K. K. Wang, E. P. Shin, S. L. Oh, J. S. Jung, H. K. Kim and Y. R. Kim, *J. Phys. Chem. C*, 2011, **115**, 3212–3219.

183 L. Fernández, W. Borzecka, Z. Lin, R. J. Schneider, K. Huvaere, V. I. Esteves, A. Cunha and J. P. C. Tomé, *Dyes Pigm.*, 2017, **142**, 535–543.

184 K. A. D. F. Castro, J. M. M. Rodrigues, M. A. F. Faustino, J. P. C. Tomé, J. A. S. Cavaleiro, M. G. P. M. S. Neves and M. M. Q. Simões, *J. Organomet. Chem.*, 2021, **938**, 121751.

185 V. Hasija, P. Raizada, A. Sudhaik, K. Sharma, A. Kumar, P. Singh, S. B. Jonnalagadda and V. K. Thakur, *Appl. Mater. Today*, 2019, **15**, 494–524.

186 D. Chen, K. Wang, W. Hong, R. Zong, W. Yao and Y. Zhu, *Appl. Catal., B*, 2015, **166–167**, 366–373.

187 S. Liu, S. Zhou, C. Hu, M. Duan, M. Song, F. Huang and J. Cai, *J. Mater. Sci.: Mater. Electron.*, 2020, **31**, 10677–10688.

188 J. Zhang, A. Wang, W. Zhao, C. Li, X. Chen, Y. Wang, W. Zhu and Q. Zhong, *Dyes Pigm.*, 2018, **153**, 241–247.

189 H. Jia, D. Ma, S. Zhong, L. Li, L. Li, L. Xu and B. Li, *Chem. Eng. J.*, 2019, **368**, 165–174.

190 T. Xiong, M. Chen, M. Li, Q. Chen, G. Liu, Y. Li, Y. He, W. Tang and X. Liu, *Mater. Lett.*, 2023, **352**, 135114.

191 G. Piccirillo, N. Maldonado-Carmona, D. L. Marques, N. Villandier, C. A. Calliste, S. Leroy-Lhez, M. E. S. Eusébio, M. J. F. Calvete and M. M. Pereira, *Catal. Today*, 2023, **423**, 113903.

192 Q. Xu, X. Guo, C. Hou and Z. Wang, *Appl. Organomet. Chem.*, 2023, **37**, 1–9.

193 Y. Zhao, Y. Dong, F. Lu, C. Ju, L. Liu, J. Zhang, B. Zhang and Y. Feng, *J. Mater. Chem. A*, 2017, **5**, 15380–15389.

194 Z. L. Ma, G. F. Huang, D. S. Xu, M. G. Xia, W. Q. Huang and Y. Tian, *Mater. Lett.*, 2013, **108**, 37–40.

195 G. Mele, I. Pio, A. Scarlino, E. Bloise, R. del Sole, L. Palmisano and G. Vasapollo, *J. Catal.*, 2013, **2013**, 7.

196 R. Słota, G. Dyrda, K. Szczegot, G. Mele and I. Pio, *Photochem. Photobiol. Sci.*, 2011, **10**, 361–366.

197 R. Rahimi, M. M. Moghaddas and S. Zargari, *J. Sol-Gel Sci. Technol.*, 2013, **65**, 420–429.

198 J. Niu, B. Yao, B. Yao, Y. Chen, C. Peng, X. Yu, J. Zhang and G. Bai, *Appl. Surf. Sci.*, 2013, **271**, 39–44.

199 R. Rahimi, E. Honarvar Fard, S. Saadati and M. Rabbani, *J. Sol-Gel Sci. Technol.*, 2012, **62**, 351–357.

200 M. A. Ahmed, Z. M. Abou-Gamra, H. A. A. Medien and M. A. Hamza, *J. Photochem. Photobiol., B*, 2017, **176**, 25–35.

201 M. Rabbani, H. Bathaee, R. Rahimi and A. Maleki, *Desalin. Water Treat.*, 2016, **57**, 25848–25856.

202 R. Rahimi, S. Saadati and E. Honarvar Fard, *Environ. Prog. Sustainable Energy*, 2015, **34**, 1341–1348.

203 L. Shao, H. Xie, J. Mo, Z. Yang, Z. Fan and C. Qi, *Environ. Eng. Sci.*, 2012, **29**, 807–813.

204 M. Cantarella, R. Sanz, M. A. Buccheri, F. Ruffino, G. Rappazzo, S. Scalese, G. Impellizzeri, L. Romano and V. Privitera, *J. Photochem. Photobiol., A*, 2016, **321**, 1–11.

205 L. Shao, J. Chen, L. He, G. Xing, W. Lv, Z. Chen and C. Qi, *Turk. J. Chem.*, 2012, **36**, 700–708.

206 X. Zhang, H. Yang, F. Zhang and K. Chan, *Mater. Lett.*, 2007, **61**, 2231–2234.

207 J.-H. Cai, Y.-J. Ye, J.-W. Huang, H.-C. Yu and L.-N. Ji, *J. Sol-Gel Sci. Technol.*, 2012, **62**, 432–440.

208 X. B. Ren, M. Chen and D. J. Qian, *Langmuir*, 2012, **28**, 7711–7719.

209 Z. Youssef, P. Arnoux, L. Colombeau, J. Toufaily, T. Hamieh, C. Frochot and T. Roques-Carmes, *J. Photochem. Photobiol., A*, 2018, **356**, 177–192.

2388 | *Catal. Sci. Technol.*, 2024, **14**, 2352–2389

This journal is © The Royal Society of Chemistry 2024

210 J. Wan, M. Wei, Z. Hu, Z. Peng, B. Wang, D. Feng and Y. Shen, *Int. J. Hydrogen Energy*, 2016, **41**, 14692–14703.

211 M. Wei, J. Wan, Z. Hu, Z. Peng and B. Wang, *Appl. Surf. Sci.*, 2016, **377**, 149–158.

212 S. Zargari, R. Rahimi, A. Ghaffarinejad and A. Morsali, *J. Colloid Interface Sci.*, 2016, **466**, 310–321.

213 W. Zhu, Z. Xia, B. Shi and C. Lü, *Langmuir*, 2023, **39**, 15665–15675.

214 H. Ghafuri, Z. Movahedinia, R. Rahimi and H. R. Esmaili Zand, *RSC Adv.*, 2015, **5**, 60172–60178.

215 B. Krishnakumar, A. Balakrishna, S. A. Nawabjan, V. Pandiyan, A. Aguiar and A. J. F. N. Sobral, *J. Phys. Chem. Solids*, 2017, **111**, 364–371.

216 Y. Zhou, W. Yang, M. Qin and H. Zhao, *Appl. Organomet. Chem.*, 2016, **30**, 188–192.

217 H. Li, Y. Zhang, G. Chang, S. Liu, J. Tian, Y. Luo, A. M. Asiri, A. O. Al-Youbi and X. Sun, *ChemPlusChem*, 2012, **77**, 545–550.

218 T. T. Nguyen, H. T. Bui, G. T. Nguyen, T. N. Hoang, C. Van Tran, P. H. Ho, P. T. Hoai Nguyen, J. Y. Kim, S. W. Chang, W. J. Chung, D. D. Nguyen and D. D. La, *Environ. Res.*, 2023, **231**, 115984.

219 M. Mahyari, Y. Bide and J. N. Gavgani, *Appl. Catal., A*, 2016, **517**, 100–109.

220 M. Mahyari and J. Nasrollah Gavgani, *Res. Chem. Intermed.*, 2018, **44**, 3641–3657.

221 S. Aghakhaninejad, S. Zargari and R. Rahimi, *SN Appl. Sci.*, 2020, **2**, 1–12.

222 H. Yi, L. Qin, D. Huang, G. Zeng, C. Lai, X. Liu, B. Li, H. Wang, C. Zhou, F. Huang, S. Liu and X. Guo, *Chem. Eng. J.*, 2019, **358**, 480–496.

223 T. Chen, L. Liu, C. Hu and H. Huang, *Chin. J. Catal.*, 2021, 1413–1438.

224 K. Hu, C. Chen, Y. Zhu, G. Zeng, B. Huang, W. Chen, S. Liu, C. Lei, B. Li and Y. Yang, *J. Colloid Interface Sci.*, 2019, **540**, 115–125.

This journal is © The Royal Society of Chemistry 2024

*Catal. Sci. Technol.*, 2024, **14**, 2352–2389 | **2389**